

Investigating landing and take-off contact dynamics of host-seeking *Anopheles coluzzii* malaria mosquitoes using frustrated total internal reflection

Luc van den Boogaart



Investigating landing and take-off contact dynamics of host-seeking *Anopheles coluzzii* malaria mosquitoes using frustrated total internal reflection

Master of science thesis

Luc Mathijs van den Boogaart

4296044

To obtain the degree of

Master of Science

in Biomedical Engineering

at the

Department of BioMechanical Engineering,

Delft University of Technology,

to be defended publicly on Friday December 3, 2021 at 13:30 AM.

Supervisors:

dr. G.J. Amador

dr. ir. F.T. Muijres

dr. D. Dodou

Assessment committee

Committee Chair

Dr. D. Dodou

Department of Biomechanical Engineering
Medical Instruments & Bio-Inspired Technology

Faculty of Mechanical, Maritime and Materials Engineering
Delft University of Technology

Supervisor

Dr. G.J. Amador

Experimental Zoology

Animal Sciences Group
Wageningen University & Research

Supervisor

Dr. Ir. F.T. Muijres

Experimental Zoology

Animal Sciences Group
Wageningen University & Research

External Member

Prof. Dr. Ir. J.L. van Leeuwen

Experimental Zoology

Animal Sciences Group
Wageningen University & Research

Student

L.M. van den Boogaart

Department of Biomechanical Engineering

Faculty of Mechanical, Maritime and Materials Engineering
Delft University of Technology

Preface

As I am sat here, marking down the final words of this 8,5 year journey to legitimately call myself an engineer, I suddenly feel myself drowning in an immense sense of gratitude towards everyone who has, in one way or another, helped me get to this point. Despite the occasional hardships, sleepless nights and so many more resits than I am willing to admit, I carry with me so many beautiful memories of this time and the people I've got to spend it with. So I wish to dedicate this this preface to those fantastic people, the absolute legends, who helped me become the person I am proud to be today.

First of all, for all their continued support throughout all the years of my life, I wish to thank my parents. We did not and will not always agree on what is most important in life. But despite our occasional differences in opinion, and my outspoken and outlived desire to figure the simple things out the hard way, you have always supported me and provided for me the means and the freedom to do so. For that I am eternally grateful.

Then is to all my friends, who I am blessed to have made many. Without you I would not have been the person I've come to be today. The experiences I've shared with you and the many, many, things I have learned from you I will carry with me, in the hope I can some day pay them forward. My housemates from the Chillmode Institute who showed me that home is not the place but the people you share it with: Marc, Sietske, Thomas, Mick, Wouter, Joe, Lucas, Martin, Irene, Rob, Jetteke, Anna, Mimi, Tamy, Lennert, Itamar, Elias, Barry, Marko, Freek, Coen, Roos, Aisha, Eric, Dincer, Jorne, Ruben, Flavie, Pleun, Eddie, Siward, Aafje, Bart, Jorrit, Margot, Sabine, and everyone else, thank you for being excellent and for kicking me to the UB when it counted. Blikje Serdijntjes, forever shall we Masterlife, never again shall we reparatiebaco. The Drivers of board 14, Luca, Brum, Jamesz, JW, TesTes, Sant and Lotte, who welcomed me in their midst and made my master Biomedical Engineering so much more meaningful. The absolute legends of the Activity Committee always striving to be the life of the party: Marielle, Andrew, Bram, Maaïke, Freddy, Sarah and the others. The boys of JC Zodiac, don't you ever change. The absolute legends that do not fit within any of the previous categories: Geert, Dodo, Ilva, Janna, Rohan, Johan, Andres, The Oostplein Crew, 138-aan-de-gracht, de magische muziekanten, Huize Hendriks, GO Force, SchmomusV and everyone else. And a special shout-out to those who have suffered me while I needed to complain about my thesis and motivated me to get work done when I struggled the most, the true OG's and support group: Ilva, Jans, Janna, Andrew, Sietske, Marc, Tawab and Luca. Lobi!

Finally I want to thank Guillermo, Florian, Julian, Jeroen, Remco, Henk and Dimitra for all your help during this thesis. I could not have wished for more supportive, pleasant and insightful supervisors and colleagues during this project. Despite working in a dark bunker in a strange city in the height of Covid lockdown you made me feel very welcome during my time in Wageningen. It was my absolute pleasure to work with such a multi-talented team and I have truly learned a lot during the past 15 months.

*Luc van den Boogaart
Delft, November 2021*

Contents

Research Paper	1
Abstract	1
Introduction	2
Materials and Methods	5
Results	10
Discussion	15
Outlooks	17
Supplements	22

Investigating landing and take-off contact dynamics of host-seeking *Anopheles coluzzii* malaria mosquitoes using frustrated total internal reflection

First author:

Luc M. van den Boogaart

Other authors (alphabetical on last name):

Guillermo J. Amador, Dimitra Dodou, Julian K. A. Langowski, Florian T. Muijres, Jeroen Spitzen.

Author for correspondence: (luc1.vandenboogaart@wur.nl)

Affiliations

Experimental Zoology Group, Department of Animal Sciences, Wageningen University & Research, De Elst 1, Wageningen, 6708 WD, The Netherlands

Luc M. van den Boogaart, Guillermo J. Amador, Julian K. A. Langowski, Florian T. Muijres

Laboratory of Entomology, Department of Plant Sciences, Wageningen University & Research, Droevendaalsesteeg 1, Wageningen, 6708PB, The Netherlands

Jeroen Spitzen

Department of BioMechanical Engineering, Faculty of Mechanical, Maritime and Materials Engineering, Delft University of Technology, Mekelweg 2, Delft, 2628 CD, The Netherlands

Luc M. van den Boogaart, Dimitra Dodou

Abstract

To avoid detection during a bloodmeal, a mosquito must minimize contact forces during attachment and detachment contact while maintaining sufficient grip to insert their proboscis and feed. Measuring contact mechanics of the mosquito is technically challenging due to the small length and force scales. Because of this, many aspects of blood feeding are still poorly understood. We developed an optic measurement set-up that enables the observation of contact dynamics when mosquitoes are host-seeking and blood feeding. Using frustrated total internal reflection (FTIR) we were able to record contact dynamics of freely flying mosquitoes at a spatial resolution of $25\mu\text{m}^2$ per pixel and a temporal resolution of 500 Hz. While useful given its non-invasiveness, FTIR as a technique may lack reproducibility due to the subjectivity in defining an intensity threshold that signifies contact. At these time and length scales, low signal-to-noise ratio may amplify variations in contact areas measured given selections in intensity thresholds. We developed a systematic approach to select contact thresholds for large image sets, allowing for standardized high-throughput FTIR studies. Our results suggest that probing behaviour, characterized as rapid pulling of the fore and mid legs towards the body during contact, might be less related to surface evaluation via sensing than previously thought, and more related to establishing sufficient grip to insert the proboscis. This new perspective illustrates the need for further investigation into the contact dynamics of mosquitoes during blood feeding to understand the mechanisms that enable the transmission of vector-borne diseases, such as malaria, between hosts.

Introduction

Vector borne diseases in humans, the majority of which are transferred by mosquitoes, are among the leading causes of death worldwide. Although the spread of these vector diseases happens during blood-feeding, many aspects of this process are still poorly understood. The initial steps of host seeking and approach flight have been studied well, revealing mosquitoes to detect possible hosts through temperature, CO₂ presence and odour (Dekker & Cardé, 2011; Spitzen et al., 2013; McMeniman et al., 2014; van Breugel et al., 2015; Hawkes & Gibson, 2016; Dickerson et al., 2018; Cribellier et al., 2020). The last step of take-off and escape has also been characterized in recent studies, showing mosquitoes employ strategies to limit take-off forces and modulate leg dynamics to overcome surface roughness and control body pitch (Muijres et al., 2017; Smith et al., 2018; Veen et al., 2020). What takes place during the feeding process in between, however, is understood in much less detail (Benton, 2017).

Mosquitoes are believed to utilize multiple sensing modalities to select a feeding location after touchdown. Part of these modalities take place through the labella and proboscis (Sparks et al., 2013; Jové et al., 2020). An increasing number of studies also suggest mosquitoes sense surface characteristics through their legs (Sparks et al., 2013; Dennis et al., 2019; Hol et al., 2020; Iikura et al., 2020), thus suggesting tarsal contact sensing as one of the key pathways to non-volatile DEET effectiveness. These discoveries led to the association of commonly observed leg and proboscis probing behaviour before blood feeding (Clements, 1963; Smith et al., 2018; Hol et al., 2020) and before landing on a host (Parket et al., 2015; Hawkes & Gibson et al., 2016; Bougatsia, 2021) with sensing for host cues. However, due to a lack of standardized behavioural studies, resulting from a large number of confounding factors such as internal and external host cues or pathogen infections (Stanczyk et al., 2017), these associations are left subject to debate.

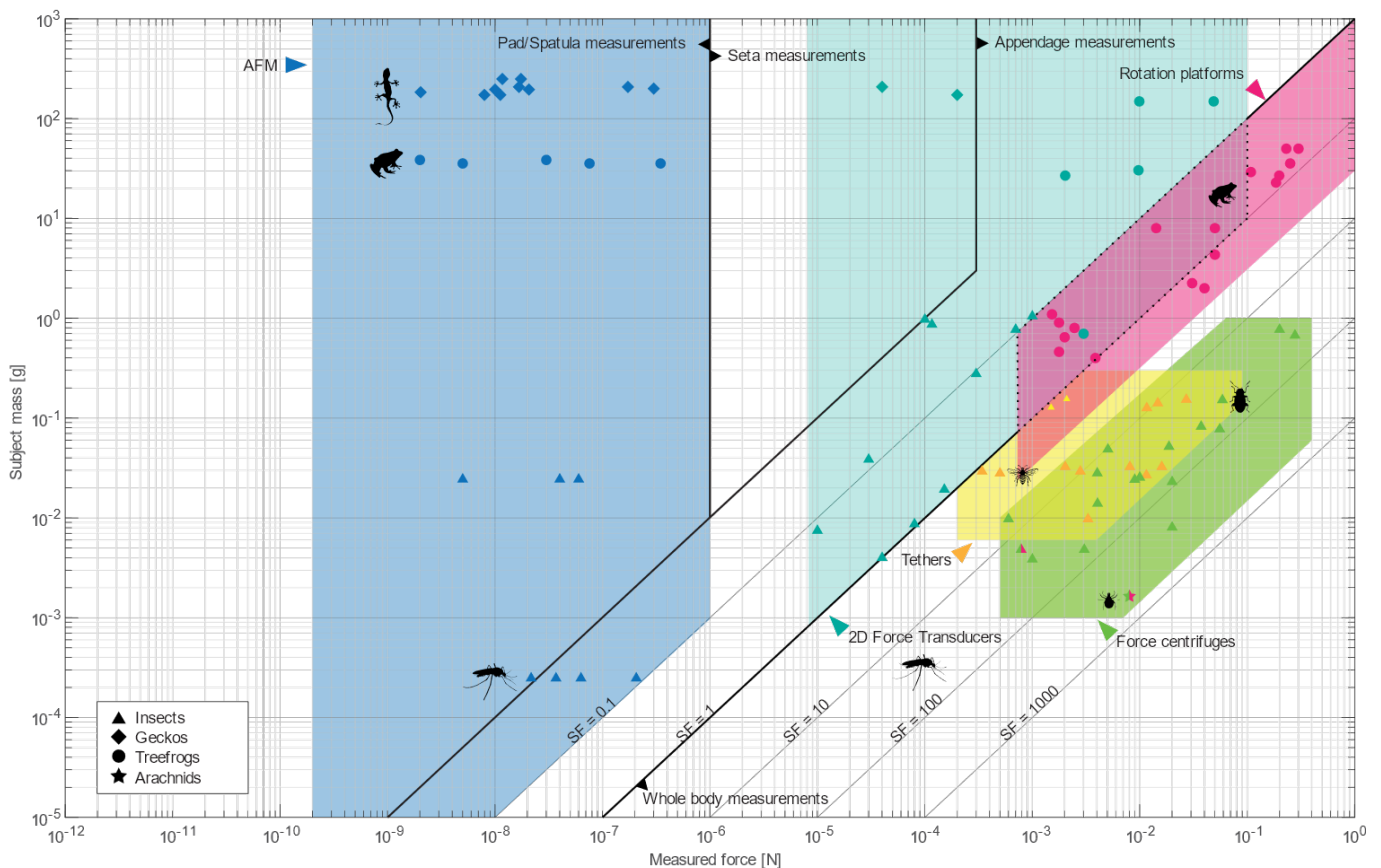


Fig 1: Regime map of the most common adhesion and friction force measurements, showing most common methods not to be viable for mosquitoes, having a body mass in the order of 1 mg. AFM (dark blue), 2D (biaxial) force transducers (light blue), force centrifuges (green), rotation platforms (pink) and tethers: 1D force transducers in tethered configuration (orange). (Van den Boogaart et al., 2021). Available in supplements: S1.

The investigation of tarsal contact mechanics from the angle of bio-adhesion could shed new light on the discussion. There currently exists a gap in literature investigating contact mechanics of mosquitoes. This gap exists in part due to the technical complexity of filling it. The most conventional way to assess adhesive performance is through force measurements. This is impossible for mosquitoes, seeing most of the commonly used techniques to directly measure adhesive forces lack the required precision to measure forces on the scale of the mosquito with an estimated body

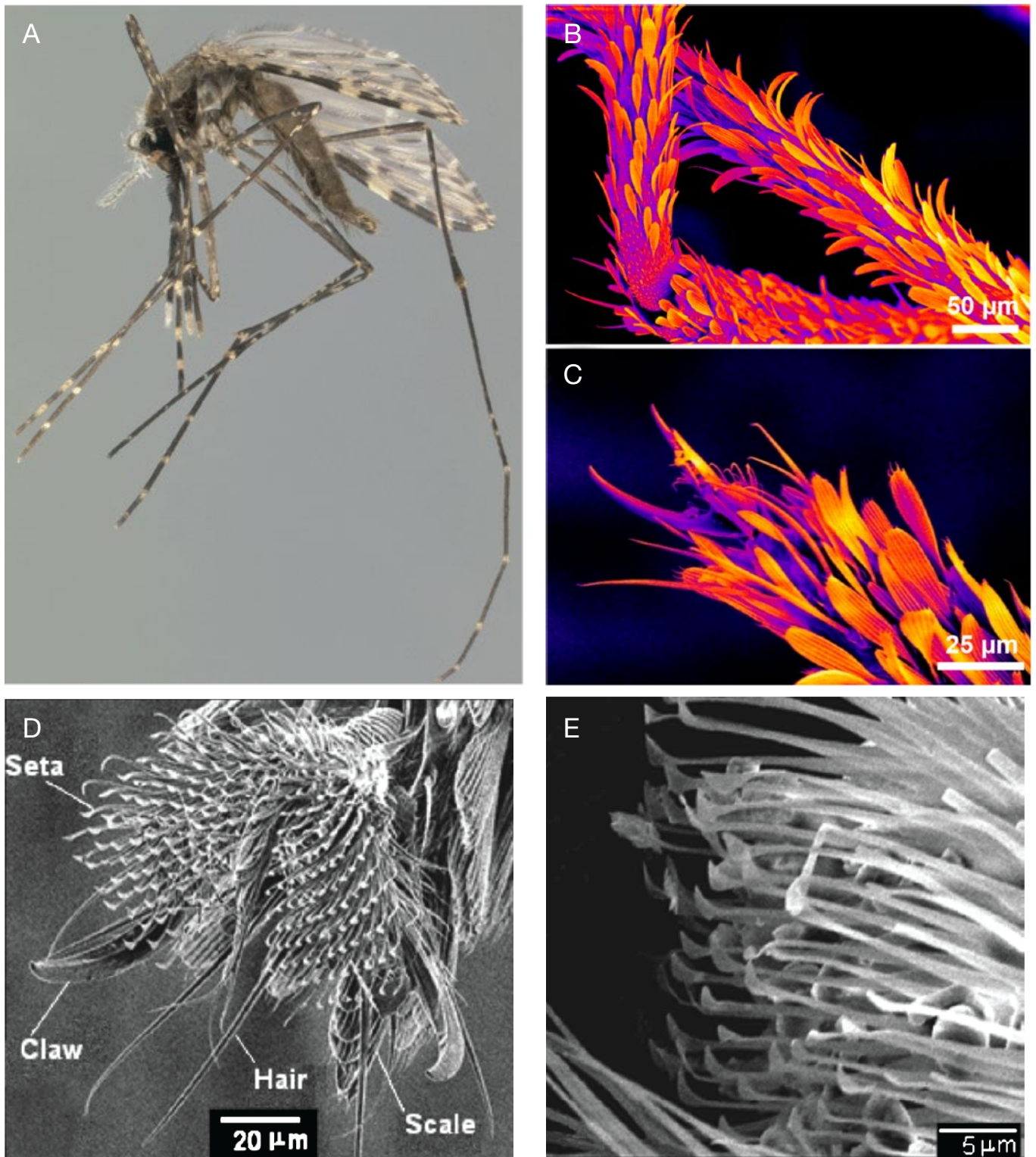


Figure 2: Morphological characteristics of the mosquito adhesive pad, and experimental setup. (A) *Anopheles coluzzii* Coetzee et al. (2013) Adapted from: photograph by Lyle Buss, University of Florida. (B) SEM (colorized) of the mosquito leg covered in hydrophobic scales. Scales are believed to interlock with rough surfaces generating Van der Waals force dominated adhesion as their main attachment mechanism. Adapted from: Pashazanusi et al. (2017). (C) SEM (colorized) of the mosquito claw, having a size in the order of 20-30μm. Adapted from: Pashazanusi et al. (2017). (D) SEM of the mosquito adhesive pad used for strict adhesion to smooth surfaces. Adapted from: Wu et al. (2007). (E) SEM of the setae that make up the adhesive pad. Each seta has a second level pad in the order of 2 – 3μm, believed to align with smooth surfaces to generate Van der Waals forces.

mass in the order of 1 mg (figure 1) (Muijres et al., 2017; Bhushan, 2018; van den Boogaart et al., 2021). So far, only Atomic Force Microscopy (AFM) has the required resolution to measure a mosquito's adhesive forces. An AFM study showed van der Waals forces to be the main adhesion mechanism employed by mosquitoes (Pashazanusi et al., 2017). AFM, however, has a key drawback: it requires an isolated leg to be attached to an AFM cantilever. This makes it impossible to measure forces of freely flying and blood feeding mosquitoes. To this point there have been no studies with mosquitoes focussing on contact mechanics in which behaviour is included.

Frustrated total internal reflection (FTIR), a way of investigating contact mechanics using light that has seen increased attention over the past decade, could provide new insights (Federle and Endlein, 2004; Endlein et al., 2013; Hill et al., 2018; Langowski et al., 2019). By trapping a sheet of light inside a substrate, contact with a wet or oily subject can be imaged through a local change of the relative refractive index between interfaces (Betts et al., 1980; van den Boogaart et al., 2021). Dynamic visualisation of the contact area while the mosquito is engaged with the substrate, provides insight into what tarsal structures are engaged with the substrate during contact, and allows us to assess their adhesive performance by analysing amount and rate of change of contact (Labonte & Federle, 2015). Like most dipterans, mosquitoes have adhesive pads (figure 2) and an oily secretion covering their legs making it in theory possible to image their leg contact using FTIR (Gorb, 2001; Pashazanusi et al., 2017; Féat et al., 2019).

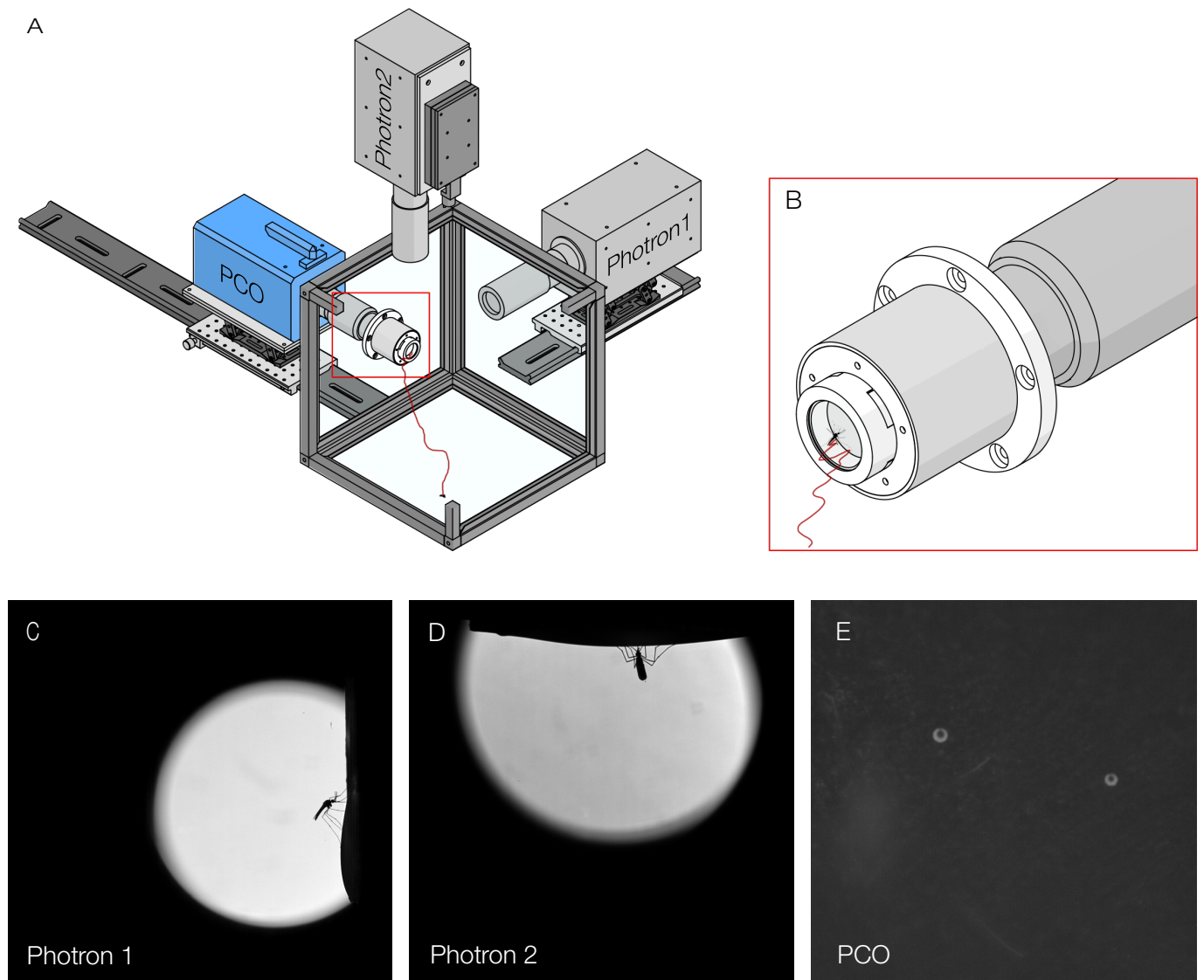


Figure 3: Overview of the experimental setup and raw image data. (A) The experimental setup consists of three High Speed cameras used to capture the landing and contact mechanics of free flying mosquitoes. Mosquitoes are released inside a cubic flight arena and motivated to land on the internally lit landing platform. The Photron cameras (grey) capture approach flight and landing of the mosquitoes with a resolution of 1MPx at 2000 FPS. PCO camera (blue) captures FTIR contact of the mosquito through the landing substrate at a resolution of 4MPx at 500 FPS. (B) The landing platform suspending a fluid cell with transparent fake blood is mounted to a tunnel attached to one of the flight arena walls. The fluid cell is covered by a parafilm membrane functioning as skin substrate to allow the mosquitoes to feed after landing. (C,D) Raw camera feed of the Photron cameras. When a mosquito is in the centre of both views, a signal is detectable on the PCO. (E) Camera feed of the PCO camera after colour correction. PCO video data is stored at 16 bit, resulting in the contact illumination to take place in the lower 1% of the dynamic range. This makes it impossible to detect contact on the PCO without image processing.

In this study we have developed an FTIR based optic measurement setup to visualize these contact mechanics during a bloodmeal. Using 3 high speed cameras we were able to capture substrate interaction. 2 cameras were used to film the approach and one camera captured substrate interaction through the substrate at a maximum resolution of $25\mu\text{m}^2$

per pixel at 500Hz. To elicit host search and feeding, FTIR was integrated into a transparent fluid cell containing fake blood and closed with a parafilm membrane as transparent artificial skin phantom. Integrating phantom skin as contact substrate and other host cues, came at a cost of signal to noise ratio however, resulting in larger relative errors from subjectivity in contact threshold selection compared to other FTIR studies. To decrease this subjectivity, we developed a custom segmentation algorithm and image processing algorithm to be used for thresholding FTIR images.

We filmed the landing and substrate interaction of 17 unfed malaria mosquitoes, *Anopheles coluzzii* (Coetzee et al., 2013). Before and after touchdown we observed probing behaviour at the skin phantom, but no successful feeding events inside the FOV of all cameras were recorded. Instead, most mosquitoes opted to move to the edge of the fluid cell, feeding while their legs were engaged with the fluid cell mount. These observations suggest mosquitoes had difficulty generating sufficient attachment to the skin phantom and that observed probing behaviour is mostly directed at getting a better grip off the substrate. Our results show that to completely dissect the interplay between mosquitoes and host cues during blood feeding, contact mechanics and substrate properties must be considered carefully.

Materials and methods:

Experimental animals

Experiments were performed with 7- to 11-day old female malaria mosquitoes, *A. coluzzi*, kept in a laboratory stock at RADIX Klima, Wageningen University, The Netherlands. The colony is reared using blood obtained from the blood bank (Sanquin, The Netherlands) using a Hemotek membrane feeding system (Discovery Workshops, Accrington, UK). Since *A. coluzzi* are nocturnally active, the colony was reared on a clock-shifted 12h:12h day/night cycle to overlap their active period with morning office hours. 15-16 hours prior to the experiments (lab closing hours the previous day) a set of mated female mosquitoes was collected and stored in custom storage containers made from an acrylic tube and gauze. While housed in these containers, the mosquitoes were starved on tap-water to motivate feeding behaviour during the morning. At the beginning of the day when experiments were conducted, mosquitoes were moved in a dark container from the rearing facility to the experimental setup. After an acclimatization period of 15-60 minutes the landing experiments were performed. Mosquitoes used during the experiment did not receive a blood meal prior or during the experiments, and were therefore free of malaria parasites (Becker et al., 2010).

Experimental setup and procedure

The experimental setup consisted of a cubic enclosure (40x40x40 cm) with transparent acrylic walls (figure 2b). During the experiments, the environment was kept at 27.5 ± 0.5 °C (mean \pm std, n) and a relative humidity of $70 \pm 1\%$. Light intensity inside the enclosure was between 1-5 lux during experiments, simulating dusk conditions. A custom landing platform was mounted on a camera port attached to one of the acrylic walls. Mosquitoes would be released in the enclosure, land on the landing platform to feed, and fly away to hide in a corner of the enclosure.

To compare footpad, contact dynamics during adhesion or friction-mediated attachment, two orientations were chosen for the enclosure and landing. First the landing platform was mounted on a horizontal axis with the substrate oriented vertically. In this vertical orientation mosquitoes support their weight primarily through friction forces. Second, the landing platform was mounted on the vertical axis with the substrate oriented horizontally from the top of the enclosure. In this inverse orientation mosquitoes support their weight through adhesive forces. Earlier results by our group investigating mosquito approach behaviour in both a regular horizontal (i.e., the mosquitoes landing from above) and vertical substrate orientation suggested a strong preference for *A. coluzzi* to land in the vertical orientation (Bougatsia, 2021). This has been observed before, hypothesized to be related to the preferred resting orientation of mosquitoes being vertical (Paaijmans and Thomas, 2011).

Because we wanted to investigate contact dynamics of the mosquitoes' legs, having a width of $\sim 50\mu\text{m}$, a high spatial resolution is required, at the cost of the field of view. To increase the number of landings inside the field of view the experiment was designed to stimulate host-seeking behaviour. A custom landing platform was developed which allowed for the imaging of the contact dynamics using FTIR while incorporating various host cues that elicit mosquito landing and feeding. The landing platform consisted of a fluid cell, made from a 35mm plastic Petri dish filled with a transparent fake blood emulsion (1 mM ATP in PBS) covered with a parafilm membrane, similar to the BitOscope as developed by Hol et al. (2020). The Petri dish was suspended inside a custom 3D printed PLA+ mounting ring lined with a 940nm IR LED-strip used to illuminate the substrate (figure setup diagram c, supplements). The resulting assembly was mounted on the camera port.

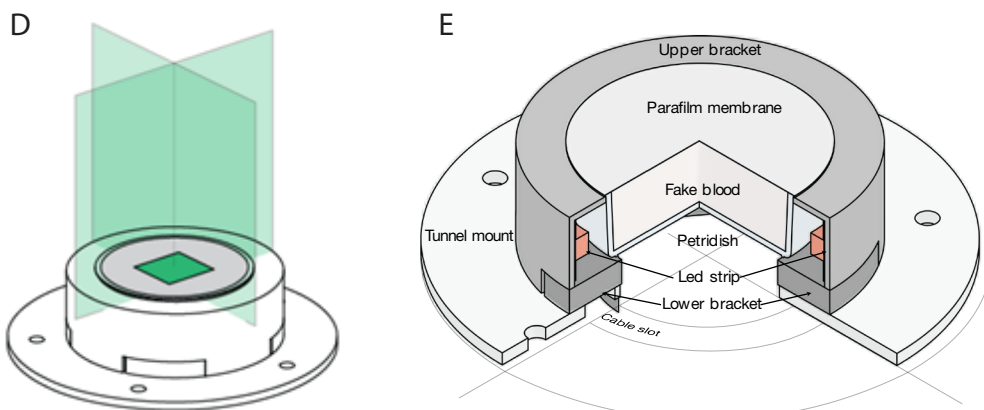
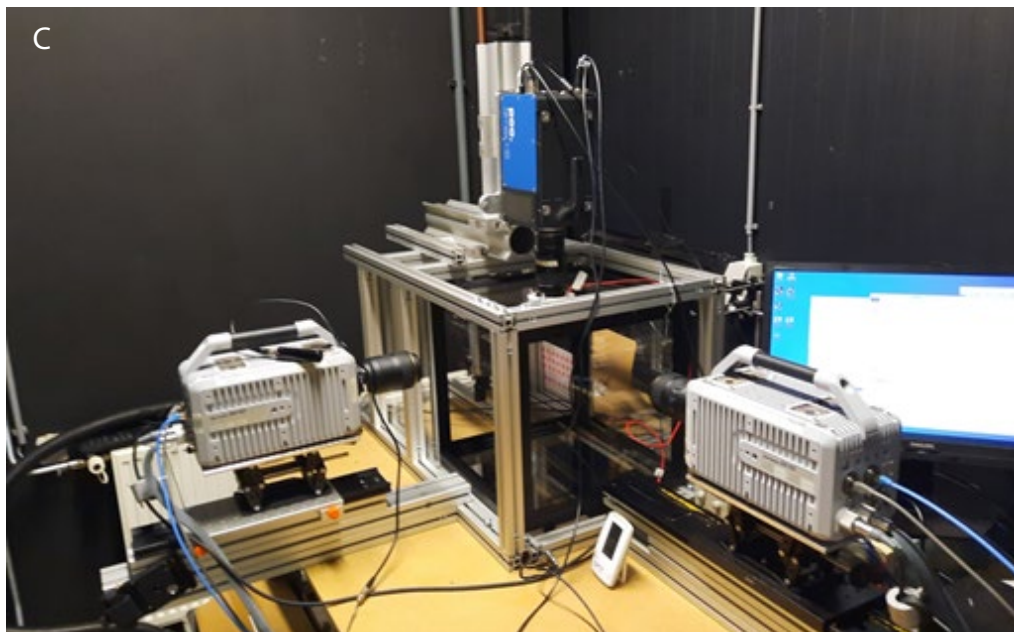
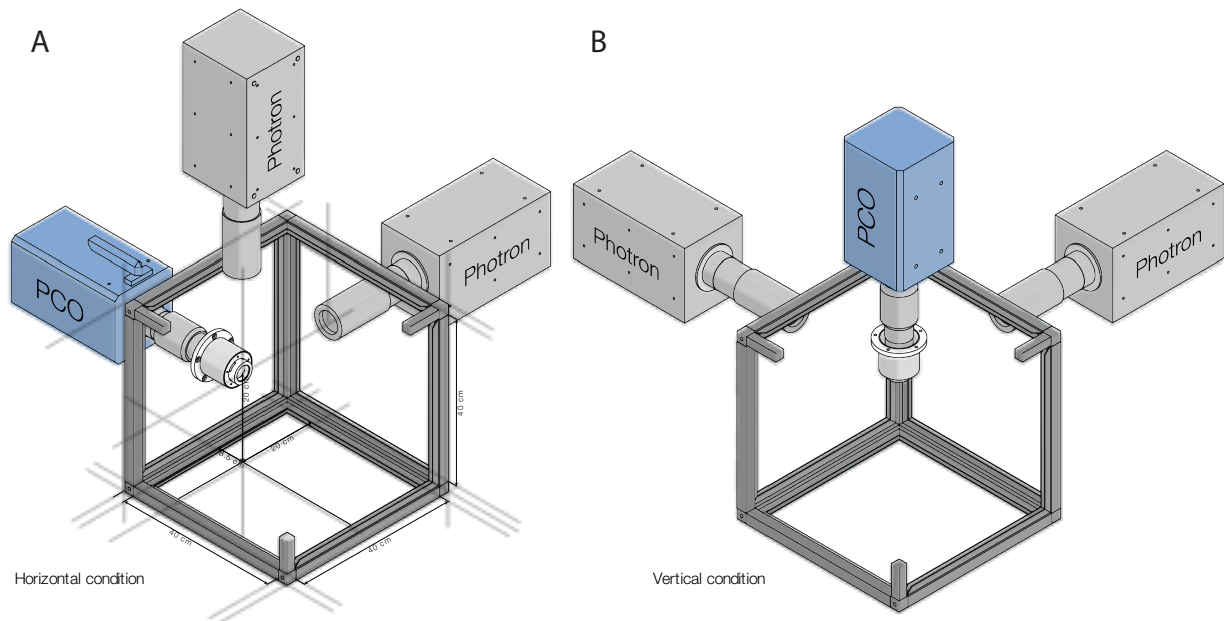


Figure 4: Two experimental conditions orientations, the experimental in the 2nd configuration, the target area indicating the FOV and focal plane of all cameras and a crosssection of the landing platform. (A,B) Overview showing both experimental conditions: the PCO Dimax HS4 (shown in blue) images through the substrate in the vertical plane (A: condition 1) and horizontal plane (B: condition 2). The cameras and flight arena are rotated between setups. (C) The experimental setup as built in the lab in condition 2. (D) The landing platform indicating the FOV of all cameras in green. (E). Crosssection of the landing platform, showing the LED strip lining the outer casing and the petridish suspended in the center. For a detailed description of the setup and components see supplements S2.

The membrane surface temperature was kept at 34 ± 1 °C, to simulate the skin temperature of a sleeping adult (te Lindert & van Someren, 2018), using the residual heat generated by the LED-strip while operated at 10V. At higher voltages, overheating would occur causing the parafilm membrane to rupture. In addition to temperature, CO₂ and odour were introduced as host cues. CO₂ was added to the system via a tube through which the experimenter could blow into the enclosure once every minute. Pumping pure CO₂ into the enclosure resulted in oversaturation, so it was not implemented in the experiments. Odour was added by placing a strip of nylon sock, worn by a human for 12 hours, around the port and rubbing a sheet of parafilm against skin for 120 seconds prior to covering the Petri Dish.

Mosquitoes were released into the enclosure in groups of 20. After an acclimatisation period of 10 minutes, CO₂ was introduced to activate the mosquitoes. When a mosquito landed in the target area, inside the FOV of all cameras, we manually triggered the recording system to record the approach and landing. Landings were recorded using three highspeed IR cameras (figure 3,4). Two Photron Fastcam SA-X2 (12 bits) 1MPx cameras were used to capture the approach and landing from the sides. A PCO Dimax HS4 (16 bits) 4MPx camera was mounted behind the landing platform to capture the FTIR light through the landing platform. The Photron cameras used a Nikkor 105mm AF-S f2.8G lens and the PCO camera used a Nikkor 105mm AF f2.8D lens with a 21.5mm extension tube, a +5-dioptre conversion lens and a 940nm filter. Both Photron Fastcam SA-X2 cameras were backlit using an 850nm 900mW mounted IR LED spot. During the experiments the cameras continuously recorded in end-trigger mode. The Photron Fastcam SA-X2 cameras recorded at 2000 frames s⁻¹ and were clocked via an external pulse generator to the PCO Dimax HS4 camera, which was set to record at 2000, 1000 and 500 frames s⁻¹ between different experiments to increase maximum exposure time. At the end of a series of experiments, mosquitoes were collected and killed, and the enclosure was cleaned using a 30% ethanol solution.

Video data processing

Due to the low signal to noise ratio and greater image size on the contact view PCO camera, event frames were first identified manually from the Photron feed capturing the approach and landing. To work with the PCO images, additional processing of the video data was required. Because of the various framerates and exposure times used during recording and uncontrollable membrane deformations, setting a uniform contact threshold was impossible. To standardize threshold selection for all recordings, a six-step computer-vision approach was developed (figure 5,6). First the image is pre-processed through subtracting the background and filtering salt- and pepper-noise. Next the image is segmented using an initial low predictor threshold, lower than the expected contact threshold. After segmentation, a computer vision-based object recognition script is used to classify and group pixel clusters as structures of interest or noise. Following structure identification, structures are classified as body, leg or noise objects and grouped based on their orientation and position. Next, splines are created to represent the legs, which are imposed over the raw image to be used as a base for sampling the actual Grey values along the leg. Finally, using these splines an outline of the leg was created, wherein pixels were grouped to the sample points to extract the average Grey value at each sample point.

The processing pipeline is designed to be modular and universal. Any of the function blocks can be tweaked or exchanged with minimal effort, and allows for the use of a range of options. The notable exception to algorithm universality is the image classification block, which is designed specifically for this data set and will need to be replaced per study. The pipe-line is designed such that blocks can be called individually, as a group or as part of a subset of blocks. Data is organised in struct objects per image frame, streamlining function calls and allowing the complete access of all data inside each of the function blocks to allow for easy local parameter tweaking and graphic debugging. To improve debugging and streamline data presentation, various data visualization algorithms are provided, which can be called from anywhere in the pipeline. Detailed explanation of the pipeline can be found in supplement (S3), code is available in supplement (S4).

Image classification

Legs can often be hard to distinguish from noise, both by the naked eye and by the computer. Contact illumination intensity levels are in the same order as illumination intensity levels from background illumination and internal refraction of the opaque parafilm membrane. Furthermore, in some cases the image is further contaminated by physical artifacts such as bubbles (figure:6A). Because of this, simple thresholding is not a feasible approach and

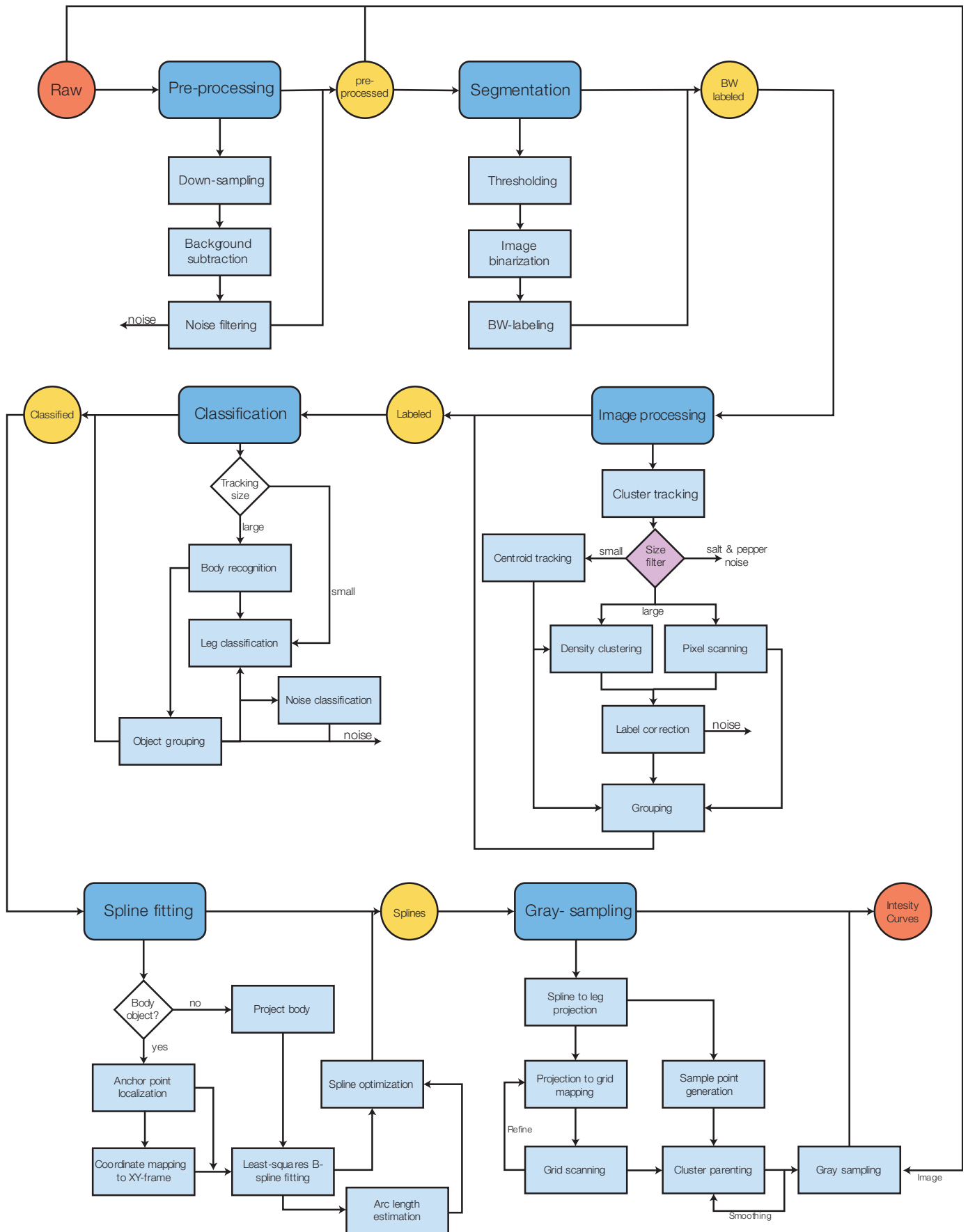


Figure 5: Flow diagram of the processing pipeline. The diagram shows the six main steps of the pipeline (dark blue) with intermediate function blocks (light blue). Each of these blocks is designed to be modular, and can be tweaked or replaced with minimal effort to fit different data sets. For a detailed description see supplements (S3). For the code availability see supplements (S4)

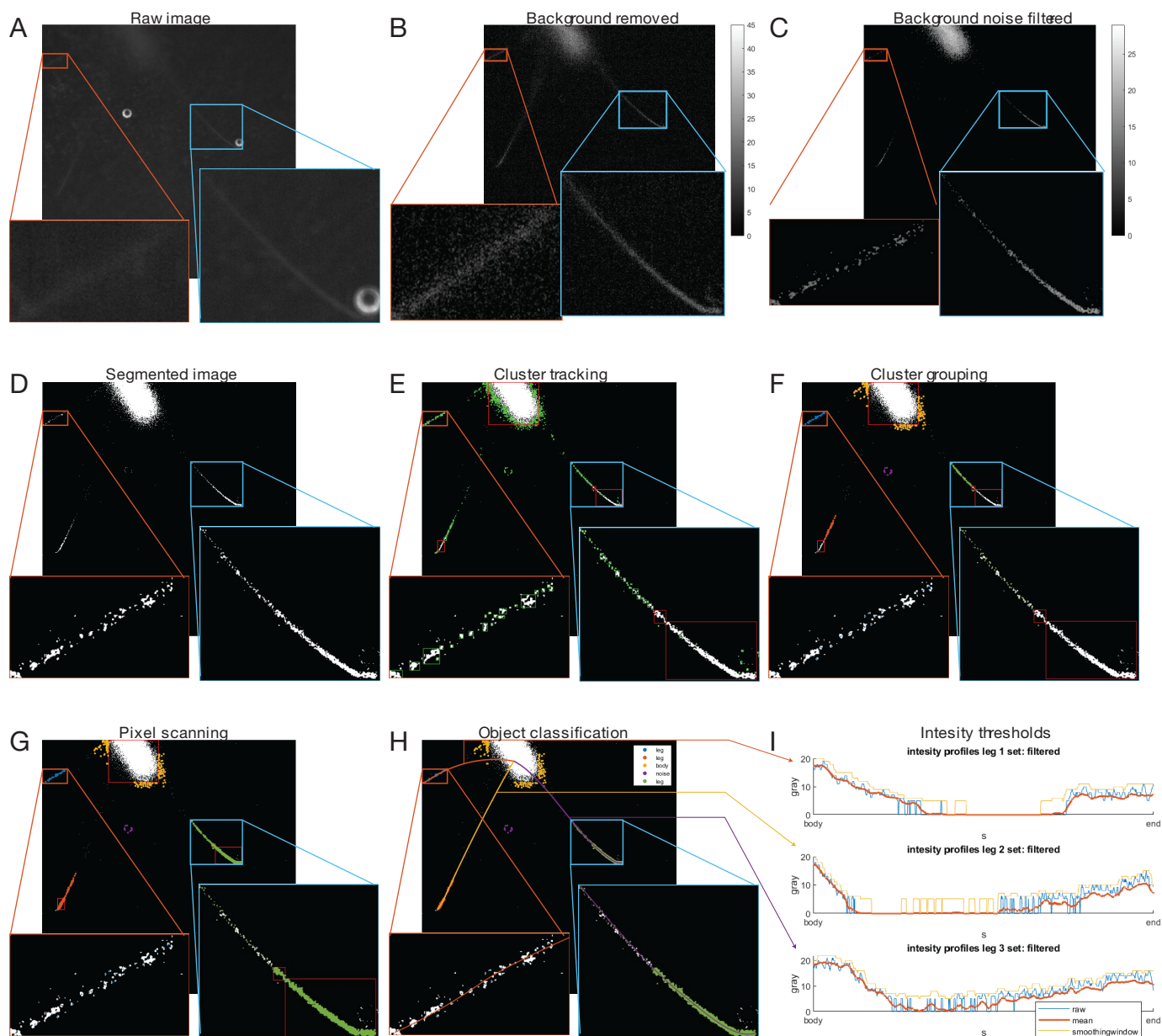


Figure 6: Example frame processing and classification, showing the extracted intensity profiles of all legs in the close-up extracted from the background noise filtered image. (A) Example raw frame (frame 30, set 13; converted to 8-bit). The left closeup image shows one of the mid-legs barely distinguishable from surrounding background noise by the naked eye. The right closeup image shows one of the hind legs in contact with a droplet noise structure. (B) Background subtraction removes most of the high intensity noise structures. Structures are no longer perceivable without scaling the image using the *imagesc* function (MATLAB®). (C) Residual noise is removed by sampling the intensity of residual noise and thresholding the image, leaving only structures of interest. (D) After background and noise removal, the image is binarized for further classification. (E) Pixel-clusters are tracked using MATLAB's image processing toolbox. Clusters are filtered using two size thresholds to remove individual pixels (salt and pepper noise) and identify expected contact areas (red boxes). (F) To reduce computational load, pixels are labelled per cluster based on centroid proximity using a density-based scanning algorithm. In this process, expected contact clusters (red boxes) are often mislabelled as noise and must be labelled separately based on Euclidean distance to pre-existing groups. (G) To improve fitting in expected contact areas, a second scanning algorithm is used to track the location of all pixels inside these areas (right close-up image). A region-size threshold is used to skip the expected body object to reduce computational load. (H) Clusters are classified to be body, leg or noise structure (top right legend) and then grouped into leg, body and noise objects based on location, orientation and group spread. Splines are then interpolated to estimate leg position. (I) The spline objects are mapped to the raw or filtered image. An offset projection is used to create a boundary to estimate the leg area. Local and mean (using a predefined smoothing window) intensity values are sampled from inside the estimated leg area along the spline object. Intensity curves show body illumination to be higher than contact illumination. This shows it is impossible to extract contact area using simple thresholding without classification. Video available in supplements (S5)

classification of visible structures is necessary. To extract local intensity profiles, leg objects need to be recognized and tracked separately. Object classification for the current data set is done using a custom computer vision-based approach. This has the benefit of allowing us to set the classification parameters ourselves making it a useful approach for a qualitative assessment of the dataset during the development of this pipeline. Custom computer vision algorithms have a downside, they are complex to program and will likely underperform neural network-based image classification algorithms. Neural networks do require a large set of annotated training data, which was unavailable in this study due to the limited size of the data set, making computer vision the method of choice.

Contact area threshold

The image processing pipeline extracts averaged raw, maximum, and averaged grey values around a user defined number of sample points. In default settings, the maximum number of sample points used are the total number of pixels intersecting the spline through the classified legs. A boundary object is created around the spline with a width of 11 pixels, corresponding to the width of a mosquito's leg. Averaging is done by taking the pixels in a specified radius r around the sample point that coincide with the boundary set. This way, r functions as a smoothing factor along the length of the leg. Taking the grey values directly from the raw image is not possible for data this noisy. Figure (7a) shows an example intensity plot of a raw image and the same image background subtracted, corresponding to figure (classification on raw). Without background subtraction, noise from imperfections in the parafilm is in some locations higher than contact illumination. To improve the signal, the image is first background subtracted and then filtered using a gaussian filter to remove residuals. The resulting signal is much cleaner, and shows a clear body, leg, and no-object area.

Contact area over time

The local intensity profiles can be used to derive contact dynamics. This is done by taking a threshold value from the intensity profiles. This can be done either by providing a maximum curve steepness, minimum value or both, depending on the data set. After thresholding, a window is created from the cut-off point to the end of the object or second cut-off point if present. Contact area per frame is calculated by taking the size of the object inside the window and multiplying this by a scaling factor calculated from the FOV and the camera resolution. Resulting contact area over time (figure 7b) shows frame by frame discrepancies of factor 3 to 4. These are artifacts from segmentation and classification, directly resulting from poor signal to noise ratio. This shows the signal to noise ratio of this dataset is too low to extract meaning-full contact dynamics from this dataset.

Results

Observed landing preferences

In total we released 423 unfed mosquitoes (383 female, 40 male) in the flight arena. We captured 17 landing events inside the target area (16 in vertical orientation (7 successful), 1 in inverse horizontal orientation (0 successful)) (overview available in supplements: S6) Landing events were characterized as successful when wing-motion ceased while engaged with the parafilm skin phantom (figure 8) (Iikura et al., 2020). During these successful landings inside the target area, no successful feeding was observed. Successful feeding was characterized by engorging of the abdomen (Hol et al., 2020). Mosquitoes were observed to successfully land and feed outside the target area, in the FOV of only one camera. This corresponds to a mosquito located on the edge of the fluid cell, standing partially or completely on the mounting bracket. These events were not recorded, however.

Our results show a lower successful landing rate than we had expected. The reported success-rate is skewed because only landings in the target area were recorded, resulting in a significant under-estimation of overall landing success. However, despite this underestimation, overall activity in the target area was also significantly lower than expected. We hypothesized that mosquitoes, in order to feed, would actively try to engage the parafilm skin phantom with all their legs to search for host-cues through tarsal sensing. When a mosquito would land with all legs on the parafilm skin phantom, on most occasions at least one of the legs would be partially inside the target area. Our experiments clearly showed mosquitoes to have a preference to land and feed from the edge of the substrate, minimizing tarsal contact with the parafilm skin phantom.

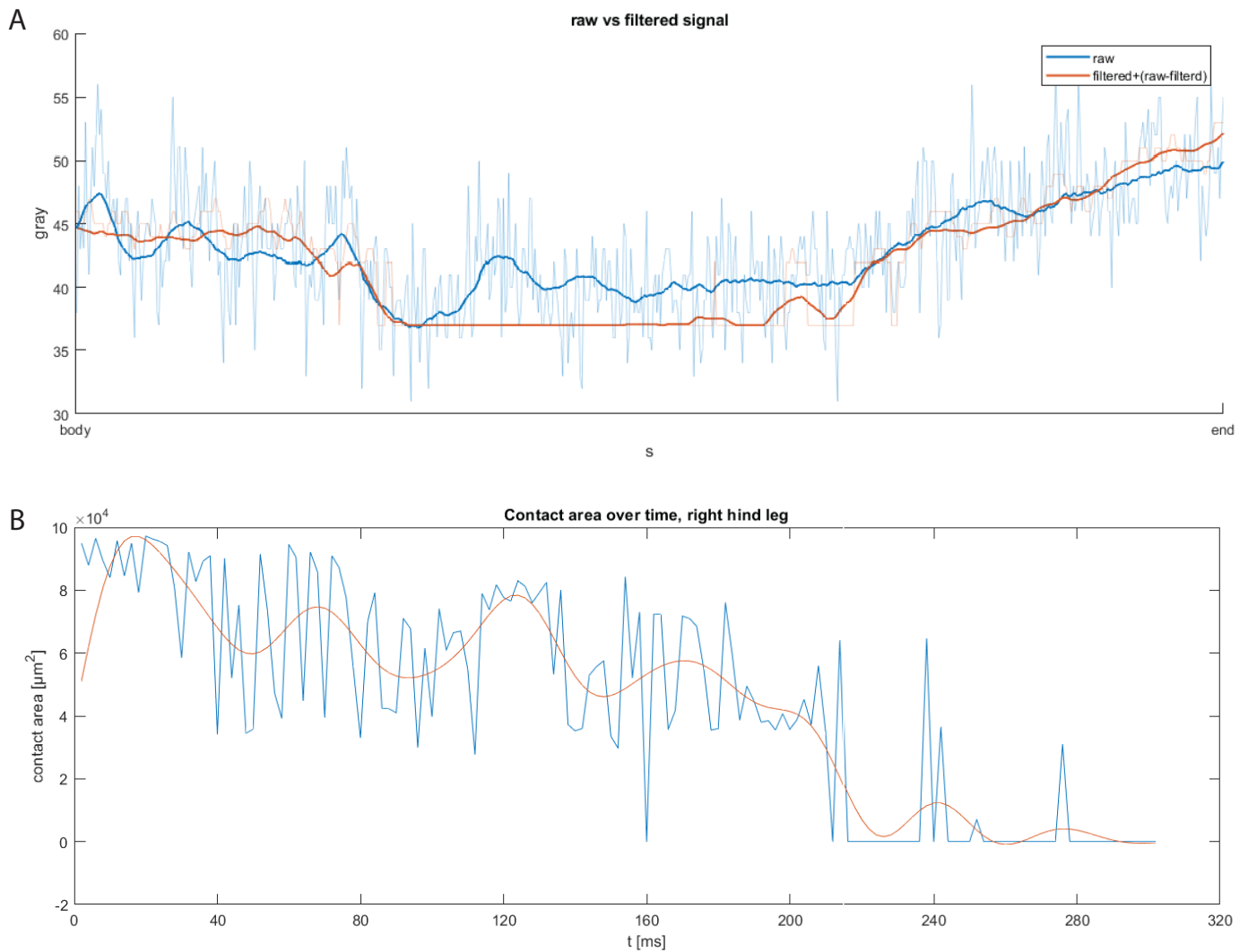


Figure 7: Example intensity profile and contact area over time extracted from FTIR signal. (A) Comparison between raw and filtered intensity profiles of a raw (blue) and processed image (red). Both signals are smoothed by averaging intensity inside a smoothing window sized by the width of the leg. Resulting averages are compared by transposing the filtered (red) signal. (B) The blue line shows extracted contact area signal over time for the right hind leg of the timeseries analysed in figure 6 (red: lowpass filtered). Plot including frames in supplements (S6). Video available in supplements (S7).

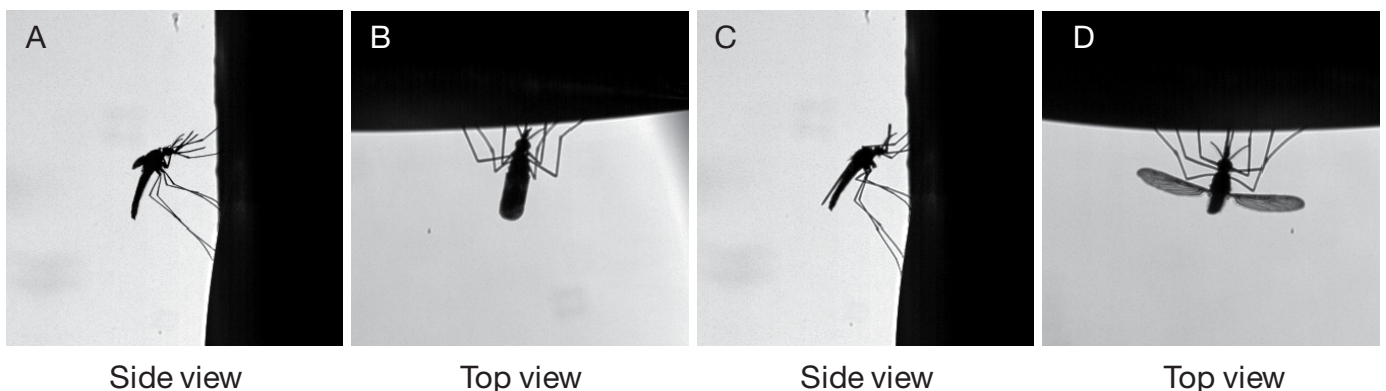


Figure 8: Mosquito attempting a landing on the parafilm membrane, showing both a complete and incomplete landing. (A,B) A mosquito probing the surface with its wings folded now fully supporting its weight through its legs, indicating a successful landing. (C,D) A mosquito probing the surface with its wings still beating, supporting part of its weight by lift generated from wingbeat kinematics, indicating an incomplete landing. Video available in online supplements (S8)

Besides the observed preference to attach at the edge of the target area, the observed difficulty feeding inside the target area was also unexpected. It is however not impossible for mosquitoes to feed through a parafilm membrane. The rearing stock of the *Anopheles coluzzii* mosquitoes used for the experiments is exclusively fed with Hemotek membrane feeding systems (Discovery Workshops, Accrington, UK) using parafilm as membrane. There, mosquitoes do not show any problem to engage with and feed through the parafilm skin phantom. Results shown on the BiteOscope (Hol et al., 2020) and by our group (Bougatsia et al., 2021) also show mosquitoes able to land on and feed through parafilm substrates. The primary differences between the Hemotek feeding setup, used for rearing, and our setup, are the use of real or fake blood and the presence of a worn thin nylon sock covering the feeding membrane to introduce odour. Transparent fake blood was used to allow for imaging, as was done in previous studies by Hol et al. (2020) and Bougatsia et al. (2021). In our setup, odour was applied directly to the membrane by rubbing the parafilm membrane against skin for 2 minutes, and a thin strip of worn nylon sock was placed nearby but not over the parafilm membrane to allow for imaging through the parafilm membrane.

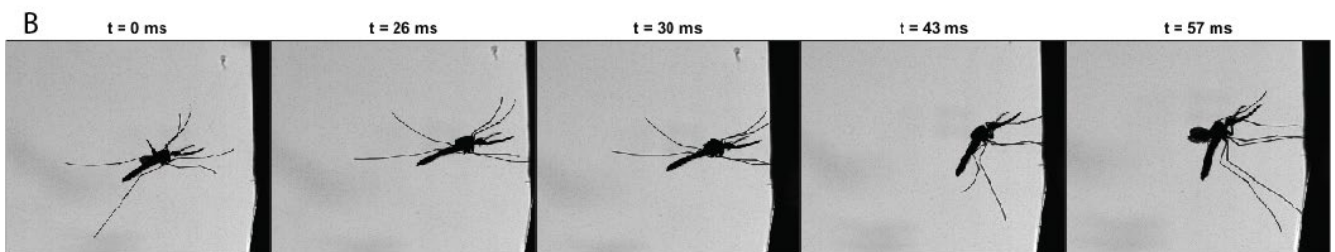
The effect of orientation on landing performance and attachment strategy

A typical landing starts with a highly controlled dipping approach flight in which the mosquito lowers its velocity prior to contact (figure 8a). The final approach phase before contact is similar in both vertical and inverse orientations (figure 8b,c). Initial surface contact is typically made using the mid-legs, with contact of the forelegs following within 10ms after initial contact by a striking motion. After engaging their mid- and forelegs, the mosquito starts an inward pulling motion with the legs in contact with the surface, dragging its distal tarsomeres across the surface. During this motion, the mosquito starts to rotate its centre of gravity towards the surface to bring its hind legs in contact. While rotating the mosquito needs to find a foothold on the surface to prevent over rotation causing its front legs to detach (figure 9a). In both orientations, mosquitoes seem to mostly use their tarsal tips when attempting a vertical or inverse landing. This could indicate the attempted engaging of claws. The primary difference between landings is that body rotation in the inverse position seems to be more demanding, suggesting the mosquito is required to rely significantly more on tarsal grip and less on wingbeat generated lift forces to maintain contact with the substrate.

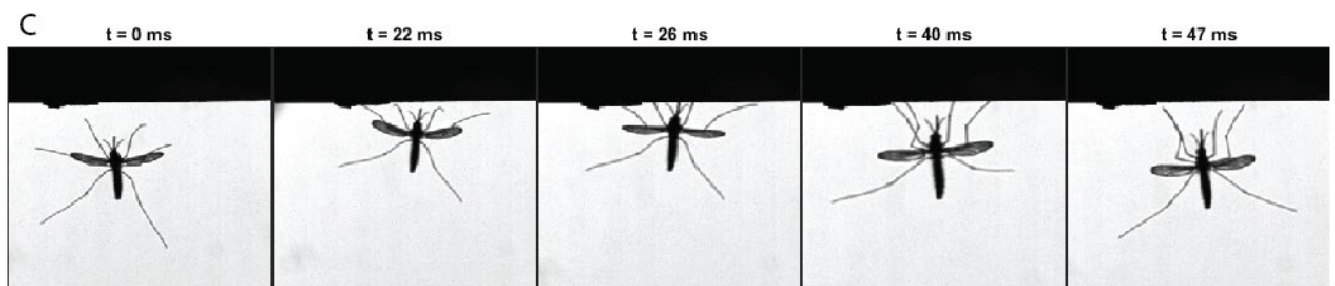
Inward dragging behaviour of the forelegs is also observed in partial attachment or after a completed landing on the parafilm substrate (figure 9b,c). Similar behaviour is observed on a horizontal parafilm substrate on the BiteOscope (Hol et al., 2020), showing this behaviour is not unique to the vertical orientation we show in our results. In partial attachment or after completed landing the duration and amplitude of the fore-leg strokes is increased compared to the bouncing flights.

Our results and observations suggest a higher success-rate in the vertical landing orientation compared to the inverse horizontal orientation. This indicates a preference for friction-mediated attachment over strictly adhesive attachment to the parafilm skin phantom. These results are in line with results from Bougatsia et al. (2021), which compared regular horizontal and vertical landings, also showing a preference for vertical landings. Even though no successful landings were recorded inside the target areas, mosquitoes were able to feed from the edge of the fluid cell, evident from the presence of engorged mosquitoes during clean-up after experiments in both experimental conditions.

Notably, despite the perceived difficulty to interact with the parafilm skin phantom, mosquitoes did not show any evidence of using their claws to pierce the skin phantom. Any piercing of the parafilm, either by claw or proboscis, would show up on the FTIR camera as a bright spot due to light trapped inside the fluid cell illuminating the protruding object directly (supplements: S9). Videos from the study on the BiteOscope show a similar lack of protrusion of claws into the substrate, but do show mosquitoes interlocking their legs while trying to feed suggesting their claws were engaged. The most likely explanation for this is that mosquitoes use their claws exclusively to catch surface asperities because they do not generate enough force to pierce skin or parafilm. The edge of the fluid cell is outside of the target area of the PCO camera making it impossible to verify claw engagement.



Landing attempt in vertical condition



Landing attempt in horizontal condition

Figure 9: Action sequence of a typical dipping approach flight and image reels showing a mosquito attempting to land in both experimental conditions, showing the similarity in landing approach. (A) A typical dipping approach flight trajectory showing a highly controlled approach trajectory to minimize impact velocity. (B). Mosquito attempting a landing on the vertical substrate. After first contact with its midlegs, the forelegs are planted in under 5 ms. Center of mass is rotated to engage the hindlegs while the other legs are dragged across the surface in the next 15 ms. Sufficient grip with the forelegs must prevent overrotation while the mosquitoes weight is still supported through wingbeat kinematics (at $t=57\text{ms}$) (C). Mosquito (back towards camera) attempting a landing on the inverted substrate. The landing strategy is remarkably similar to the previous approach, with initial contact established with the mid legs followed by planting of the forelegs within 5 ms. In the next 15 ms the mosquito drags the fore- and mid-legs across the surface to find enough grip to rotate its center of gravity towards the substrate and engage its hindlegs. In contrary to the vertical landing in (A) the mosquito is not able to support its weight through wingbeat kinematics. Videos available in online supplements (S10, S11).

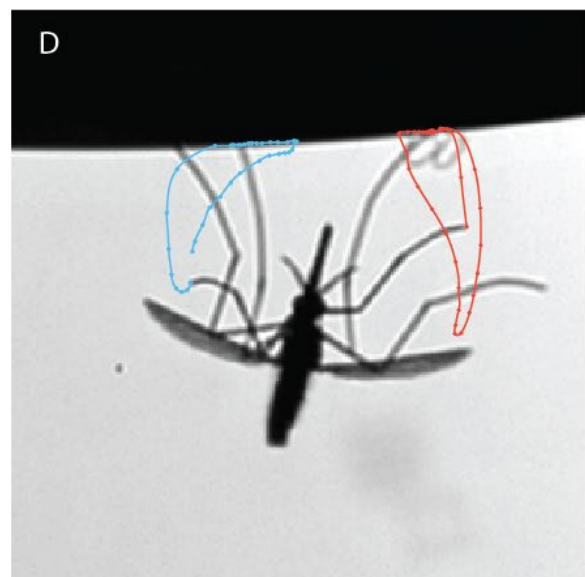
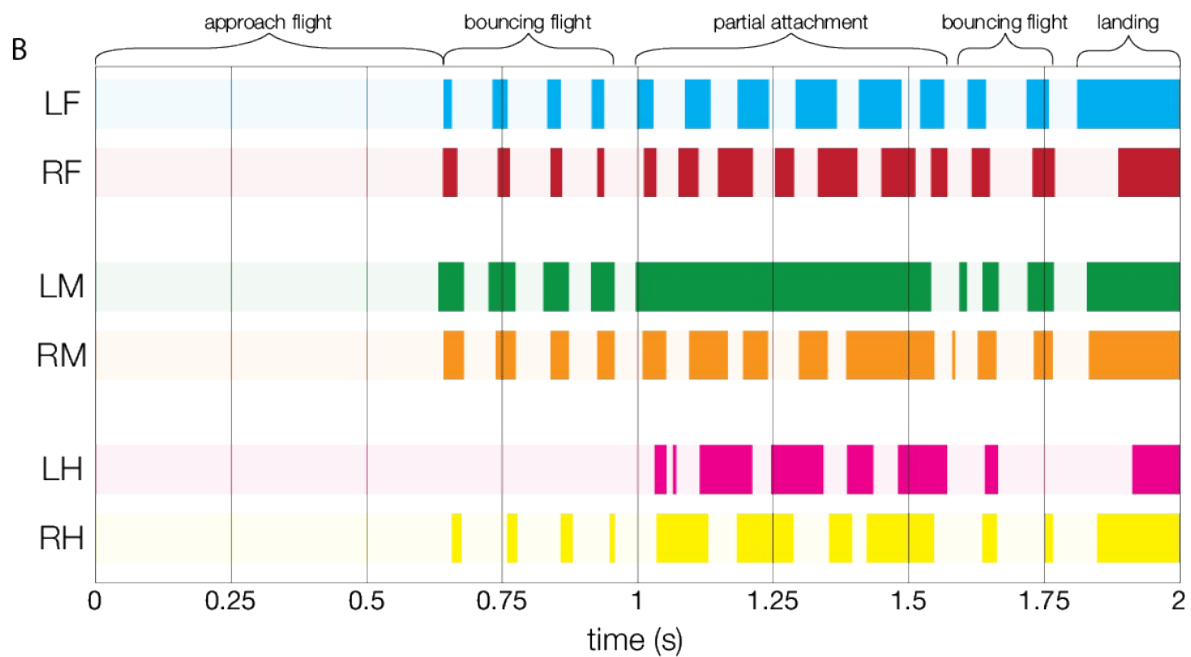
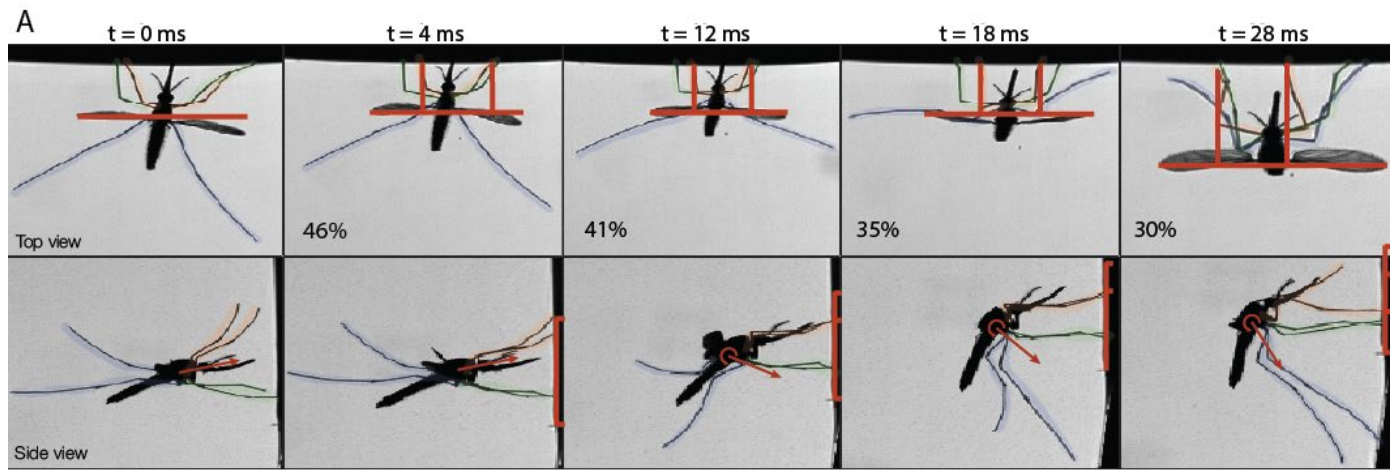


Figure 10: Typical mosquito approach flight and landing. (A) Time series of mosquito in bouncing flight showing dragging motion of front legs after initial contact with mid-legs (orange = forelegs, green is mid-legs, blue = hindlegs) Top: percentages show lateral foreleg position as fraction of wingspan. Bottom: red line shows front leg position with respect to visual artifact. Arrows denotes motion direction of body centre. (B) Ethogram showing leg contact duration. Bouncing flight landing attempts always start with one of the mid-legs and are followed by short dragging motions of the forelegs. During partial contact dragging attempts of the forelegs are amplified in amplitude and duration. (C,D) Traces of the foreleg dragging during partial attachment (duration 92ms) showing excessive dragging of the tarsal tips over the parafilm substrate (blue = left foreleg (LF), red = right foreleg (RF)) Video available in supplements: S10.

Discussion

Substrate probing and foreleg dragging behaviour

Our results show that mosquitoes prefer to be minimally engaged with the parafilm skin phantom while feeding. This observation contrasts the hypothesis that tarsal probing is used for host identification based on earlier studies using parafilm as landing substrate. Argued from the tarsal contact sensing hypothesis our results are unexpected and seemingly conflicting: if the substrate has been deemed inappropriate for feeding by a tarsal contact sensing modality, why not abort feeding altogether? A more fitting narrative for this probing behaviour becomes evident when we interpret these movements systematically: tarsal probing is primarily a strategy to improve grip.

Insects are believed to control attachment forces on four different levels: through body kinematics, by moving their centre of gravity and altering their gaits; through leg movements, influencing the surface contact angles and force directions; through (pre)tarsal movements, moving the claws or adhesive pad to improve attachment; and through active modifications of the adhesive system, using adhesive secretions or altering material properties of their adhesive pads (Federle and Endlein, 2004). During an attempted landing, we can clearly observe the first two levels of attachment control. The first contact is typically made with the tarsal tip where the mosquito's adhesive pad is located. Quickly thereafter mosquitoes made contact with both fore- and mid-legs, dragging their legs inward. This dragging motion increases contact area and positions the claws to be aligned with any surface asperities. During this motion, the mosquito shifts its centre of gravity forward and rotates its body to align with the substrate. When the mosquitoes were not able to generate sufficient grip with their legs, the body would over rotate, causing the landing attempt to fail (figure 9).

Parafilm is a less than ideal surface for mosquitoes to adhere to. A minimal surface asperity height is required to engage claws, shown to be in the order of 10 μm for the dock beetle *Gastrophysa viridula* (Bullock & Federle, 2011), which is around 10% of their claw size. While dock beetle claws are significantly larger than mosquito claws, the surface roughness of the parafilm membrane is believed to be much smaller (<10% of mosquito claw size) and is considered smooth. In these conditions it is virtually impossible for mosquitoes to use their claws to catch asperities, and attachment ability is primarily dependent on the adhesive system (Song et al., 2016). The adhesive pad surface is extremely small compared to the total leg surface covered in micro scales.

Because of this, contact area and Van der Waals forces increase greatly with increased surface roughness. Pashazanusi et al. (2017) have shown the mosquito adhesive system to be dominated by Van der Waals forces, further supported by capillary forces when the target surface is hydrophilic and conditions are humid.

This explains the lack of successful feeding events inside the target area and the observed tarsal dragging behaviour. Continued substrate engagement suggests not a lack of trying to feed, but an inability of the mosquitoes to puncture the membrane with their proboscis while exclusively engaged with the membrane. Successful feeding taking place at the edge of the fluid cell can be explained through the same narrative. At the edge of the fluid cell, the mosquito can engage with the 3D printed PLA+ mounting bracket. The bracket has an estimated surface roughness RMS in the order of several 10's of μm 's (Alsoufi and Elsayed, 2017; Alsoufi and Elsayed, 2018). This roughness is sufficient for mosquitoes to use friction-mediated adhesion force generated through van der Waals interactions between the surface and the micro/nano setae structures covering their legs (Pashazanusi et al., 2017) and for their claws to engage (Bullock & Federle, 2011). This suggests that not the presence of surface cues, but sufficient grip seems to be the deciding factor for a successful feeding event. Observed tarsal probing behaviour seems to be an adhesion related artifact from parafilm as a substrate.

Further evidence hinting towards the hypothesis of foreleg dragging to increase grip rather than to sense surface characteristics comes from observations of climbing beetles. Beetles with adhesive pads soiled with microbeads show similar dragging behaviour of their forelegs while climbing (Amador et al., 2017), indicating this dragging behaviour is the result of failed attachment.

Foreleg dragging behaviour during host-seeking is also unexpected considering the increased risk of detection it introduces. The fitness of mosquitoes as a species seems highly related to their stealthy nature. Mosquitoes are known to employ strategies to mitigate landing and take-off forces through their long legs and wingbeat kinematics (Muijres et al., 2017; Smith et al., 2018; Smith et al., 2020). Von Frey detection threshold of low threshold mechanoreceptors

(LTMRs) is estimated to be around 70 μ N (Johansen et al., 1980; Li et al., 2011). Von Frey thresholds are measured by placing a thin Von Frey hairs perpendicular on skin (Gebhart & Schmidt, 2013) and are a good estimation of landing force detectability (Smith et al., 2020). The force detection threshold of the Root hair plexus is expected even lower due to force amplification through the human hair acting as a moment arm when loaded perpendicular. Mosquito leg dragging motion therefore increases risk of detection significantly.

Preferred biting locations of mosquitoes on man seem to coincide regions with little to no hair such as the face and ankles (De Jong & Knols, 1995; Dekker et al., 1998). The preference for biting locations has previously been mostly attributed to specific combinations of skin temperature, eccrine sweat gland density and convection currents. Hair as a confounding factor for biting success has been largely unconsidered. To the authors knowing, there have not been any studies investigating the presence of hair and blood-feeding success, and women, being naturally less hairy in the facial region, have been largely excluded from studies investigating mosquito behaviour in general due to their scent patterns varying with hormonal cycles. Because of this it is impossible to say if the observed preference for hairless biting location, and local bite distribution, is simply the result of skin availability or increased detection due to mosquitoes touching hairs.

Parafilm as substrate for adhesion studies

Parafilm as a substrate for our experiments was inspired by its status as feeding membrane of choice in the rearing of mosquitoes, used to cover Hemotek feeding systems, and its use in previous studies through-substrate imaging studies with the BiteOscope (Hol et al., 2020). Despite appearing to introduce behavioural artifacts when studying free mosquitoes it is also difficult to gauge absolute adhesive performance on parafilm as a substrate. Parafilm is difficult to control and hard to classify. The surface properties of parafilm are largely unknown, only contact angle and surface energy have been reported in a study by Shi et al. (2013), showing parafilm to have a surface energy lower than Teflon, used for non-stick coatings, and to be extremely hydrophobic (table 1). Hydrophobicity makes parafilm suitable to seal the fluid cell and Hemotek feeders, but is likely to reduce fluid mitigated adhesion. Moreover, surface tension and membrane thickness vary between samples due to stretching the membrane by hand, introducing further uncertainty between measurements.

Table 1. Surface properties of parafilm and similar materials compared to glass

Material	Contact angle (°)	Surface energy (mJ/m ²)	Reference
Parafilm	109.6 \pm 8.8	9.02 \pm 3.16	Shi et al., 2013
Glass	55.7	83.4	Rhee, 1977
PTFE (Teflon) polytetrafluorethen	106.9	18.5	Kinloch, 1987, Włoch et al., 2018
PDMS (polydimethyloxane)	110	19 - 21	Vudayagiri et al., 2013

The influence of contact angle and surface energy on bio-adhesion is still largely under debate (Feát et al., 2019). While capillary adhesiveness is likely limited for parafilm compared to glass, it is unclear to what extent this influences adhesive performance. Insect pad secretion, as an emulsion, is shown to an effective wetting agent for hydrophobic and hydrophilic substrates alike, hinting contact angle is not the limiting factor in adhesive performance (Attipoe et al., 2020). One study by Izadi et al. (2014) investigated gecko adhesion to Teflon and PDMS. They found that geckos relied mostly on electrostatic adhesion forces to adhere to these substrates. Both substrates are comparable to parafilm in terms of hydrophobicity, surface energy, and smoothness (table 1). In terms of expected electrostatic forces, parafilm is expected to perform better than PDMS with parafilm, Teflon and PDMS having a dielectric constant of 2.2 (Zulkepli et al., 2018), 2.65 and 1.93 (Izadi et al., 2014). This indicates parafilm might be a suitable substrate for studies investigating electrostatic adhesion. Compared to insects, gecko adhesive pads are considered to be dry, allowing for the build-up of electrostatic charge on their setae. Mosquitoes, and other insects, are however not likely to be able to rely on electrostatic adhesion due to charge dissipation through insect pad secretion.

Limitations of this study

Both in inverse landing and vertical landing, time between first contact and contact with all fore-legs is between 5 to 10 ms. To measure fracture propagation within this time window, a temporal resolution of 500 FPS, corresponding to 2ms/frame, is on the low end. This provides at most 2 frames between initial contact and full contact with all legs. This is insufficient to use a fracture mechanics approach to assess contact performance for mosquitoes, as proposed by Labonte and Federle (2015). During our experiments we have tried to image the FTIR contact at 1000 frames s^{-1} , at the expense of exposure time and consequently SNR (supplements: S12) At this framerate, SNR was not sufficient to distinguish contact. A spatial resolution of 4MPx at a FOV of 1cm² is high enough to see the legs, but is on the low end to image the adhesive pad even at higher signal to noise ratio.

Besides introducing behavioural artifacts, using a parafilm membrane as cover for the fluid cell also introduces imaging complications. When stretched, parafilm can deform under the weight of the liquid contained in the fluid cell. Because of this, the surface area, surface angle, and distance from the focal point, are hard to control. Membrane deformation also made it difficult to assess contact from the Photron camera feeds, especially in slow movements. As a medium for FTIR imaging, the parafilm membrane proved too thin to serve as medium to trap the light from the LED light source. To overcome this challenge, light was trapped inside the fluid cell and the parafilm substrate was considered thin, having a neglectable thickness. Due to the height of the fluid cell and the distance of the LED-strip to the fluid cell, it was difficult to avoid light traveling through the cell at high enough angles to escape through the parafilm. Moreover, parafilm is slightly opaque. While this is useful to focus the camera, light refracting inside the membrane also escapes the fluid cell. These combined effects result in illumination of objects directly behind, but not in contact with the membrane. This reduces the signal to noise ratio significantly, making it more difficult to separate contact from near contact.

Due to COVID-19 related delays in the production of setup components and lab opening hours restrictions, the amount of time available for measuring was severely limited, and various concessions had to be made to the setup. The lack of camera anchors and rail spacers during the measurement made it impossible to guard the imaging setup from vibrations. Combined with the short measurement windows and the already highly uncontrollable nature of the parafilm membrane it was unrealistic to spatially calibrate the cameras before each set of measurements. Combined with the already low amount of successful landings previously discussed this had implications for the size of the dataset, and its useability of for the extraction of absolute adhesive performance metrics. Moreover, the short window in which the setup was fully operational and measurements could be done left little to no time for pilots with mosquitoes. While it was sufficient to address software and hardware failures, the level of standardization in CO₂ and odour host cue introduction leaves considerable room for improvement.

Outlooks

This study has both displayed the difficulties in estimating adhesive performance while preserving natural behaviour, as the use for such an approach to advance the debate on mosquito behaviour and the need for this approach to close the current knowledge gap surrounding blood feeding. In this pilot study we have attempted to push FTIR imaging above and beyond. Our preliminary results were not sufficient to do a quantitative assessment of adhesive performance, as was the original outset of the study. However, from our results it also became evident that we did not yet succeed to draw out the setups full potential. Considering this, there is a place for a follow up study in which some of our key lessons are addressed.

In the current setup low signal to noise ratio can be attributed to several factors. Already discussed is the need for a more transparent membrane, reducing the bleeding of light due to refraction inside the membrane and high angle light penetrating the membrane and illuminating the object before contact. Ideally light is trapped directly inside the membrane, though this remains a technical challenge and turned out to be impossible using an LED-strip as light source integrated into the landing platform while conserving host-cues.

When strictly looking at general attachment performance, parafilm membranes have turned out to be problematic as a target substrate. However, we also observed that mosquitoes would still attempt to feed with their legs minimally engaged with the substrate. Considering this fact, in a follow up study there is no need to integrate both host cues and FTIR into the fluid cell. Mosquitoes can land on a stiff transparent landing platform (e.g. glass or acrylic) with an integrated FTIR light source, and feed from the edge of the landing platform. Part of the landing platform can also be

covered with DEET or cleaned with ethanol, creating an ideal spot for mosquitoes to land while not being restricted in the size of the platform for FTIR integration while still being able to use a small FOV. Being unrestricted in landing platform size allows the light source to be placed further from the target area. This will reduce the amount of high angle light escaping at the target area further increasing SNR. Illuminating a stiff substrate, rather than the liquid cell, also removes any restriction on LED strip power levels. This way both signal increases and background noise decreases, making it possible to image at higher framerates.

Choosing to use a membrane as the landing platform introduces some challenges. Firstly, the choice of membrane is difficult. Selecting a membrane that more closely resembles skin and is easier to adhere to than parafilm is paramount to success. PDMS is not likely to be a suitable alternative, seeing it is remarkably similar to parafilm in terms of surface energy and hydrophobicity. Further research into thin and transparent skin phantoms is necessary. Next to membrane choice, various technical challenges need to be addressed. To reduce membrane deformation due to fluid load, it is desirable to either use the membrane in a horizontal position, having mosquitoes land from the top down, or minimizing the cells height to reduce fluid volume contained. Either way, in both orientations the use of a LED strip as a light source is not ideal due to the difficulties trapping the light in a thin object. Further experiments using a laser generate light sheet are needed to see if this increases SNR compared to LED illumination.

To obtain more conclusive evidence if observed tarsal probing during bouncing flight and tarsal dragging during partial attachment is an indicator of failed attachment, it is probably unnecessary to include a feeding cell. Considering tarsal contact sensing seems not to be as important as previously believed, we hypothesize mosquitoes will engage with any substrate provided sufficient host cues (CO₂, temperature and odour) are present. A simple experiment observing landing performance on partially roughened glass or acrylic substrates without a feeding cell would be sufficient to assess free mosquito adhesive performance. We expect to see a significant increase in the frequency of substrate bounces on the smooth part of the substrate compared to the roughened part of the substrate. Showing bouncing flight to be an indicator of failed attachment would provide us with an easily observable and countable metric to assess adhesive performance. This could allow us to design simple high throughput studies in which we control key parameters of the substrate, such as hydrophobicity, surface energy, roughness and surface chemistry, and investigate adhesive performance of free flying mosquitoes by assessing bounce frequency. This could prove to be instrumental in closing the knowledge gap existing between a mosquitoes touchdown and take-off.

Acknowledgements

We thank: Remco Pieters for his assistance in the development of the experimental setup; Radix Klima mosquito rearing group for the rearing of the mosquitoes.

Competing interests

The authors declare no competing or financial interests

Author contributions

Conceptualization: L.M.v.d.B., G.J.A., F.T.M.; Study design: L.M.v.d.B., G.J.A., F.T.M., J.K.L., J.S.; Writing – original draft: L.M.v.d.B.; Supervision: G.J.A., D.D., F.M.; Experiments: L.M.v.d.B., Data analysis: L.M.v.d.B.

Funding

The high-speed cameras were co-financed by Shared Research Facilities of Wageningen University & Research.

References

- Alsoufi, M. S., & Elsayed, A. E. (2017). How Surface Roughness Performance of Printed Parts Manufactured by Desktop FDM 3D Printer with PLA+ is Influenced by Measuring Direction. *American Journal of Mechanical Engineering*, 5(5), 211–222. <https://doi.org/10.12691/ajme-5-5-4>
- Alsoufi, M. S., & Elsayed, A. E. (2018). Surface Roughness Quality and Dimensional Accuracy—A Comprehensive Analysis of 100% Infill Printed Parts Fabricated by a Personal/Desktop Cost-Effective FDM 3D Printer. *Materials Sciences and Applications*, 09(01), 11. <https://doi.org/10.4236/msa.2018.91002>
- Amador, G. J., Endlein, T., & Sitti, M. (2017). Soiled adhesive pads shear clean by slipping: A robust self-cleaning mechanism in climbing beetles. *Journal of The Royal Society Interface*, 14(131), 20170134. <https://doi.org/10.1098/rsif.2017.0134>
- Attipoe, A.E.L., Kaimaki, D-M., Labonte, D.(2020) Surface Tension of the Insect Pad Secretion. (n.d.). *SICB*. Retrieved 10 November 2021, from <https://sicb.org/abstracts/surface-tension-of-the-insect-pad-secretion/>
- Becker, N., Petrić, D., Zgomba, M., Boase, C., Madon, M., Dahl, C., & Kaiser, A. (2010). Medical Importance of Mosquitoes. In N. Becker, D. Petric, M. Zgomba, C. Boase, M. Madon, C. Dahl, & A. Kaiser (Eds.), *Mosquitoes and Their Control* (pp. 25–42). Springer. https://doi.org/10.1007/978-3-540-92874-4_3
- Betts, R. P., Duckworth, T., Austin, I. G., Crocker, S. P., & Moore, S. (1980). Critical light reflection at a plastic/glass interface and its application to foot pressure measurements. *Journal of Medical Engineering & Technology*, 4(3), 136–142. <https://doi.org/10.3109/03091908009161107>
- Bhushan, B. (2018). Insects locomotion, piercing, sucking and stinging mechanisms. *Microsystem Technologies*, 24(12), 4703–4728. <https://doi.org/10.1007/s00542-018-4175-9>
- van den Boogaart, L.M., Amador, G.J., Dodou, D., Langowski, J.K.A., Muijres, F.T. (2021). Studying Stickiness: Methods, trade-offs, and limitations in measuring reversible biological adhesion. *Available in supplement 1*.
- Bougatsia, A. (2021). Landing approach of the mosquito *Anopheles coluzzii* under the presence of host cues. *MSc thesis*.
- van Breugel, F., Riffell, J., Fairhall, A., & Dickinson, M. H. (2015). Mosquitoes Use Vision to Associate Odor Plumes with Thermal Targets. *Current Biology*, 25(16), 2123–2129. <https://doi.org/10.1016/j.cub.2015.06.046>
- Bullock, J. M. R., & Federle, W. (2011). The effect of surface roughness on claw and adhesive hair performance in the dock beetle *Gastrophysa viridula*: Effect of surface roughness on attachment. *Insect Science*, 18(3), 298–304. <https://doi.org/10.1111/j.1744-7917.2010.01369.x>
- Clements, A. N. (1963). *The Physiology of Mosquitoes* (1st ed., Vol. 17). Pergamon. <https://www.elsevier.com/books/the-physiology-of-mosquitoes/clements/978-1-4831-9773-9>
- Coetzee, M., Hunt, R. H., Wilkerson, R., Torre, A. D., Coulibaly, M. B., & Besansky, N. J. (2013). *Anopheles coluzzii* and *Anopheles amharicus*, new members of the *Anopheles gambiae* complex. *Zootaxa*, 3619(3), 246–274. <https://doi.org/10.11646/zootaxa.3619.3.2>
- Cribellier, A., Spitzen, J., Fairbairn, H., van de Geer, C., van Leeuwen, J. L., & Muijres, F. T. (2020). Lure, retain, and catch malaria mosquitoes. How heat and humidity improve odour-baited trap performance. *Malaria Journal*, 19(1), 357. <https://doi.org/10.1186/s12936-020-03403-5>
- Dekker, T., Takken, W., Knols, B. G. J., Bouman, E., van de Laak, S., de Bever, A., & Huisman, P. W. T. (1998). Selection of biting sites on a human host by *Anopheles gambiae* s.s., *An. Arabiensis* and *An. Quadriannulatus*. *Entomologia Experimentalis et Applicata*, 87(3), 295–300. <https://doi.org/10.1046/j.1570-7458.1998.00334.x>
- Dekker, T., & Cardé, R. T. (2011). Moment-to-moment flight manoeuvres of the female yellow fever mosquito (*Aedes aegypti* L.) in response to plumes of carbon dioxide and human skin odour. *Journal of Experimental Biology*, 214(20), 3480–3494. <https://doi.org/10.1242/jeb.055186>
- Dennis, E. J., Goldman, O. V., & Voshall, L. B. (2019). *Aedes aegypti* Mosquitoes Use Their Legs to Sense DEET on Contact. *Current Biology*, 29(9), 1551-1556.e5. <https://doi.org/10.1016/j.cub.2019.04.004>
- Dickerson, A. K., Olvera, A., & Luc, Y. (2018). Void Entry by *Aedes aegypti* (Diptera: Culicidae) Mosquitoes Is Lower Than Would Be Expected by a Randomized Search. *Journal of Insect Science*, 18(6), Article 6. <https://doi.org/10.1093/jisesa/iey115>
- Endlein, T., Ji, A., Samuel, D., Yao, N., Wang, Z., Barnes, W. J. P., Federle, W., Kappl, M., & Dai, Z. (2013b). Sticking like sticky tape: Tree frogs use friction forces to enhance attachment on overhanging surfaces. *Journal of The Royal Society Interface*, 10(80), 20120838. <https://doi.org/10.1098/rsif.2012.0838>
- Féat, A., Federle, W., Kamperman, M., & van der Gucht, J. (2019). Coatings preventing insect adhesion: An overview. *Progress in Organic Coatings*, 134, 349–359. <https://doi.org/10.1016/j.porgcoat.2019.05.013>
- Federle, W., & Endlein, T. (2004). Locomotion and adhesion: Dynamic control of adhesive surface contact in ants. *Arthropod Structure & Development*, 33(1), 67–75. <https://doi.org/10.1016/j.asd.2003.11.001>
- Gebhart, G. F., & Schmidt, R. F. (Eds.). (2013). Von Frey Hair. In *Encyclopedia of Pain* (pp. 4243–4243). Springer. https://doi.org/10.1007/978-3-642-28753-4_202454
- Gorb, S. (Ed.). (2001). Attachment pads. In *Attachment Devices of Insect Cuticle* (pp. 135–175). Springer Netherlands. https://doi.org/10.1007/0-306-47515-4_9

- Hawkes, F., & Gibson, G. (2016). Seeing is believing: The nocturnal malarial mosquito *Anopheles coluzzii* responds to visual host-cues when odour indicates a host is nearby. *Parasites & Vectors*, *9*(1), 320. <https://doi.org/10.1186/s13071-016-1609-z>
- Hill, I. D. C., Dong, B., Barnes, W. J. P., Ji, A., & Endlein, T. (2018). The biomechanics of tree frogs climbing curved surfaces: A gripping problem. *Journal of Experimental Biology*, *221*(5). <https://doi.org/10.1242/jeb.168179>
- Hol, F. J., Lambrechts, L., & Prakash, M. (2020). BiteOscope, an open platform to study mosquito biting behavior. *eLife*, *9*, e56829. <https://doi.org/10.7554/eLife.56829>
- Ikura, H., Takizawa, H., Ozawa, S., Nakagawa, T., Matsui, Y., & Nambu, H. (2020). Mosquito repellence induced by tarsal contact with hydrophobic liquids. *Scientific Reports*, *10*(1), 14480. <https://doi.org/10.1038/s41598-020-71406-y>
- Izadi, H., Stewart, K. M. E., & Penlidis, A. (2014). Role of contact electrification and electrostatic interactions in gecko adhesion. *Journal of The Royal Society Interface*, *11*(98), 20140371. <https://doi.org/10.1098/rsif.2014.0371>
- Johansson, R. S., Vallbo, Å. B., & Westling, G. (1980). Thresholds of mechanosensitive afferents in the human hand as measured with von Frey hairs. *Brain Research*, *184*(2), 343–351. [https://doi.org/10.1016/0006-8993\(80\)90803-3](https://doi.org/10.1016/0006-8993(80)90803-3)
- De Jong, R., & Knols, B. G. J. (1995). Selection of biting sites on man by two malaria mosquito species. *Experientia*, *51*(1), 80–84. <https://doi.org/10.1007/BF01964925>
- Jové, V., Gong, Z., Hol, F. J. H., Zhao, Z., Sorrells, T. R., Carroll, T. S., Prakash, M., McBride, C. S., & Vosshall, L. B. (2020). Sensory Discrimination of Blood and Floral Nectar by *Aedes aegypti* Mosquitoes. *Neuron*, *108*(6), 1163–1180.e12. <https://doi.org/10.1016/j.neuron.2020.09.019>
- Labonte, D., & Federle, W. (2015a). Rate-dependence of ‘wet’ biological adhesives and the function of the pad secretion in insects. *Soft Matter*, *11*(44), 8661–8673. <https://doi.org/10.1039/C5SM01496D>
- Langowski, J. K. A., Rummenie, A., Pieters, R. P. M., Kovalev, A., Gorb, S. N., & Leeuwen, J. L. van. (2019). Estimating the maximum attachment performance of tree frogs on rough substrates. *Bioinspiration & Biomimetics*, *14*(2), 025001. <https://doi.org/10.1088/1748-3190/aafc37>
- Li, Y., Krahn, J., & Menon, C. (2016). Bioinspired dry adhesive materials and their application in robotics: A review. *Journal of Bionic Engineering*, *13*(2), 181–199. [https://doi.org/10.1016/S1672-6529\(16\)60293-7](https://doi.org/10.1016/S1672-6529(16)60293-7)
- Te Lindert, B. H. W., & Van Someren, E. J. W. (2018). Chapter 21—Skin temperature, sleep, and vigilance. In A. A. Romanovsky (Ed.), *Handbook of Clinical Neurology* (Vol. 156, pp. 353–365). Elsevier. <https://doi.org/10.1016/B978-0-444-63912-7.00021-7>
- McMeniman, C. J., Corfas, R. A., Matthews, B. J., Ritchie, S. A., & Vosshall, L. B. (2014). Multimodal Integration of Carbon Dioxide and Other Sensory Cues Drives Mosquito Attraction to Humans. *Cell*, *156*(5), 1060–1071. <https://doi.org/10.1016/j.cell.2013.12.044>
- Muijres, F. T., Chang, S. W., Veen, W. G. van, Spitzen, J., Biemans, B. T., Koehl, M. a. R., & Dudley, R. (2017). Escaping blood-fed malaria mosquitoes minimize tactile detection without compromising on take-off speed. *Journal of Experimental Biology*, *220*(20), 3751–3762. <https://doi.org/10.1242/jeb.163402>
- Paaijmans, K. P., & Thomas, M. B. (2011). The influence of mosquito resting behaviour and associated microclimate for malaria risk. *Malaria Journal*, *10*(1), 183. <https://doi.org/10.1186/1475-2875-10-183>
- Pashazanusi, L., Lwoya, B., Oak, S., Khosla, T., Albert, J. N. L., Tian, Y., Bansal, G., Kumar, N., & Pesika, N. S. (2017). Enhanced Adhesion of Mosquitoes to Rough Surfaces. *ACS Applied Materials & Interfaces*, *9*(28), 24373–24380. <https://doi.org/10.1021/acsami.7b06659>
- Rhee, S. K. (1977). Surface energies of silicate glasses calculated from their wettability data. *Journal of Materials Science*, *12*(4), 823–824. <https://doi.org/10.1007/BF00548176>
- Shi, X., Li, L., Ostrovidov, S., Shu, Y., Khademhosseini, A., & Wu, H. (2014). Stretchable and Micropatterned Membrane for Osteogenic Differentiation of Stem Cells. *ACS Applied Materials & Interfaces*, *6*(15), 11915–11923. <https://doi.org/10.1021/am5029236>
- Smith, N. M., Clayton, G. V., Khan, H. A., & Dickerson, A. K. (2018). Mosquitoes modulate leg dynamics at takeoff to accommodate surface roughness. *Bioinspiration & Biomimetics*, *14*(1), 016007. <https://doi.org/10.1088/1748-3190/aaed87>
- Song, Y., Dai, Z., Wang, Z., Ji, A., & Gorb, S. N. (2016). The synergy between the insect-inspired claws and adhesive pads increases the attachment ability on various rough surfaces. *Scientific Reports*, *6*. <https://doi.org/10.1038/srep26219>
- Sparks, J. T., Vinyard, B. T., & Dickens, J. C. (2013). Gustatory receptor expression in the labella and tarsi of *Aedes aegypti*. *Insect Biochemistry and Molecular Biology*, *43*(12), 1161–1171. <https://doi.org/10.1016/j.ibmb.2013.10.005>
- Spitzen, J., Spoor, C. W., Grieco, F., Braak, C. ter, Beeuwkes, J., Brugge, S. P. van, Kranenbarg, S., Noldus, L. P. J. J., Leeuwen, J. L. van, & Takken, W. (2013). A 3D Analysis of Flight Behavior of *Anopheles gambiae* sensu stricto Malaria Mosquitoes in Response to Human Odor and Heat. *PLOS ONE*, *8*(5), e62995. <https://doi.org/10.1371/journal.pone.0062995>
- Stanczyk, N. M., Mescher, M. C., & De Moraes, C. M. (2017). Effects of malaria infection on mosquito olfaction and behavior: Extrapolating data to the field. *Current Opinion in Insect Science*, *20*, 7–12. <https://doi.org/10.1016/j.cois.2017.02.002>
- Veen, W. G. van, Leeuwen, J. L. van, & Muijres, F. T. (2020). Malaria mosquitoes use leg push-off forces to control body pitch during take-off. *Journal of Experimental Zoology Part A: Ecological and Integrative Physiology*, *333*(1), 38–49. <https://doi.org/10.1002/jez.2308>
- Vudayagiri, S., Junker, M. D., & Skov, A. L. (2013). Factors affecting the surface and release properties of thin polydimethylsiloxane films. *Polymer Journal*, *45*(8), 871–878. <https://doi.org/10.1038/pj.2012.227>

Włoch, J., Terzyk, A. P., Wiśniewski, M., & Kowalczyk, P. (2018). Nanoscale Water Contact Angle on Polytetrafluoroethylene Surfaces Characterized by Molecular Dynamics-Atomic Force Microscopy Imaging. *Langmuir: The ACS Journal of Surfaces and Colloids*, 34(15), 4526–4534. <https://doi.org/10.1021/acs.langmuir.8b00257>

Zulkepli, S. N. I. S., Hamid, N. H., & Shukla, V. (2018). Droplet Velocity Measurement Based on Dielectric Layer Thickness Variation Using Digital Microfluidic Devices. *Biosensors*, 8(2), 45. <https://doi.org/10.3390/bios8020045>

Supplements:

S1. <i>Van den Boogaart et al., 2021, Studying Stickiness: Methods, trade-offs and limitations in measuring reversible biological adhesion</i>	23
S2. Setup parts list	39
S3. Code manual	40
S4. Online code availability	48
S5. Online video PCO analysed data set	49
S6. Table of recordings	49
S7. Figure 7b extended	50
S8. Online video: 2021-03-31 Run6	51
S9. Parafilm puncture	51
S10. Online video: 2021-04-01 Run2	51
S11. Online video: 2021-04-02 Run1	51
S12. 1000FPS PCO data	52
S13. Digital lab journal	53
S14. Online videos	56

S1. Studying stickiness: Methods, trade-offs, and limitations in measuring reversible biological adhesion.

Studying stickiness

First author:

Luc M. van den Boogaart

Other authors (alphabetical on last name):

Guillermo J. Amador, Dimitra Dodou, Julian K. A. Langowski, Florian T. Muijres

Author for correspondence: (luc1.vandenboogaart@wur.nl)

Affiliations

Experimental Zoology Group, Department of Animal Sciences, Wageningen University & Research, De Elst 1, Wageningen, 6708 WD, The Netherlands

Luc M. van den Boogaart, Guillermo J. Amador, Julian K. A. Langowski, Florian T. Muijres

Department of BioMechanical Engineering, Faculty of Mechanical, Maritime and Materials Engineering, Delft University of Technology, Mekelweg 2, Delft, 2628 CD, The Netherlands

Luc M. van den Boogaart, Dimitra Dodou

Summary statement

A review of force measurement methods for bio adhesion studies, presenting methods from a functional perspective, highlighting novel limitations and trade-offs for experimental study design.

Abstract

Animal adhesion has fascinated biologists and engineers for decades. Utilizing a complex interplay of frictional and adhesive forces, animals can control their attachment allowing them to run, cling or slide along a multitude of surfaces. A better understanding of the fundamentals of biological attachment has the potential to benefit a large range of applications, from biomimetic commercial tapes to bioinspired surgical tools. The feat of controlled adhesion is shared by a large range of animals: from ticks to treefrogs whose weights are over 6 orders of magnitude apart, and from geckos to mosquitoes who adhere under vastly different circumstances. In this review we report the methods currently used for measuring adhesion and friction forces on terrestrial animals, focussing on the most studied groups: geckos, treefrogs, and insects. While previous reviews have already focussed on animal size, adhesion speed, or animal type, this review focusses on the force measurement methods used in animal adhesion research, classifying them with respect to the type of study: considering free and perturbed animals, and studying the whole animal or any of its parts. This approach gives a unique perspective on some of the limitations of adhesion force measurement methods, and highlights considerations and trade-offs in terms of veracity, controllability and variability which should be considered in the design phase of any biological adhesion study.

Introduction

Controlled reversible adhesion is a key strategy towards the survival of a large range of animals, and is effectively applied in a wide range of environments. Between ticks, ants, mosquitoes, treefrogs and geckos, various highly versatile adhesion strategies have evolved. Adhering to a vertical or overhanging substrate requires a combination of strong adhesion (the attachment force normal to the substrate) and strong friction (the attachment force parallel to the substrate surface) (Langowski et al., 2018). Geckos and some spiders rely on what is referred to as “dry” adhesion, dominated by weak intermolecular forces (Autumn et al., 2000; Autumn et al., 2002, Gao et al., 2005). Insects and tree frogs are believed to rely on what is referred to as “wet” adhesion, generating adhesion through capillary forces, hydrodynamic forces, and possibly Van der Waals forces (Gorb, 1998; Gorb & Beutel, 2001; Gorb, 2005). In the case of frogs adhesion in wet environments is further enabled through drainage (Langowski et al., 2018). Most animals rely on additional mechanisms to control or aid their adhesiveness, such as utilizing friction through different body parts (Federle & Labonte, 2019; Langowski, 2019), or claws to latch on to protrusions (Gorb, 2002; Song et al., 2016). These mechanisms are also employed at various temporal and spatial scales, and have been studied in insects and spiders of a couple micrograms, to lizards of several hundreds of grams in weight (Labonte et al., 2016).

Remarkably, some of these animals can establish and reverse adhesion at an extremely rapid pace, having stride frequencies of up to 10 steps s^{-1} for geckos or even 100 steps s^{-1} for mites (Federle and Labonte, 2019). The leading theory is that geckos and other animals use peeling mechanisms to rapidly detach from surfaces (Persson & Gorb, 2003, Federle and Labonte, 2019), and control their adhesiveness using shear-sensitivity of their adhesive pads (Federle and Labonte, 2019). Certain surface characteristics, such as roughness, surface chemistry, wettability, and surface energy, affect an animal's general adhesive capacity to the substrate and the effectiveness of their adhesive. Furthermore, there is increasing evidence of self-cleaning during locomotion (Amador et al., 2017; Amador & Hu, 2015; Crawford et al., 2012; Hansen & Autumn, 2005). How these factors interplay, to what extent, and through what mechanisms, is still under debate. A fundamental understanding why some animals employ different strategies in seemingly similar environments, or to what makes some strategies more effective than others under specific circumstances, is still lacking.

This fundamental understanding of biological rapidly reversible adhesion can find many applications that would benefit humans in daily life. Reversible adhesion finds applications in commercial tapes, robotic grippers (Hawkes et al., 2014; Song et al., 2014; Zhou et al., 2013), and climbing robots (Henrey et al., 2014; Kim et al., 2008; Murphy et al., 2011). Also the development of surgical tools or surgical robots benefits greatly from studies into reversible adhesion, for the manipulation of, or navigation through, soft, wet, delicate and slippery tissues (Bergeles & Yang, 2014; Glass et al., 2008; Kwon et al., 2006). Other applications can be found in architecture or agriculture. Findings can, for example, be used to protect crops from animal pests (Salerno et al., 2018a; 2018b), protect buildings from termites (Féat et al., 2019b) to improve pollination of flowers (Bräuer et al., 2017), or to protect people from disease carrying parasitic animals such as malaria mosquitoes or ticks (Féat et al., 2019a; Pashazanusi et al., 2017; Voigt & Gorb, 2017).

Accurate measurements of adhesion and friction forces play an important role in unravelling the mechanics of biological adhesion. In order to understand and transfer the fundamentals of biological adhesion into applications, models need to be developed. In development and validation of these models, force data, or its derivatives such as normal or shear stress, are crucial. Getting an accurate measurement of these forces poses a number of challenges however. In animal force measurements the behaviour of the animal needs to be considered. When an animal is free (not perturbed by any forces applied by the observer and freely moving) it might employ a completely different strategy than when it is perturbed or constrained, and reacting stressed. Similarly, measuring the adhesiveness of a single organ, or measuring adhesion

forces of the animal in its entirety, might paint a different picture.

In this review, we will give an overview of various methods for force measurement used in animal adhesion studies, and their limitations and trade-offs. This review will limit itself to methods used in studies on terrestrial animals, because terrestrial animals are most widely studied in adhesion studies, and the understanding of their adhesive structures has the greatest potential to find applications that will benefit us in daily, terrestrial life. In this review we present a novel perspective on force measurement methods, focussing on the design of the study from the subjects perspective. To this extent we will review the most used force measurement methods considering free and perturbed animals, and whole body and isolated body part measurements. We will compare methods in their versatility, veracity and controllability, comparing them based on their force measurement resolution and spatial scale. This approach gives a unique perspective on adhesion force measurement methods, and highlights considerations and trade-offs which should be considered early in the design of an adhesion study.

Force measurement methods

Free animal measurements

In climbing or adhering, an animal might employ different locomotive strategies for various reasons: predators benefit from stealthy movement and fast accelerations, climbing and resting animals benefit from energy efficient postures, and parasitic insects, such as mosquitos, benefit from stealthy approach and limited contact forces to avoid detection. Sometimes it is necessary to perturb an animal to get a measurement. When we do this, there is always a risk the animal no longer employs the strategy we try to study, but is now using some sort of a stress induced survival strategy, such as escaping or clinging on to their best capacity. It is therefore often desirable to perturb the animal as little as possible trying to measure quantitative data, while still retaining control over the environment. Several methods have been developed to measure forces between climbing animals and substrates for these studies where the animal can be considered “free”.

Force platforms are the most commonly used method to quantify forces in free animal experiments. The standard 3D force platforms allow for the measurement of the magnitude and direction of ground reaction forces during locomotion and attachment. These measurements can be used to quantify gait patterns of studied animals, calculating a measure of adhesion forces through calculating stabilizing moments during locomotion (Autumn et al., 2006b). The simplest setups consist off a single force platform for reaction force recording (i.e. Autumn et al., 2006b or Dai et al., 2011). The main limitation using a single force platform is the inability to separate the force contributions of individual legs.

Because of this, later studies sought to increase the spatial resolution of the experimental setups by adding additional force platforms, creating force measurement arrays (FMA's). FMA's (figure 1a) have been predominantly used to investigate the gait patterns of lizards (Dai et al., 2011) and tree frogs (Endlein et al., 2013b; Endlein et al., 2017; Ji et al., 2019). Reinhardt et al. (2009) and Endlein & Federle (2015) have also used micro force platforms to measure the reaction force of a single leg of an ant during climbing. While 3D force platforms are among the few methods that allow simultaneous measurement of frictional and adhesive forces, it can be difficult to interpret the measured force in terms of adhesive and frictional components, and typically impossible to measure the contact area during attachment. Increasing the resolution of the force platform to enable contact area measurements would require multiple individual sensors per contact point. Upscaling and increasing the amount of sensors quickly becomes impractical due to exponentially growing cost and calibration time. Adhesion forces, however, correlate strongly with contact area (Irschick et al., 1996). A more robust metric to report adhesive capacity is normalizing adhesion forces to adhesive stress (Autumn et al., 2002), for which the contact area is a required metric.

Optic tactile sensors have been developed to measure the contact area during locomotion, so addressing one of the major limitations of force platforms. Earlier optic sensors used in insect studies worked with photo-elastic gelatine (Full et al., 1995), making use of polarizing filters. This method, however, is limited in substrate selection and impractical due to calibration requirements. Later optic sensors rely on frustrated total internal reflection (FTIR), a technique first developed by Betts et al. in 1980. FTIR works by trapping a beam of light inside a transparent substrate of a high refractive index compared to air (e.g. glass $n \sim 1.5$) by shining it into the substrate in a shallow enough angle for it to reflect internally. When in the substrate comes into contact with a sample, the relative reflective index will be lowered locally, allowing light to escape the substrate and to be imaged. FTIR is limited by camera resolution. Stride frequencies of up to 100 strides s^{-1} require adhesion to be established and reversed within milliseconds (Federle & Labonte, 2019). Capturing these dynamics requires a high temporal resolution. This high temporal demand often conflicts with the requirement for a high spatial resolution needed for small insects (i.e. the leg of a mosquito has a diameter of 50 μm (Pashazanusi et al., 2017)). Having both a high temporal and spatial resolution requires a very efficient data processing procedure and very expensive cameras. This makes tactile optic sensors and FTIR good alternatives for slow and large adhesive studies. Eason et al. (2015) have developed a force sensor based on FTIR to measure the normal stress distribution during adhesion of a gecko foot. This sensor makes use of a PDMS sensing membrane covered in flexible pyramidal bumps,

named taxels, placed on an acrylic waveguide. When force is applied to the membrane, the pyramidal bumps buckle and the contact area between the sensing membrane and the waveguide increases, causing more light to scatter (figure 1b). This way measurable light intensity is related to applied pressure, allowing the mapping of pressure distributions during contact at a high spatial and temporal resolution, about 60 taxels/mm² filmed at 60Hz. In animal studies the technique of FTIR has mostly seen use for tree frogs in a completely free animal experiment (Hill et al., 2018) and in combination with rotating platforms (Endlein et al., 2013b; Langowski et al., 2019) (figure 1c). Federle and Endlein (2004) have also successfully used FTIR to image contact area during locomotion of ants, measuring contact areas of several hundreds of μm^2 at framerates of 125 and 250 FPS.

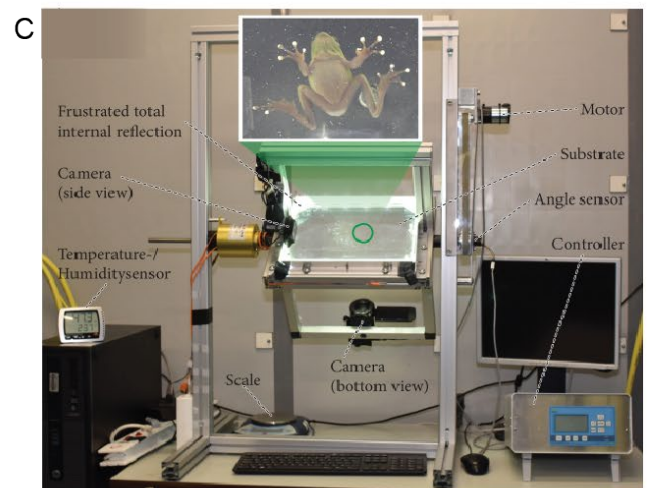
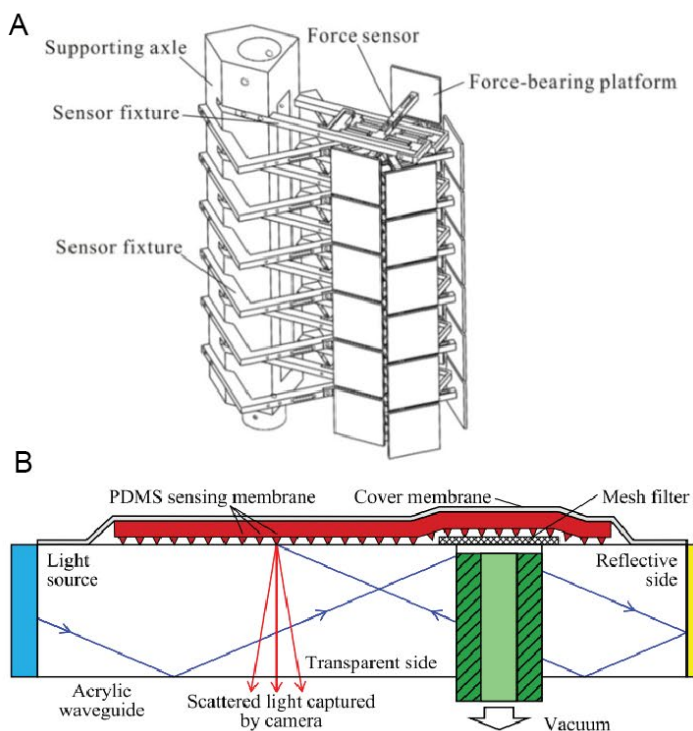
Perturbed animal measurements

The main limitation of free animal experiments manifests in the difficulty to separate adhesive, frictional and reaction forces. Often we seek to investigate or compare an animals adhesive capacity to different substrates and closely study the frictional and adhesive force components of the whole animal, its legs, pads or adhesive structures. For these studies it is unavoidable to

perturb the animal, but doing so with consideration we can measure quantitative data unavailable to us in free animal studies. In this section we will review the various methods used to study animal adhesion in which the animal has to be perturbed, and can no longer be considered “free”. We will make the distinction between whole animal measurements, and appendage measurements focussing on a single toe, pad or seta.

Perturbed whole animal measurements

Perturbed whole animal studies are all those studies in which the animal is free to use all of its appendages, or other body parts, to establish and maintain adhesion, but the forces compensated by the adhesive forces are controlled by the experimenter. This way we accurately measure the magnitude of the adhesive or frictional forces produced by the studied animal. By carefully selecting animal orientations and force directions, we can separate adhesive forces and frictional forces reasonably well. Various methods have seen use in perturbed whole animal studies. In this section a distinction will be made between methods that are predominantly used to quantify adhesive forces, and methods that are predominantly used to measure frictional forces of whole animal force measurements.



Adhesion force measurements

Vertical pull studies are the most basic studies to quantify adhesive forces (figure 2a). They prove an effective way to quantify adhesive forces and are easy to setup, but on a downside they are invasive (i.e. highly affect animal behaviour). Vertical pulling requires a strain gauge or scale to be attached to some part of the animal, at which point a local force is applied. This has implications for the behaviour of the studied animal, which can be assumed to react stressed and possibly finds itself in an unnatural posture. E.g. a vertical pull study on Tokay Geckos (*Gekko gecko*) was done by Pugno et al. (2011) to investigate normal adhesive forces vs body displacement. Whilst the study was effective in showing a clear trend in decreased adhesion over multiple trials resulting from feet damage, it underestimated the adhesive capacity of the gecko by more than a factor 30. The authors suggest this to be the result of macro imperfections on the toes, however another likely explanation for the reduced adhesive capacity lies in the forced posture. The subjects limbs were pulled in unnatural angles wherein it was unable to fully engage its adhesive structures. In any case it is hard to rule out or quantify these effects in pull studies.

Rotation platforms (figure 2b) are the most common alternative to vertical pulling studies. After the animal is placed on the platform, the platform is rotated until the animal is pulled off by gravity. The major limitation of this method is the maximum force which can be applied, which is equal to the weight of the studied animal. The upside is that the inversion platform is minimally invasive. The angle of the platform at which the animal drops off, can be used to quantify adhesive force, with a completely inverted platform coinciding with an adhesive force equal to (or greater than) the animal weight. For this reason, rotation platforms are most effective for animals whose safety factor (SF: the amount of times an animal can support its own body weight) in pure adhesion is around 1 or lower. Theoretically rotation platforms are not limited by animal weight or adhesion force, as long as the animal can be weighed precisely and its safety factor is lower than 1. In practice rotation platforms are mostly suitable for climbing frogs and salamanders, the lightest species of which investigated are around 50 mg. Rotation platforms have been used most predominantly with tree frogs (Barnes et al., 2006; Crawford et al., 2012; Endlein et al., 2013b; Langowski et al., 2019) and can be combined with FTIR measurements, as stated earlier. Rotation platforms have also been used to study salamanders (O'Donnel & Deban, 2020) beetles (Gorb & Gorb, 2002), mirid bugs (Voigt et al., 2007), and ticks (Voigt & Gorb, 2017). Due to the typically high S.F. of hexapods and arthropods, rotation platforms are not really suited to measure adhesion forces, but instead serve to statistical test effects through high number of repetitions or a large number of experimental conditions (e.g. the likelihood of attachment between different surfaces (Voigt & Gorb, 2017)).

Adhesion force centrifuges are the most used alternative for direct vertical pull studies for insects (figure 2c). When used to measure adhesive forces, the studied animal is placed on the side of a drum or platform attached to an arm. The drum is then rotated at increasing velocity (typically up to 3000 RPM) until the studied animal falls off, at which point the centrifugal force exceeds the adhesion force. This allows the method to be effective for animals with high S.F.'s. As a downside, their effectiveness is limited with increased subject mass. Increased inertia of the system will lead to higher forces and vibrations, requiring a more robust setup. Moreover, higher forces in order to overcome adhesion result in higher impact forces after release, which increases the risk of injury for test subjects. This makes using force centrifuges for heavier animals ethically challenging. Because of this force centrifuges are best suited for insect studies, or animals of a mass in the range {1mg, 1g}. Gorb et al. (2001) investigated the influence of aerodynamic drag on the friction force and concluded that for insects at these velocities the effects are negligible. At lower masses, however, aerodynamic forces can no longer be neglected. Force centrifuges are able to record forces in a range between around {500 μ N, 500mN} (lower bound: motor precision, upper bound: max motor RPM). These ranges could be expanded by optimizing the centrifuge motor. Centrifuging techniques used to measure adhesion forces were first introduced by Dixon et al., (1990) and later used to study ants (Brainerd, 1994; Federle et al. 2000; Federle et al., 2002; Labonte & Federle, 2015b), moths (Al Bitar et al., 2009), and stick insects (Labonte et al., 2019). As a second downside of force centrifuges, they only work with animals unable to jump or fly away. E.g. in their study with moths, Al bitar et al. (2009) had to cut the wings of the subjects wings to prevent the subjects from fleeing during the force centrifuge experiments.

Friction force measurements

Friction force centrifuges use the principle of controlling centripetal force for friction force measurements (figure 2d). Force centrifuges are capable of measuring static and dynamic friction. In friction force centrifuge measurements, subjects are placed on top of a rotating disk or drum. A laser or camera is used to monitor the subjects distance from the centre of the disk. Measuring the tangential acceleration and the centrifugal force component, the friction force can be calculated. Keeping the RPM constant after static friction is overcome by centrifugal force, dynamic friction can be calculated by measuring the sliding velocity and deriving acceleration. Similarly to the adhesion force centrifuges, they are most effective for insects with high S.F.'s and low body mass. Friction force centrifuges are equally limited in recordable force and animal mass as adhesion force centrifuges. Most of the friction force centrifuge experiments done are based on the set up developed by Gorb et al. (2001). This, or a similar, setup has been used to study ants (Federle et al., 2004), beetles (Lüken et al., 2009; Grohman et al.,

2014), coddling moths (Al bitar et al., 2010), sawfly larvae (Voigt & Gorb, 2012) and syrphid flies (Gorb et al., 2001).

Tethered animals studies (figure 2e) are the most common friction force studies. In a tethered animal experiment, a wire is used to attach an animal to a strain or force gauge, or to pull on an animal positioned on a force sensor. Tethered animal studies are cheap, requiring only a simple force transducer, a wire and some super glue. The method is invasive however, insects capable of flight need to be incapacitated by gluing or trimming their wings. The method was first used by Walker et al. (1985) in a study on blowflies, in which the substrate was pulled whilst the animal remains stationary. This way, dynamic friction was measured for various pulling directions. As a downside of this study design, the insect is dragged along the surface, resulting in an increased contact area and subsequently increased friction. Later

studies addressed this by making the animal walk over the substrate, pulling on the force transducer, thus measuring static friction (also referred to as traction). Reviewed studies suggest a measurable force range of {200 μ N, 10mN}, due to sensor limitations. All studies reviewed made use of the same force transducer: 10 g capacity, Biopac Systems Ltd., Santa Barbara, CA, USA. Bounds could be expanded by using force transducers of a higher capacity or higher precision. The method has been used as means of validation for force centrifuge tests (Federle et al., 2000), as well as to study attachment ability of insects to various substrates. Examples include studying the effects of surface energy (Gorb et al., 2008), surface structure (Gorb et al., 2010), or surface chemistry (England et al., 2016). Additionally tethered animal trials have also been used to study the attachment capacity to various plants (Salerno et al., 2018a; 2018b; 2020), and flower petals (Bräuer et al., 2016).

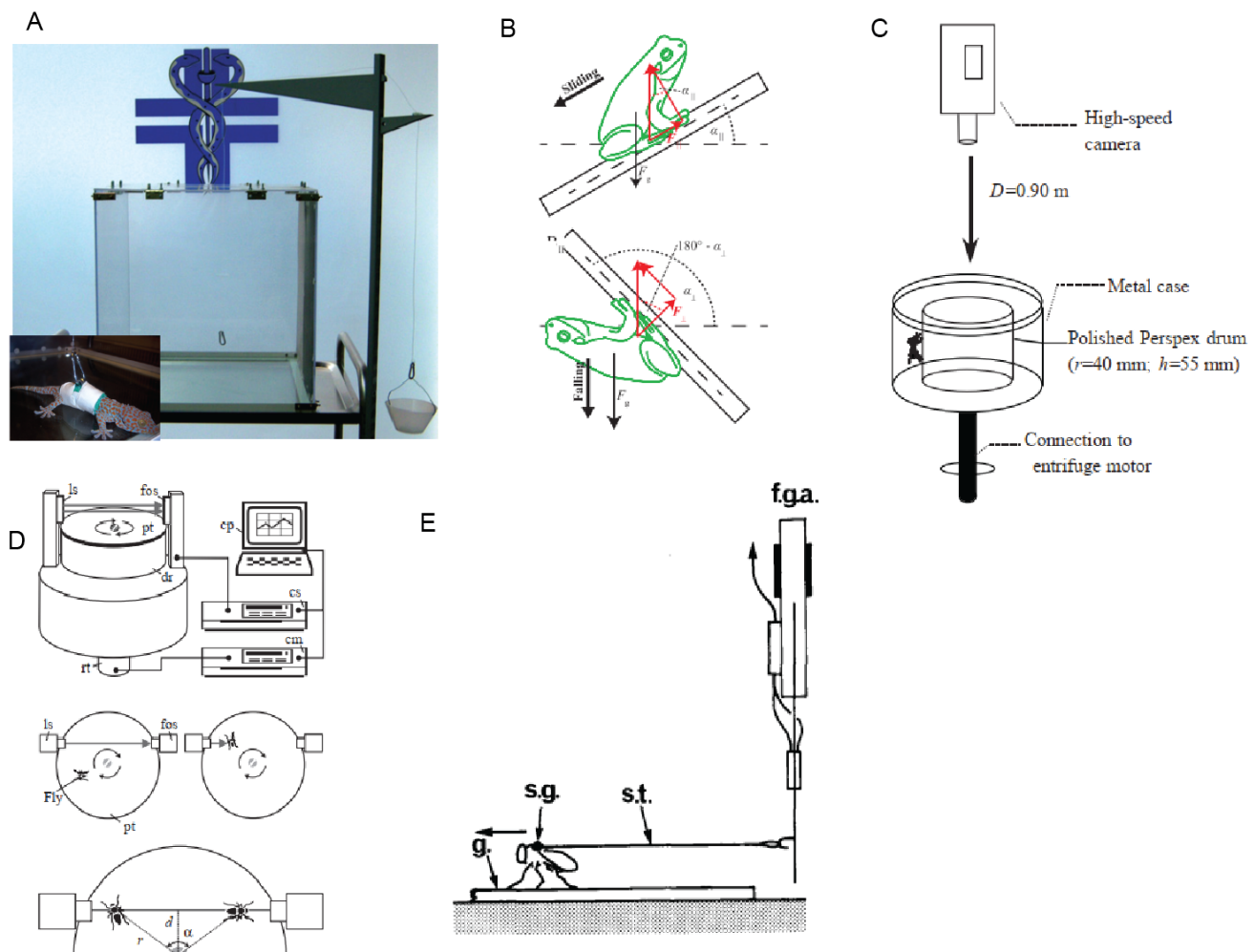


Fig 2: Graphic overview of perturbed whole animal adhesion and friction force measurement setups. (A) Scale pulley system to measure adhesive force (inset: attachment of the cable to the test animal), adapted from Pugno et al., 2013. (B) Principle of the rotating platform for adhesive force measurement. α_{\perp} falling angle, α_{\parallel} sliding angle, F_g body weight, F_{\perp} adhesion, F_{\parallel} friction. Adapted from Langowski et al., 2019. (C) Force centrifuge in adhesion measurement configuration, adapted from Federle et al., 2000. (D) Force centrifuge in friction configuration used to measure dynamic friction. A laser is used to measure the position of the studied animal. Adapted from Gorb et al., 2001. (E) Traction measurement setup used to measure static friction of test animal walking over substrate, adapted from Walker et al., 1985.

Appendages and beyond

When we are interested in learning how certain microstructures enable adhesion, or what kind of interplay between various adhesive or frictional forces is at play during attachment, it is often irrelevant what the macro behaviour of the studied animal is. In this case it makes sense to isolate the body part, or microstructure, of interest for our study. Doing so correctly, increases the controllability of the experiment and allows us to measure forces in greater detail than we could measuring the entire animal. Moreover, when we exclude the animals behaviour or natural strategies from the experiment, we can also estimate the maximum capacity of various adhesive structures. This information is of great importance for the design of biomimetic adhesives.

Force transducers (FT's) are widely used to measure adhesion and friction of the toes, feet, hairs, and pads of geckos, frogs, and insects. Several different configurations have been developed between studies, but most of them are either uniaxial or biaxial FT's. Uniaxial FT's in appendage studies are mostly used to measure adhesive forces (figure 3a). Biaxial FT's, mounted to a robotic stage in combination with a closed loop controller, can be used to keep adhesive forces constant to isolate frictional forces or apply a shear load to measure adhesive forces. Several different types of sensors have been used. Uniaxial FT's typically rely on fibre optic springs (Jiao et al., 2000; Labonte & Federle, 2015a), or piezoelectric sensors (Hansen & Autumn, 2005). Spinner et al. (2014) used a uniaxial FT to measure friction forces, by sliding the feet of a chameleon over a rod attached in direction of the FT (figure 3b). Biaxial FT's (figure 3c) mostly rely on strain gauges placed in perpendicular directions (Autumn et al., 2000; 2002; Crawford et al., 2012; Drechsler & Federle, 2006; Federle et al., 2006; Zhou et al., 2014). Force transducers are able to record forces in a range between {80 μ N, 100mN} (lower bound: sensor precision [Labonte et al., 2019]), upper bound: sensor limitation of used 10g force transducers). One study by Autumn et al. (2006a) uses a 3-axis force sensor to measure the friction force of an array of setae from a gecko for various directions. One study by Gillies et al. (2014), also on a gecko, uses a 6-axis force sensor, though this was most likely due to availability. Keeping the amount of measuring axes to a minimum is beneficial through reducing: the amount of calibration needed, the controller complexity (in case used), the financial costs, and the data analysis.

Atomic Force Microscopy (AFM) is an indispensable method in adhesion studies, either to measure adhesive forces directly or functioning in a support role. AFM relies on the optic imaging or piezoresistive sensing of the deflection of a cantilever, which is brought into contact with a substrate (figure 3d-e). AFM can measure adhesion

forces with a resolution of 70 Pico Newtons (Huber et al., 2005a; 2005b; 2007). This makes AFM suitable to measure adhesive forces in a range of around {200 pN, 1 μ N} (lower bound: precision of 70pN [Huber et al., 2005a, upper bound: maximum force in flexible probe range (Park et al., 2007)). AFM is not limited to a specific animal group or limited by animal weight, seeing AFM is only able to measure at a very small spatial range, measuring at the (sub-)seta range. AFM has for example been used to measure the adhesive capacity of gecko setae (Autumn et al., 2002), capillary forces on the terminal plates of fly setae (Langer et al., 2004) and the adhesion of mosquito legs to rough surfaces (Pashazanusi et al., 2017). Beyond just force measurements, AFM is a very versatile method. Many studies which investigate the topography or effects of surface roughness use AFM to measure the root-mean square roughness (R_{RMS}) of the substrate or structure. Alternatives to measure surface roughness of biological samples, such as Scanning Electron Microscopy (SEM) imaging, are prone to artefacts from the sample preparation such shrinkage or drying, and are not suitable for living animals (Scholz et al., 2009). AFM can also be used for measuring the elasticity or stiffness of soft materials through nano indentation. Micro indentation using a micro tribometer is sufficient for larger structures such as tree frog toes (Barnes et al., 2011). For smaller structures AFM is required, for example to measure the stiffness of the epithelial (cells) or local friction profiles over single pillars of tree frogs toes (Kappl et al., 2016), or the stiffness of the adhesive tarsal setae of ladybird beetles (Peisker et al., 2013) (figure 3f).

Discussion

In the previous section we have presented a broad overview of methods currently, or previously, used to study biological adhesion on terrestrial animals. Table 1 gives an overview of all presented methods and studies in which they were employed. When deciding on a method for a new study, there are a couple of questions one should consider. Is the method suitable for measuring the type of data of interest? Is the method suitable for the type of animal of interest? Does the method provide the freedom to choose experimental conditions of interest? What are the limitations of a given method? Does the method limit the behavioural freedom of the test subject? Are there alternative methods available for this study? In this section we will present a couple of considerations in selecting a method for an animal adhesion study. First we will consider some of the limitations in scale and subject of the most prevalent methods. Then, the main trade-off in selecting a method found through this review will be discussed. Lastly, we will review some outlooks for future development and topics of interest for animal adhesion studies.

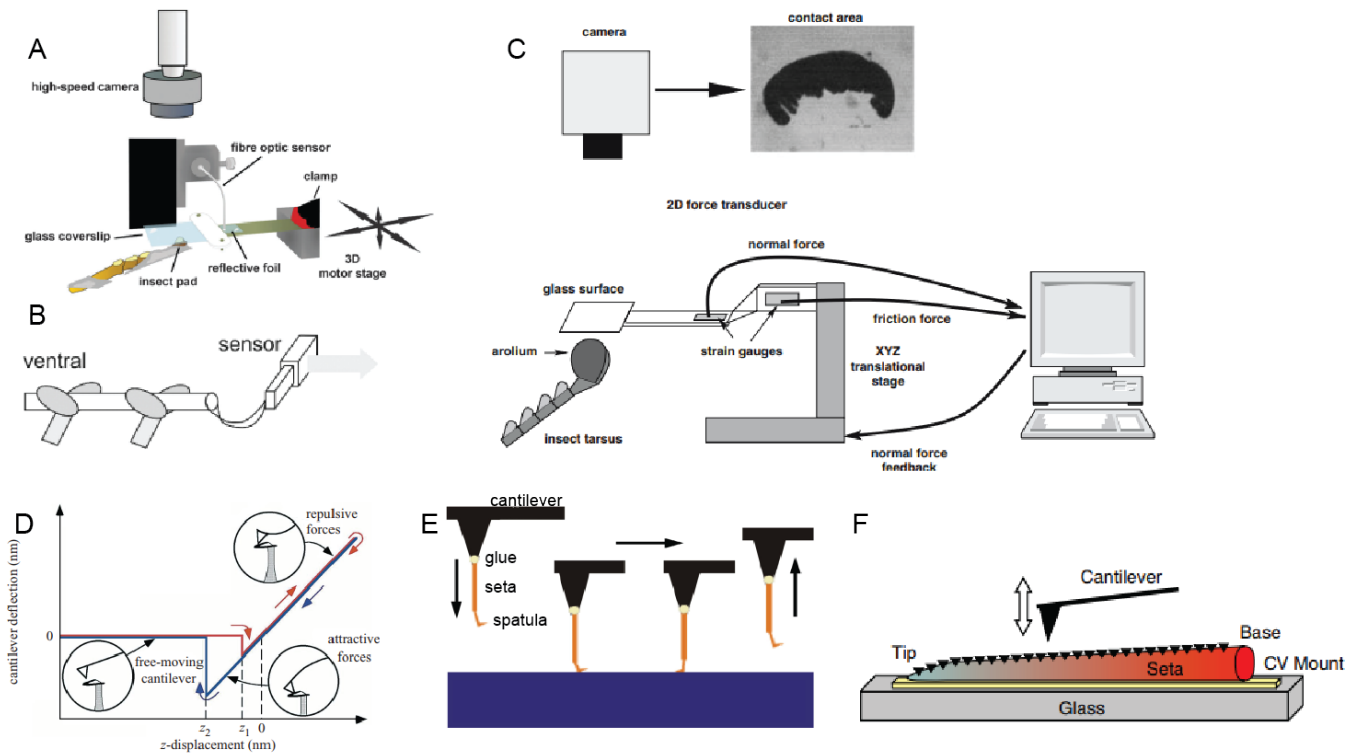


Fig 3: Force measurement methods focusing on appendages, setae and spatulas. (A) A fiberoptic uniaxial force transducer setup used to measure adhesion forces, adapted from Labonte & Federle, 2015a (B) A uniaxial force transducer setup used to measure friction forces, adapted from Spinner et al., 2014. (C). A biaxial force transducer setup using strain gauges and a closed loop controller to keep normal forces constant during friction forces measurement, adapted from Drechsler & Federle 2006. (D) AFM probe in contact mode used to measure adhesive forces, adapted from Langer et al., 2004. (E) AFM probe with seta attached to cantilever to measure forces at the spatula, adapted from Huber et al., 2005a. (F) AFM probe in nano-indentation configuration to measure material stiffness gradient in seta, adapted from Peisker et al., 2013.

Limitations

Spatial scale effects limit all methods. Figure 5 shows a regime map of the most common adhesion and friction force study methods. Only AFM, 2D (biaxial) force transducers, 1D (uniaxial) force transducers in tethered configuration, rotation platforms and force centrifuges are included. Force platform studies are excluded because they report reaction forces which are difficult to compare to adhesion forces. There were not sufficient ($n < 3$) data points available in the reviewed studies to make a meaningful estimate of the regimes of the other methods. Their limitations have already been discussed in the results section. Measured force was plotted against subject mass as reported in reviewed studies, resulting in an estimate for method regimes. Data points showed 2 distinct trends: (1) whole animal studies follow Iso Safety Factor (ISF) lines, and (2) body part measurements are limited by sensor precision. As noted before, rotation platform limits are explained well by SF, and SF should be considered during design of the experiment. For the other whole animal force measurement methods, tethers and force centrifuge measurements, ISF bounds are suggested by the reviewed studies. Tethered studies are not effective below SF 1: animals that cannot sustain their own weight through friction will likely start slipping when pulling their own body weight. Force centrifuges are expected to become more reliable for animals of higher safety factors. At higher centrifuge RPM, correlating with

higher safety factor, the relative variance over measurements is lower. There is a considerable overlap between tethers and force centrifuge studies, suggesting both are capable of studying the same type of animals, and expected SF or animal weight should not be strongly considered when choosing between them.

Table 1: Dependent and independent variables per method of reviewed studies

Method	Configuration	Subject class	Type ¹	Dependent variables	Independent variables	Study
3D force platforms	Single platform	Geckos	W-F	Reaction force	Walking direction	Autumn et al., 2006b; Dai et al., 2011
		Insects	A-F	Reaction force	-	Reinhardt et al., 2009; Endlein & Federle, 2015
	Force Measurement Array (FMA)	Geckos	W-F	Reaction force	Substrate R _{RMS}	Dai et al., 2011
		Treefrogs	W-F	Reaction force	Substrate R _{RMS} , platform angle	Endlein et al., 2013b; Endlein et al., 2017; Ji et al., 2019
Photo-elastic	-	Insects	W-F	Reaction force	-	Full et al., 1995
Optic tactile	-	Geckos	A-F	Normal stress	Load angle	Eason et al., 2015
FTIR	-	Insects	W-P	Contact area	Load	Federle & Endlein, 2004
	Free	Treefrogs	W-F	Contact area	Substrate curvature	Endlein et al., 2017 Hill et al., 2018;
	Rotation platform	Treefrogs	W-P	Contact area	Surface roughness	Endlein et al., 2013, Langowski et al., 2019
Scale	Vertical pull	Geckos	W-P	Adhesion force	Load	Pugno et al., 2013
Rotation platforms		Arachnid	W-P	Adhesion %	Substrate R _{RMS}	Voigt et al., 2017
		Insects	W-P	Adhesion %	Substrate R _{RMS} , Surface type, Surface structure,	Gorb & Gorb., 2002; Voigt et al., 2007
		Treefrogs	W-P	Adhesion force Shear force	Surface R _{RMS}	Barnes et al., 2006; Crawford et al., 2012; Langowski et al., 2019
Force centrifuge	Horizontal	Insects	W-P	Dynamic friction force	Substrate R _{RMS} , contact angle, angular velocity	Al Bitar et al., 2010; Gorb et al., 2001; Grohman et al., 2014; Lükken et al., 2009; Voigt & Gorb, 2012; Voigt & Gorb, 2017
	Vertical	Insects	W-P	Adhesion force	angular velocity, subject orientation	Al Bitar et al., 2009; Brainerd 1994; Federle et al., 2000; Federle et al., 2002; Labonte & Federle, 2015b; Labonte et al., 2019; Voigt & Gorb, 2012
Tethered studies	Tethered	Insects	W-P	Static friction force	Substrate R _{RMS} , chemistry, wettability, surface energy	Bräuer et al., 2016; England et al., 2016; Federle et al., 2000; Gorb et al., 2008; Gorb et al., 2010; Salerno et al., 2018a; 2018b; 2020; Voigt et al., 2007, Walker et al., 1985
1D (uniaxial) force transducers	Adhesion	Insects	A-P	Adhesive force	Preload, retraction speed,	Jiao et al., 2000; Hansen & Autumn, 2005; Labonte & Federle, 2015a
	Friction	Geckos	A-P	Friction force	Curvature, substrate R _{RMS} , pull velocity	Spinner et al., 2014
2D (biaxial) force transducers	-	Geckos	A-P	Friction force	Preload, wettability	Autumn et al., 2000; 2002;
		Insects	A-P	Friction force	Substrate R _{RMS} , preload, humidity, sliding speed, retraction speed	Drechsler & Federle, 2006; Labonte et al., 2019; Zhou et al., 2014
		Tree frogs	A-P	Friction force	Substrate R _{RMS} , pad preload	Crawford et al., 2012; Endlein et al., 2017; Federle et al., 2006;
Multiaxial force transducer	3-axis	Geckos	A-P	Friction force	Drag direction	Autumn et al., 2006a
	6-axis	Geckos	A-P	Friction force	Substrate roughness	Gillies et al., 2014
AFM	Force	Geckos	A-P	Adhesion force	Humidity, contact angle, preload, substrate R _{RMS}	Autumn et al., 2002 Huber et al., 2005a; 2005b; 2007;
		Insects	A-P	Adhesion force	Substrate R _{RMS} , relative humidity, buffer presence	Langer et al., 2004; Pashazanusi et al., 2017
	Nano-indentation	Treefrogs	A-P	Stiffness	Indenter size, indentation: speed, depth	Kappl et al., 2016; Peisker
	Topography	Treefrogs	A-P	R _{RMS}	AFM tip shape, preload, scan direction	Kappl et al., 2016; Scholz et al., 2009

1: F = free, P = perturbed, A = appendage, W = whole body

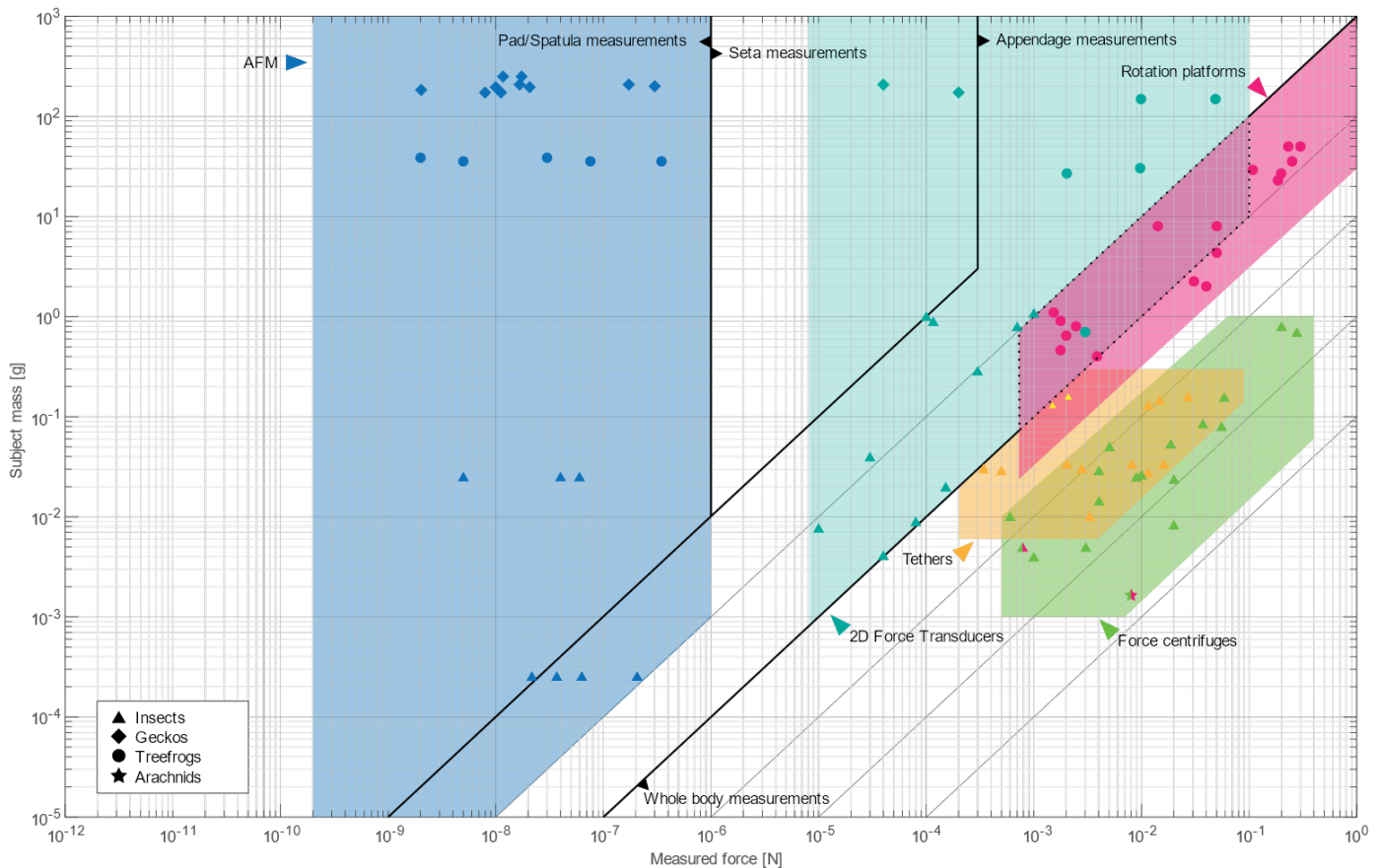


Fig 4: Regime map of the most common adhesion and friction force measurements: AFM (dark blue), 2D (biaxial) force transducers (light blue), force centrifuges (green), rotation platforms (pink) and 1D force transducers in tethered configuration (tethers; orange). Data points indicate animal mass and measured force, symbols denote animal type. Diagonal lines indicate iso safety factor (SF) lines. Thick lines denote boundary regions of pad/spatula measurements, seta measurements, appendage measurements and whole body measurements. The area in between dashed dotted lines shows an overlap of the appendage measurements and whole body measurements range. Studies reviewed investigated animals ranged over 6 orders of magnitude in weight, and reported forces ranged over 9 orders of magnitude. 2 studies are 2 colours, indicating study made use of 2 methods.

Trade-offs in study design

The main trade-off in study design is between controllability (the extent to which the experimental conditions can be controlled and the repeatability of the study), variability (the range of experimental conditions, subjects and scales the method can be used for) and veracity (the extent to which the study is representative of natural behaviour). Figure 6 shows a trade-off diagram mapping all considered studies to three axes representing Veracity, Controllability and Variability. Methods are scored in relative to each other with a score of 1 to 5. Individual scores, are displayed in table 2, presented as Controllability/Variability/Veracity. Methods closer to the centre of the triangle can be considered more balanced; the theoretically universal method, making equal compromises to all three parameters, would lie in the centre of the diagram. Methods located towards one of the corners sacrifice one of the three conditions to benefit the other two criteria. It is possible to score high in two categories, but never in all three.

Veracity is dictated by how free the animal can be considered to be. Veracity is scored looking at the level of perturbation needed for a measurement, the level of behavioural freedom the animal has during measurement, and the preservation of postural and kinematic data. High veracity is desirable when studying animal behaviour or strategies it might employ. Methods scoring high in veracity are methods where animals are minimally perturbed, such as FMA (force platforms), FTIR, rotation platforms and optic tactile sensors.

Controllability represents the level of control the experimenter has during the experiment. Controllability is scored by the repeatability of the experiments, the extent to which dependent parameters can be separated, the resolution of the measurement technique, the signal to noise ratio and the variance of the data collected. Optic tactile sensors, force centrifuges, 2D (biaxial) force transducers, and AFM score high in controllability.

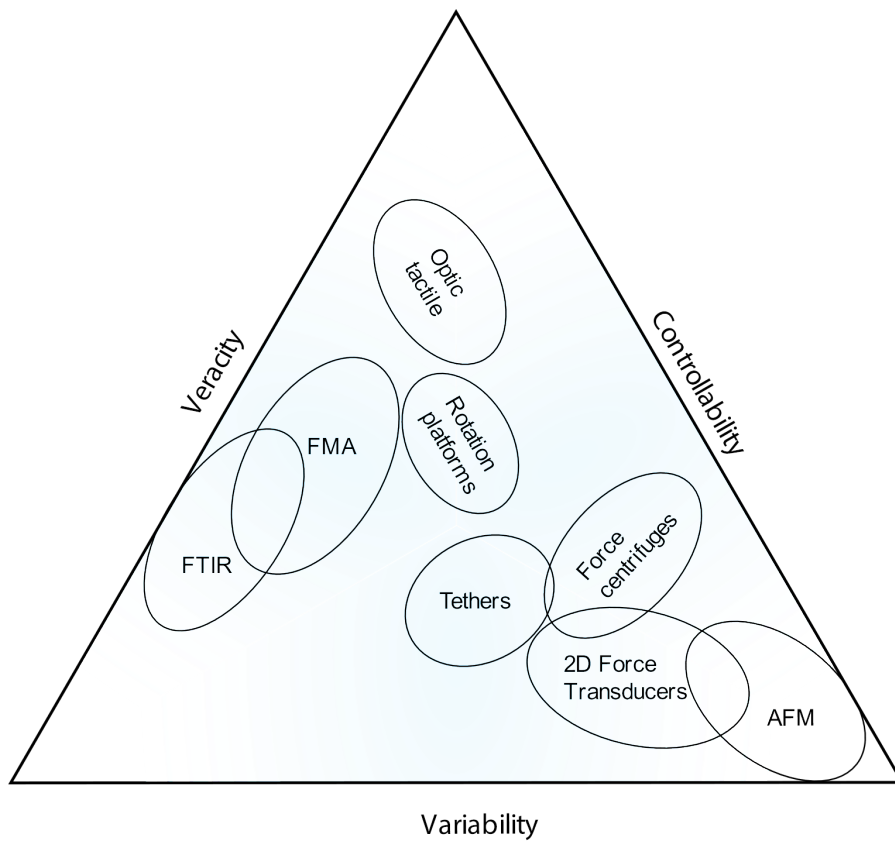


Table 2: Scores per method

Method	C/Va/Ve
2D Force transducers	4,5/4/1,5
AFM	5/4,5/1
FMA	3/3/4,5
Force centrifuges	3/3/2,5
FTIR	2,5/3/5
Optic Tactile	3/1,5/4
Rotation Platforms	3/2,5/3,5
Tethers	3/2,5/2,5

Fig 5: Methods mapped to a veracity/controllability/variability trade-off diagram

Variability represents the flexibility of the method in terms of experimental design. Variability is scored by the level of freedom in selecting independent parameters and dependent parameters during study design, the measurable range (figure 2. X-axis), and the types of animals that can be investigated with the method. Tethers, AFM and 2D force transducers score high towards variability.

Perspectives

Recent studies and developments have opened up a wide variety of new perspectives for studying animal adhesion. With the data available to us now, it was possible to map established methods to show the effectiveness and limitations of these methods. Studying adhesion for the large and slow does no longer pose a problem. The frontier seemingly lies at the extremely small and fast, and measuring small and fast processes still provides us with a considerable challenge. A renewed interest in optic methods the past few years looks promising though (Endlein et al., 2013, Endlein et al., 2017, Hill et al., 2018, Langowski et al., 2019). With visual data processing technologies, data storage and transfer capacities, and optic systems ever improving, optics based methods seem more and more promising. Future studies will have to show how small and fast we can go.

During this review we have largely skipped over Micro-ElectroMechanical Systems (MEMS) sensors. Interest in these technologies for adhesion seems to have faded in

the past decade, but MEMS sensors might be key in exploring the realm of fast and small. A MEMS force plate for studying insect locomotion developed by Bartsch et al (2003, 2007) has seen less than 5 citations in actual animal studies. The same goes for a new biaxial MEMS cantilever design by Lin & Tramer (2014). This begs the question: is MEMS really just a false promise, or have developments in this field largely gone unnoticed by the biologists doing the experiments?

Biological adhesion has always been a fascinating subject to study for biologists and engineers alike. Their hard work over the last decades resulted in the discovery of various insights into these remarkable mechanics, attracting an ever increasing interest from various other disciplines. Electrical engineers, (soft)roboticists, medical engineers, material scientists, and ecologists, all benefit from discoveries in this field and work to tackle multidisciplinary problems, such as protecting honeybees, preventing animal pests or developing new soft grippers for various purposes. Together we may contribute to our fundamental understanding of biological adhesion and investigate the smallest and the fastest.

Acknowledgements

Competing interests

The authors declare no competing or financial interests

Author contributions

Conceptualization: L.M.v.d.B., G.J.A., D.D., J.K.L., F.M.; Writing – original draft: L.M.v.d.B.; Supervision: G.J.A., D.D., J.K.L., F.M.

Funding

We acknowledge and thank the parents of L.M.v.d.B. for their continued financial support over the years leading towards the writing of this review.

Referenes

- Al Bitar, L., Voigt, D., Zebitz, C. P. W., & Gorb, S. N. (2009). Tarsal morphology and attachment ability of the codling moth *Cydia pomonella* L. (Lepidoptera, Tortricidae) to smooth surfaces. *Journal of Insect Physiology*, *55*(11), 1029–1038. <https://doi.org/10.1016/j.jinsphys.2009.07.008>
- Al Bitar, L., Voigt, D., Zebitz, C. P. W., & Gorb, S. N. (2010). Attachment ability of the codling moth *Cydia pomonella* L. to rough substrates. *Journal of Insect Physiology*, *56*(12), 1966–1972. <https://doi.org/10.1016/j.jinsphys.2010.08.021>
- Amador, G. J., Endlein, T., & Sitti, M. (2017). Soiled adhesive pads shear clean by slipping: A robust self-cleaning mechanism in climbing beetles. *Journal of The Royal Society Interface*, *14*(131), 20170134. <https://doi.org/10.1098/rsif.2017.0134>
- Amador, G. J., & Hu, D. L. (2015). Cleanliness is next to godliness: Mechanisms for staying clean. *Journal of Experimental Biology*, *218*(20), 3164–3174. <https://doi.org/10.1242/jeb.103937>
- Autumn, K., Dittmore, A., Santos, D., Spenko, M., & Cutkosky, M. (2006a). Frictional adhesion: A new angle on gecko attachment. *Journal of Experimental Biology*, *209*(18), 3569–3579. <https://doi.org/10.1242/jeb.02486>
- Autumn, K., Hsieh, S. T., Dudek, D. M., Chen, J., Chitaphan, C., & Full, R. J. (2006b). Dynamics of geckos running vertically. *Journal of Experimental Biology*, *209*(2), 260–272. <https://doi.org/10.1242/jeb.01980>
- Autumn, K., Liang, Y. A., Hsieh, S. T., Zesch, W., Chan, W. P., Kenny, T. W., Fearing, R., & Full, R. J. (2000). Adhesive force of a single gecko foot-hair. *Nature*, *405*(6787), 681–685. <https://doi.org/10.1038/35015073>
- Autumn, K., Sitti, M., Liang, Y. A., Peattie, A. M., Hansen, W. R., Sponberg, S., Kenny, T. W., Fearing, R., Israelachvili, J. N., & Full, R. J. (2002). Evidence for van der Waals adhesion in gecko setae. *Proceedings of the National Academy of Sciences*, *99*(19), 12252–12256. <https://doi.org/10.1073/pnas.192252799>
- Barnes, W. Jon. P., Goodwyn, P. J. P., Nokhbatolfoghahai, M., & Gorb, S. N. (2011). Elastic modulus of tree frog adhesive toe pads. *Journal of Comparative Physiology A*, *197*(10), 969. <https://doi.org/10.1007/s00359-011-0658-1>
- Barnes, W. Jon. P., Oines, C., & Smith, J. M. (2006). Whole animal measurements of shear and adhesive forces in adult tree frogs: Insights into underlying mechanisms of adhesion obtained from studying the effects of size and scale. *Journal of Comparative Physiology A*, *192*(11), 1179–1191. <https://doi.org/10.1007/s00359-006-0146-1>
- Bartsch, M.S., Federle, W., Full, R. J., & Kenny, T. W. (2003). Small insect measurements using a custom MEMS force sensor. *TRANSDUCERS '03. 12th International Conference on Solid-State Sensors, Actuators and Microsystems. Digest of Technical Papers (Cat. No.03TH8664)*, *2*, 1039–1042 vol.2. <https://doi.org/10.1109/SENSOR.2003.1216946>
- Bartsch, M.S., Federle, W., Full, R. J., & Kenny, T. W. (2007). A Multiaxis Force Sensor for the Study of Insect Biomechanics. *Journal of Microelectromechanical Systems*, *16*(3), 709–718. <https://doi.org/10.1109/JMEMS.2007.893677>
- Bergeles, C., & Guang-Zhong Yang. (2014). From Passive Tool Holders to Microsurgeons: Safer, Smaller, Smarter Surgical Robots. *IEEE Transactions on Biomedical Engineering*, *61*(5), 1565–1576. <https://doi.org/10.1109/TBME.2013.2293815>
- Betts, R. P., Duckworth, T., Austin, I. G., Crocker, S. P., & Moore, S. (1980). Critical light reflection at a plastic/glass interface and its application to foot pressure measurements. *Journal of Medical Engineering & Technology*, *4*(3), 136–142. <https://doi.org/10.3109/03091908009161107>
- Brainerd EL. (1994). Adhesion force of ants on smooth surfaces. *American Zoologist*, *34*. /z-wcorg/.
- Bräuer, P., Neinhuis, C., & Voigt, D. (2017). Attachment of honeybees and greenbottle flies to petal surfaces. *Arthropod-Plant Interactions*, *11*(2), 171–192. <https://doi.org/10.1007/s11829-016-9478-0>
- Crawford, N., Endlein, T., & Barnes, W. J. P. (2012). Self-cleaning in tree frog toe pads; a mechanism for recovering from contamination without the need for grooming. *Journal of Experimental Biology*, *215*(22), 3965–3972. <https://doi.org/10.1242/jeb.073809>
- Dai, Z., Wang, Z., & Ji, A. (2011). Dynamics of gecko locomotion: A force-measuring array to measure 3D reaction forces. *Journal of Experimental Biology*, *214*(5), 703–708. <https://doi.org/10.1242/jeb.051144>
- Drechsler, P., & Federle, W. (2006). Biomechanics of smooth adhesive pads in insects: Influence of tarsal secretion on attachment performance. *Journal of Comparative Physiology A*, *192*(11), 1213–1222. <https://doi.org/10.1007/s00359-006-0150-5>
- Eason, E. V., Hawkes, E. W., Windheim, M., Christensen, D. L., Libby, T., & Cutkosky, M. R. (2015). Stress distribution and contact area measurements of a gecko toe using a high-resolution tactile sensor. *Bioinspiration & Biomimetics*, *10*(1), 016013. <https://doi.org/10.1088/1748-3190/10/1/016013>
- Endlein, T., Barnes, W. J. P., Samuel, D. S., Crawford, N. A., Biaw, A. B., & Grafe, U. (2013a). Sticking under Wet Conditions: The Remarkable Attachment Abilities of the Torrent Frog, *Stauroids guttatus*. *PLOS ONE*, *8*(9), e73810. <https://doi.org/10.1371/journal.pone.0073810>
- Endlein, T., & Federle, W. (2015). On Heels and Toes: How Ants Climb with Adhesive Pads and Tarsal Friction Hair Arrays. *PLOS ONE*, *10*(11), e0141269. <https://doi.org/10.1371/journal.pone.0141269>
- Endlein, T., Ji, A., Samuel, D., Yao, N., Wang, Z., Barnes, W. J. P., Federle, W., Kappl, M., & Dai, Z. (2013b). Sticking like sticky tape: Tree frogs use friction forces to enhance attachment on overhanging surfaces. *Journal of The Royal Society Interface*, *10*(80), 20120838. <https://doi.org/10.1098/rsif.2012.0838>

- Endlein, T., Ji, A., Yuan, S., Hill, I., Wang, H., Barnes, W. J. P., Dai, Z., & Sitti, M. (2017). The use of clamping grips and friction pads by tree frogs for climbing curved surfaces. *Proceedings of the Royal Society B: Biological Sciences*, 284(1849), 20162867. <https://doi.org/10.1098/rspb.2016.2867>
- England, M. W., Sato, T., Yagihashi, M., Hozumi, A., Gorb, S. N., & Gorb, E. V. (2016). Surface roughness rather than surface chemistry essentially affects insect adhesion. *Beilstein Journal of Nanotechnology*, 7(1), 1471–1479. <https://doi.org/10.3762/bjnano.7.139>
- Féat, A., Federle, W., Kamperman, M., & van der Gucht, J. (2019). Coatings preventing insect adhesion: An overview. *Progress in Organic Coatings*, 134, 349–359. <https://doi.org/10.1016/j.porgcoat.2019.05.013>
- Féat, A., Federle, W., Kamperman, M., Murray, M., van der Gucht, J., & Taylor, P. (2019). Slippery paints: Eco-friendly coatings that cause ants to slip. *Progress in Organic Coatings*, 135, 331–344. Scopus. <https://doi.org/10.1016/j.porgcoat.2019.06.004>
- Federle, W., Barnes, W. J. P., Baumgartner, W., Drechsler, P., & Smith, J. M. (2006). Wet but not slippery: Boundary friction in tree frog adhesive toe pads. *Journal of The Royal Society Interface*, 3(10), 689–697. <https://doi.org/10.1098/rsif.2006.0135>
- Federle, W., Baumgartner, W., & Hölldobler, B. (2004). Biomechanics of ant adhesive pads: Frictional forces are rate- and temperature-dependent. *Journal of Experimental Biology*, 207(1), 67–74. <https://doi.org/10.1242/jeb.00716>
- Federle, W., & Endlein, T. (2004). Locomotion and adhesion: Dynamic control of adhesive surface contact in ants. *Arthropod Structure & Development*, 33(1), 67–75. <https://doi.org/10.1016/j.asd.2003.11.001>
- Federle, W., & Labonte, D. (2019). Dynamic biological adhesion: Mechanisms for controlling attachment during locomotion. *Philosophical Transactions of the Royal Society B: Biological Sciences*, 374(1784), 20190199. <https://doi.org/10.1098/rstb.2019.0199>
- Federle, W., Riehle, M., Curtis, A. S. G., & Full, R. J. (2002). An Integrative Study of Insect Adhesion: Mechanics and Wet Adhesion of Pretarsal Pads in Ants. *Integrative and Comparative Biology*, 42(6), 1100–1106. <https://doi.org/10.1093/icb/42.6.1100>
- Federle, W., Rohrseitz, K., & Hölldobler, B. (2000). Attachment forces of ants measured with a centrifuge: Better ‘wax-runners’ have a poorer attachment to a smooth surface. *Journal of Experimental Biology*, 203(3), 505–512.
- Full, R., Yamauchi, A., & Jindrich, D. (1995). Maximum single leg force production: Cockroaches righting on photoelastic gelatin. *Journal of Experimental Biology*, 198(12), 2441–2452.
- Gao, H., Wang, X., Yao, H., Gorb, S., & Arzt, E. (2005). Mechanics of hierarchical adhesion structures of geckos. *Mechanics of Materials*, 37(2), 275–285. <https://doi.org/10.1016/j.mechmat.2004.03.008>
- Gillies, A. G., Henry, A., Lin, H., Ren, A., Shiu, K., Fearing, R. S., & Full, R. J. (2014). Gecko toe and lamellar shear adhesion on macroscopic, engineered rough surfaces. *Journal of Experimental Biology*, 217(2), 283–289. <https://doi.org/10.1242/jeb.092015>
- Glass, P., Cheung, E., & Sitti, M. (2008). A Legged Anchoring Mechanism for Capsule Endoscopes Using Micropatterned Adhesives. *IEEE Transactions on Biomedical Engineering*, 55(12), 2759–2767. <https://doi.org/10.1109/TBME.2008.2002111>
- Gorb, E. V., Hosoda, N., Miksch, C., & Gorb, S. N. (2010). Slippery pores: Anti-adhesive effect of nanoporous substrates on the beetle attachment system. *Journal of The Royal Society Interface*, 7(52), 1571–1579. <https://doi.org/10.1098/rsif.2010.0081>
- Gorb, E. V., Voigt, D., Eigenbrode, S. D., & Gorb, S. N. (2008). Attachment force of the beetle *Cryptolaemus montrouzieri* (Coleoptera, Coccinellidae) on leaflet surfaces of mutants of the pea *Pisum sativum* (Fabaceae) with regular and reduced wax coverage. *Arthropod-Plant Interactions*, 2(4), 247–259. <https://doi.org/10.1007/s11829-008-9049-0>
- Gorb, E. V., & Gorb, S. N. (2002). Attachment ability of the beetle *Chrysolina fastuosa* on various plant surfaces. *Entomologia Experimentalis et Applicata*, 105(1), 13–28. <https://doi.org/10.1046/j.1570-7458.2002.01028.x>
- Gorb, S. N. (1998). The design of the fly adhesive pad: Distal tenent setae are adapted to the delivery of an adhesive secretion. *Proceedings of the Royal Society of London. Series B: Biological Sciences*, 265(1398), 747–752. <https://doi.org/10.1098/rspb.1998.0356>
- Gorb, S. N. (2002). Attachment Devices of Insect Cuticle, Kluwer Academic Publishers, Dordrecht, 2002, <https://doi.org/10.1007/0-306-47515-4>
- Gorb, S. N. (2005). Uncovering Insect Stickiness: Structure and Properties of Hairy Attachment Devices. *American Entomologist*, 51(1), 31–35. <https://doi.org/10.1093/ae/51.1.31>
- Gorb, S. N., & Beutel, R. (2001). Evolution of locomotory attachment pads of hexapods. *Naturwissenschaften*, 88(12), 530–534. <https://doi.org/10.1007/s00114-001-0274-y>
- Gorb, S. N., Gorb, E. V., & Kastner, V. (2001). Scale effects on the attachment pads and friction forces in syrphid flies (Diptera, Syrphidae). *Journal of Experimental Biology*, 204(8), 1421–1431.
- Grohmann, C., Blankenstein, A., Koops, S., & Gorb, S. N. (2014). Attachment of *Galerucella nymphaeae* (Coleoptera, Chrysomelidae) to surfaces with different surface energy. *Journal of Experimental Biology*, 217(23), 4213–4220. <https://doi.org/10.1242/jeb.108902>
- Hansen, W. R., & Autumn, K. (2005). Evidence for self-cleaning in gecko setae. *Proceedings of the National Academy of Sciences*, 102(2), 385–389. <https://doi.org/10.1073/pnas.0408304102>

- Hawkes, E. W., Christensen, D. L., Han, A. K., Jiang, H., & Cutkosky, M. R. (2014). *Grasping without Squeezing: Shear Adhesion Gripper with Fibrillar Thin Film*. 8.
- Heepe, L., Raguseo, S., & Gorb, S. N. (2017). An experimental study of double-peeling mechanism inspired by biological adhesive systems. *Applied Physics A*, 123(2), 124. <https://doi.org/10.1007/s00339-016-0753-9>
- Henrey, M., Ahmed, A., Boscaroli, P., Shannon, L., & Menon, C. (2014). Abigaille-III: A Versatile, Bioinspired Hexapod for Scaling Smooth Vertical Surfaces. *Journal of Bionic Engineering*, 11(1), 1–17. [https://doi.org/10.1016/S1672-6529\(14\)60015-9](https://doi.org/10.1016/S1672-6529(14)60015-9)
- Hill, I. D. C., Dong, B., Barnes, W. J. P., Ji, A., & Endlein, T. (2018). The biomechanics of tree frogs climbing curved surfaces: A gripping problem. *Journal of Experimental Biology*, 221(5). <https://doi.org/10.1242/jeb.168179>
- Huber, G., Gorb, S. N., Hosoda, N., Spolenak, R., & Arzt, E. (2007). Influence of surface roughness on gecko adhesion. *Acta Biomaterialia*, 3(4), 607–610. <https://doi.org/10.1016/j.actbio.2007.01.007>
- Huber, G., Gorb, S. N., Spolenak, R., & Arzt, E. (2005a). Resolving the nanoscale adhesion of individual gecko spatulae by atomic force microscopy. *Biology Letters*, 1(1), 2–4. <https://doi.org/10.1098/rsbl.2004.0254>
- Huber, G., Mantz, H., Spolenak, R., Mecke, K., Jacobs, K., Gorb, S. N., & Arzt, E. (2005b). Evidence for capillarity contributions to gecko adhesion from single spatula nanomechanical measurements. *Proceedings of the National Academy of Sciences of the United States of America*, 102(45), 16293–16296. Scopus. <https://doi.org/10.1073/pnas.0506328102>
- Irschick, D. J., Austin, C. C., Petren, K., Fisher, R. N., Losos, J. B., & Ellers, O. (1996). A comparative analysis of clinging ability among pad-bearing lizards. *Biological Journal of the Linnean Society*, 59(1), 21–35. <https://doi.org/10.1111/j.1095-8312.1996.tb01451.x>
- Ji, A., Yuan, S., Endlein, T., Hill, I. D. C., Wang, W., Wang, H., Jiang, N., Zhao, Z., Barnes, W. J. P., & Dai, Z. (2019). A force-measuring and behaviour-recording system consisting of 24 individual 3D force plates for the study of single limb forces in climbing animals on a quasi-cylindrical tower. *Bioinspiration & Biomimetics*, 14(4), 046004. <https://doi.org/10.1088/1748-3190/ab1d11>
- Jiao, Y., Gorb, S., & Scherge, M. (2000). Adhesion measured on the attachment pads of *Tettigonia viridissima* (Orthoptera, insecta). *Journal of Experimental Biology*, 203(12), 1887–1895. Retrieved from: <https://jeb.biologists.org/content/203/12/1887>
- Kamiyama, K., Kajimoto, H., Kawakami, N., & Tachi, S. (2004). Evaluation of a vision-based tactile sensor. *IEEE International Conference on Robotics and Automation, 2004. Proceedings. ICRA '04. 2004*, 2, 1542-1547 Vol.2. <https://doi.org/10.1109/ROBOT.2004.1308043>
- Kappl, M., Kaveh, F., & Barnes, W. J. P. (2016). Nanoscale friction and adhesion of tree frog toe pads. *Bioinspiration & Biomimetics*, 11(3), 035003. <https://doi.org/10.1088/1748-3190/11/3/035003>
- Kim, S., Spenko, M., Trujillo, S., Heyneman, B., Santos, D., & Cutkosky, M. R. (2008). Smooth Vertical Surface Climbing With Directional Adhesion. *IEEE Transactions on Robotics*, 24(1), 65–74. <https://doi.org/10.1109/TRO.2007.909786>
- Kwon, J., Cheung, E., Park, S., & Sitti, M. (2006). Friction enhancement via micro-patterned wet elastomer adhesives on small intestinal surfaces. *Biomedical Materials*, 1(4), 216–220. <https://doi.org/10.1088/1748-6041/1/4/007>
- Labonte, D., Clemente, C. J., Dittrich, A., Kuo, C.-Y., Crosby, A. J., Irschick, D. J., & Federle, W. (2016). Extreme positive allometry of animal adhesive pads and the size limits of adhesion-based climbing. *Proceedings of the National Academy of Sciences*, 113(5), 1297–1302. <https://doi.org/10.1073/pnas.1519459113>
- Labonte, D., & Federle, W. (2015a). Rate-dependence of 'wet' biological adhesives and the function of the pad secretion in insects. *Soft Matter*, 11(44), 8661–8673. <https://doi.org/10.1039/C5SM01496D>
- Labonte, D., & Federle, W. (2015b). Scaling and biomechanics of surface attachment in climbing animals. *Philosophical Transactions of the Royal Society B: Biological Sciences*, 370(1661), 20140027. <https://doi.org/10.1098/rstb.2014.0027>
- Labonte, D., Struecker, M.-Y., Birn-Jeffery, A. V., & Federle, W. (2019). Shear-sensitive adhesion enables size-independent adhesive performance in stick insects. *Proceedings of the Royal Society B: Biological Sciences*, 286(1913), 20191327. <https://doi.org/10.1098/rspb.2019.1327>
- Langer, M. G., Ruppertsberg, J. P., & Gorb, S. (2004). Adhesion forces measured at the level of a terminal plate of the fly's seta. *Proceedings of the Royal Society of London. Series B: Biological Sciences*, 271(1554), 2209–2215. <https://doi.org/10.1098/rspb.2004.2850>
- Langowski, J. K. A., Dodou, D., Kamperman, M., & van Leeuwen, J. L. (2018). Tree frog attachment: Mechanisms, challenges, and perspectives. *Frontiers in Zoology*, 15(1), 32. <https://doi.org/10.1186/s12983-018-0273-x>
- Langowski, J. K. A., Rummenie, A., Pieters, R. P. M., Kovalev, A., Gorb, S. N., & Leeuwen, J. L. van. (2019). Estimating the maximum attachment performance of tree frogs on rough substrates. *Bioinspiration & Biomimetics*, 14(2), 025001. <https://doi.org/10.1088/1748-3190/aafc37>
- Lin, H.-T., & Trimmer, B. A. (2012). A new bi-axial cantilever beam design for biomechanics force measurements. *Journal of Biomechanics*, 45(13), 2310–2314. <https://doi.org/10.1016/j.jbiomech.2012.06.005>
- Lüken, D., Voigt, D., Gorb, S. N., & WZebitz, C. P. (2009). Die Tarsenmorphologie und die Haftfähigkeit des Schwarzen Batatenkäfers *Cylas puncticolis* (Boheman). *Mitt. Dtsch. Ges. Allg. Angew. Ent.*, 17, 109–113.

- Murphy, M. P., Kute, C., Mengüç, Y., & Sitti, M. (2011). Waalbot II: Adhesion Recovery and Improved Performance of a Climbing Robot using Fibrillar Adhesives. *The International Journal of Robotics Research*, 30(1), 118–133. <https://doi.org/10.1177/0278364910382862>
- O'Donnell, M. K., & Deban, S. M. (2020). The Effects of Roughness and Wetness on Salamander Cling Performance. *Integrative and Comparative Biology*, 60(4), 840–851. <https://doi.org/10.1093/icb/icaa110>
- Park, S.-J., Goodman, M. B., & Pruitt, B. L. (2007). Analysis of nematode mechanics by piezoresistive displacement clamp. *Proceedings of the National Academy of Sciences*, 104(44), 17376–17381. <https://doi.org/10.1073/pnas.0702138104>
- Pashazanusi, L., Lwoya, B., Oak, S., Khosla, T., Albert, J. N. L., Tian, Y., Bansal, G., Kumar, N., & Pesika, N. S. (2017). Enhanced Adhesion of Mosquitoes to Rough Surfaces. *ACS Applied Materials & Interfaces*, 9(28), 24373–24380. <https://doi.org/10.1021/acsami.7b06659>
- Peisker, H., Michels, J., & Gorb, S. N. (2013). Evidence for a material gradient in the adhesive tarsal setae of the ladybird beetle *Coccinella septempunctata*. *Nature Communications*, 4(1), 1661. <https://doi.org/10.1038/ncomms2576>
- Persson, B. N. J., & Gorb, S. N. (2003). The effect of surface roughness on the adhesion of elastic plates with application to biological systems. *The Journal of Chemical Physics*, 119(21), 11437–11444. <https://doi.org/10.1063/1.1621854>
- Pugno, N., Lepore, E., Toscano, S., & Pugno, F. (2011). Normal Adhesive Force-Displacement Curves of Living Geckos. *The Journal of Adhesion*, 87(11), 1059–1072. <https://doi.org/10.1080/00218464.2011.609439>
- Reinhardt, L., Weihmann, T., & Blickhan, R. (2009). Dynamics and kinematics of ant locomotion: Do wood ants climb on level surfaces? *Journal of Experimental Biology*, 212(15), 2426–2435. <https://doi.org/10.1242/jeb.026880>
- Salerno, G., Reborá, M., Gorb, E. V., & Gorb, S. (2018a). Attachment ability of the polyphagous bug *Nezara viridula* (Heteroptera: Pentatomidae) to different host plant surfaces. *Scientific Reports*, 8(1), 10975. <https://doi.org/10.1038/s41598-018-29175-2>
- Salerno, G., Reborá, M., Kovalev, A., Gorb, E. V., & Gorb, S. (2018b). Contribution of different tarsal attachment devices to the overall attachment ability of the stink bug *Nezara viridula*. *Journal of Comparative Physiology A*, 204(7), 627–638. <https://doi.org/10.1007/s00359-018-1266-0>
- Salerno, G., Reborá, M., Piersanti, S., Gorb, E., & Gorb, S. (2020). Mechanical ecology of fruit-insect interaction in the adult Mediterranean fruit fly *Ceratitis capitata* (Diptera: Tephritidae). *Zoology*, 139, 125748. <https://doi.org/10.1016/j.zool.2020.125748>
- Scholz, I., Barnes, W. J. P., Smith, J. M., & Baumgartner, W. (2009). Ultrastructure and physical properties of an adhesive surface, the toe pad epithelium of the tree frog, *Litoria caerulea* White. *Journal of Experimental Biology*, 212(2), 155–162. <https://doi.org/10.1242/jeb.019232>
- Song, Y., Dai, Z., Wang, Z., Ji, A., & Gorb, S. N. (2016). The synergy between the insect-inspired claws and adhesive pads increases the attachment ability on various rough surfaces. *Scientific Reports*, 6. <https://doi.org/10.1038/srep26219>
- Song, S., Majidi, C., & Sitti, M. (2014). GeckoGripper: A soft, inflatable robotic gripper using gecko-inspired elastomer micro-fiber adhesives. *2014 IEEE/RSJ International Conference on Intelligent Robots and Systems*, 4624–4629. <https://doi.org/10.1109/IROS.2014.6943218>
- Spinner, M., Westhoff, G., & Gorb, S. N. (2014). Subdigital setae of chameleon feet: Friction-enhancing microstructures for a wide range of substrate roughness. *Scientific Reports*, 4(1), 5481. <https://doi.org/10.1038/srep05481>
- Voigt, D., & Gorb, S. N. (2012). Attachment ability of sawfly larvae to smooth surfaces. *Arthropod Structure & Development*, 41(2), 145–153. <https://doi.org/10.1016/j.asd.2011.10.001>
- Voigt, D., & Gorb, S. (2017). Functional morphology of tarsal adhesive pads and attachment ability in ticks *Ixodes ricinus* (Arachnida, Acari, Ixodidae). *Journal of Experimental Biology*, 220(11), 1984–1996. <https://doi.org/10.1242/jeb.152942>
- Walker, G., Yulf, A. B., & Ratcliffe, J. (1985). The adhesive organ of the blowfly, *Calliphora vomitoria*: A functional approach (Diptera: Calliphoridae). *Journal of Zoology*, 205(2), 297–307. <https://doi.org/10.1111/j.1469-7998.1985.tb03536.x>
- Zhou, Y., Robinson, A., Steiner, U., & Federle, W. (2014). Insect adhesion on rough surfaces: Analysis of adhesive contact of smooth and hairy pads on transparent microstructured substrates. *Journal of The Royal Society Interface*, 11(98), 20140499. <https://doi.org/10.1098/rsif.2014.0499>
- Zhou, M., Tian, Y., Sameoto, D., Zhang, X., Meng, Y., & Wen, S. (2013). Controllable Interfacial Adhesion Applied to Transfer Light and Fragile Objects by Using Gecko Inspired Mushroom-Shaped Pillar Surface. *ACS Applied Materials & Interfaces*, 5(20), 10137–10144. <https://doi.org/10.1021/am402815x>

S2. Setup parts list

Cameras

Photron Fastcam SA-X2

PCO Dimax HS4

Lenses

Nikkor 105mm AF-S f2.8G (Photrons)

Nikkor 105mm AF f2.8D (PCO)

21.5 mm extension tube

+5 diptre conversion lens

940nm IR filter - Thorlabs

Lights

Backlights: ML850L3 (Bergkirchen, Germany) Thorlabs

Assembly:

ER12	Thorlabs
LCP01_M	Thorlabs
LCP02_M	Thorlabs
SM1T2	Thorlabs
SM2A52	Thorlabs
VB01_M	Thorlabs

940nm IR strip:

Frame

Maytec Aluminium profiles

- Habru aluminium systeemprofielen B.V. (Doetichem, the Netherlands)

Linor X95 profiles

Flight arena

Windows: 8mm acrylic panels

Frame: 400mm double-flange-combi tube- Handytube (Maarheze, the Netherlands)

Camera mounts:

Linor FLS95 rails

Linor carrier 120mm

Linor Carrier X95

OptoSigma XTable

Thorlabs L490M

3D printed components

Printer: Ultimaker S3

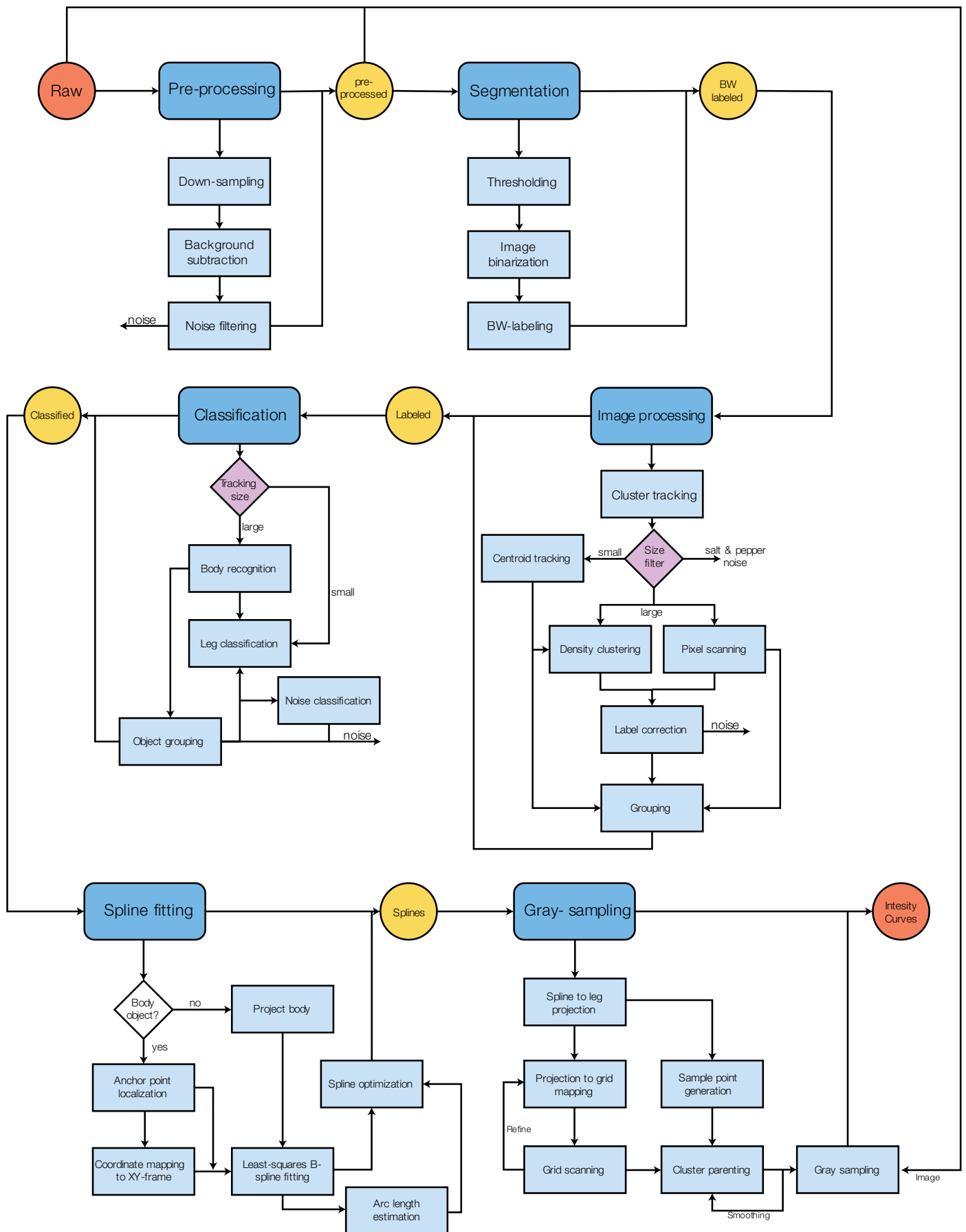
Material: Ultimaker Tough PLA Black

Slicer: Cura

Print settings: Ultimaker Tough PLA default

S3: Code manual

Processing pipeline overview.



Code manual

In the following section, the use of the MATLAB code and settings for various functions will be detailed. The pipeline can be operated from the top folder using only the *Runme.m* script. All other files are nested under the Functions folder and can be located through the directory index, at the end of the manual.

Basic operation: *Runme.m*

The script is operated through the *Runme.m* script file. The script can be executed through opening the script file and clicking on run or pressing F5. Or alternatively through the MATLAB command window through the command:

```
>> run runme.m
```

Inside *Runme.m* various operating settings can be adjusted. The operating mode sets the subset of processing modules to be used. Under Data set selection the data location and subset for analysis can be selected. And under Switches and Settings, various algorithm parameters can be edited.

Clear all:

Use the clearall switch to clean or keep the workspace. In standard operation it is recommended to clear the workspace and any figures. For plotting or analysis it can be desirable to keep the workspace intact. Clearall can be set to *true* or *false*.

```
%% Do you want to clear the workspace?
clearall = true;
if clearall == true
clc
clear all
close all
end
```

Operating modes:

Various operating modes can be selected under the **Select operating mode** section. Operating modes select the processing modules to be used during data analysis. To switch operating mode, change the char string behind operating mode to one of the defined operating modes. Custom operating modes can be defined manually inside *runtype.m*, more information at the end of this section.

```
%% Select operatingmode
Operatingmode = 'standard';

%'standard': Run the full algorithm
% recommended use: use default settings
%
%'segmentation': Only runs the segmentation part of the code.
% recommended use: to find initial segmentation thresholds. To quickly
% visualize segmentation result use: showframe(framenumber)
%
%'plotting': Only runs the figure plotting algorithm
% recommended use: set clearall to false
%
%'load_data': Only loads the image data and creates a datastore
% recommended use: using datastore for other purposes

%NOTE: Custom operating modes can be added in the runtype.m script under
%\functions\Driver and Settings
```

Data set selection

The script is pre-set to load data from the mosquito thesis experiments. Three data selection modes are available: 'manual', 'automatic', and 'sampledata'.

Manual selection: Specify the day, runnumber, drive, camera and frames. This function assumes a windows folder directory. For Linux or IOS, the data folder path needs to be supplied inside the altfolder brackets.

Automatic selection: Video data of the mosquito analysis experiment has been tagged and sorted in sets defined in the Events.xlsx worksheet. Using automatic selection these sets can be loaded by defining a setnumber.

Sampledata: A small subset (24 frames) of the data used for programming and parameter testing, in which activity and various forms of noise are visible on the PCO signal.

```
%% Data set selection

%For WINDOWS machines: Set drive selection to automatic or manual.
%  automatic: will try to locate the events.xlsx file. This will work only
%  when the file is located in the top folder of a drive, either internal or
%  external.
%  manual: specify the measurement day, run number, drive, and camera.
%  sampledata: use the sample dataset

selection = 'manual';

%For IOS/Linux systems drive selection must be adjusted by manually and by
%hand. For details see the read_data_v05.m function

switch selection
  case 'manual'
    %Select day: 'mm_dd', run: #, drive: e.g. ('D:','E:','F:','G:'),
    %camera: 'PCO','Photron1','Photron2';

    %You can change the values of these parameters
    %%%%%%%%%%%%%%%%%%%%%%%%%%%%%%%
    day = '03_31';
    runno = 6;
    drive = 'D:';
    camera = 'PCO';
    frames = [586, 706];
    %%%%%%%%%%%%%%%%%%%%%%%%%%%%%%%
    %Note that specifying an altfolder will overwrite the folder
    %selection algorithm, but the above parameters still need to be
    %filled out for the data loading algorithm to work.

    usesampleddata = 0;
    altfolder = []; %manually override the folder path (currently only way to
    select data on IOS and Linux systems)

  case 'automatic'
    %Select set number (setno), as indicated in the events.xlsx file
    setno = 19;
    run auto_selector_string.m
    usesampleddata = false;

  case 'sampledata'
    day = '03_31';
    runno = 6;
    drive = 'D:';
    camera = 'PCO';
    frames = [2, 25];
    usesampleddata = true;

    altfolder = [];

end
```

Switches

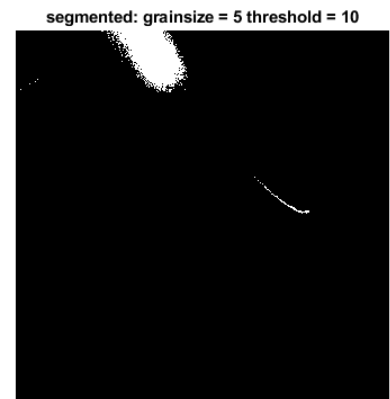
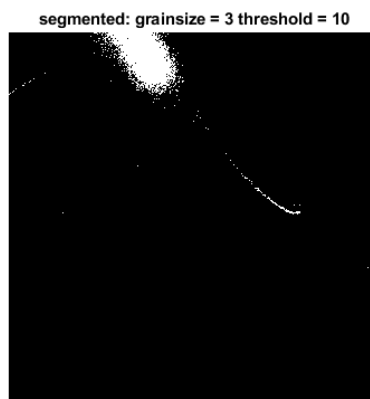
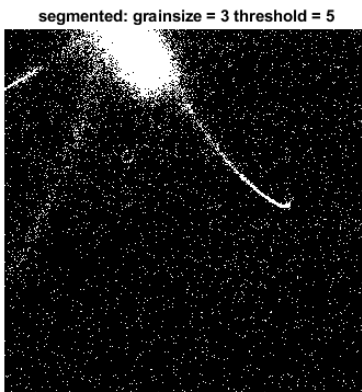
Select the filtertype and filter layout of the background subtract algorithm. Preprogramed filters are the median filter *medfilt2*, and the gaussian filter *imgaussfilt*. There are two filter layouts: single filtering and double filtering. The first filterpass is on the background image, to smooth out sensor noise. The 2nd filter-pass happens on the background-subtracted image, to filter out residual salt and pepper noise. The 2nd filter-pass will be of the type: 'medfilt2', to preserve edge clarity.

```
%% Switches
filtertype = 'medfilt2';    %possible filters: medfilt2, gaussfilt
filtertwice = true;        %apply 2nd pass filter on image (reduces salt & pepper
                             noise)
```

Settings

Under settings, various settings can be selected for the image processing pipeline.

```
%% Settings
%image and background removal
grainsize = 3;             %Sets the pixel cluster size for filtering
threshold = 10;           %Sets the noise level threshold after background removal
```



```
%Segmentation and tracking
segmentationalgorithm = 'otsuthresh';
minboundingboxarea = 750; %Minimum size (#pixels^2) of bounding box (e.g. a 10 * 75
                             pixel box)
```

```
%Boxtracking;
%DBscan:
Centersearchrange = 50;
Centerminpts = 8;
```

```
%Spline fitting
Makespline = true;
```

```
%Threshold smoothing range
smoothingrange = 15;
```

Adding operating modes.

Inside `runtype.m` custom operating modes can be set. To do so, add a case (i.e. case 'test'), and make a list of the operating modes to be turned on and off by setting the modes to true or false, like in the example below. To use a custom operating mode, after defining, enter the custom string in the `operatingmode` variable in `Runme.m`

```
switch Operatingmode
  case 'standard'
    %True
    mode.segmentation = true;
    mode.preprocessing = true;
    mode.processing = true;
    mode.classification = true;
    mode.fitting = true;
    mode.sampling = true;
    mode.plotting = true;
    mode.analysis = true;
    %False
  case 'plotting'
    %True
    mode.plotting = true;
    mode.analysis = true;
    %False
    mode.segmentation = false;
    mode.preprocessing = false;
    mode.classification = false;
    mode.fitting = false;
    mode.sampling = false;
    mode.processing = false;
...

```

Altering the image processing pipeline

The image processing pipeline is controlled by the `driver.m` script. To change parts of the pipeline, switch out functions inside the driver with new functions and place the function files inside the Functions folder.

```
%Driver script for data analysis Mosquito Thesis project
% Author: Luc van den Boogaart

time.tstart = tic;
%% Set operating mode
run runtype.m

%% Load and apply settings
run Initialize.m
ImTrackSettings = overwrite_default_settings(settings);

%% Load data
[im_datastore, imdat, background] =
read_data_v06(day, runno, camera, drive, frames, 'usesampleddata', usesampleddata, 'altfolder', a
ltfolder);

%% Image preprocessing
%_create datastore & data struct_

if mode.preprocessing == true

%_Downsample to uint 8_
[imdat, background8b] = downsample16to8b(im_datastore, imdat, background);

%_filtered background_
imdat = backgroundsubtractv3(settings, imdat, 'filtersetting', 'single');

%_apply threshold_
imdat = applythreshold(settings, imdat);

end

%% Image segmentation

```

```

%_segment the image using estimated thresholds_%
nframes = frames(2)-frames(1)+1;

if mode.segmentation == true
time.tsegment = tic;
    for i = 1:nframes
        [imdat{i},stat{i}] = imagesegmentation_v2(imdat{i},ImTrackSettings); %segment
images
        [imdat{i},stat{i}] = imagelabel(imdat{i},stat{i}); %Create BW Label
        clc
        disp('Image segmentation')
        disp(['Image ',num2str(i),' of ',num2str(nframes)])
        toc
    end

disp(newline+"segmentation time elapsed:")
toc(time.tsegment)
disp(newline+"Total time elapsed:")
toc(time.tstart)
end

... etc

```

Pipeline data format

Processing data is stored per frame in *imdat* structs. All functions in the pipeline have the *imdat* struct as in and output, allowing all data to be called from anywhere in the pipeline.

Field ^	Value
Imagedat	1x1 struct
segmentation	1x1 struct
processing	1x1 struct
identifier	"imagetracker struct"
fitting	1x1 struct
sampling	1x1 struct

Field ^	Value
camera	'PCO'
date	'2021_03_31'
run	'RUN6'
name	'2021_03_31_RUN6_PCO_09550.tif'
number	9550
string	"2021_03_31_RUN6_PCO_09550.tif"
raw	2000x2000 uint8
background	2000x2000 uint8
filteredbackground	2000x2000 uint8
backgroundremoved	2000x2000 uint8

Data visualization

Various data visualization functions have been made to work with the *imdat* structs. These are located in the Functions\plotting folder and contain detailed instructions on how to call them.

Dir-index

\Code\Functions

Mode	LastWriteTime	Length	Name
d----	11/4/2021 2:10 PM		Analysis
d----	11/3/2021 11:30 PM		Driver and Settings
d----	10/23/2021 9:04 PM		Image processing
d----	10/22/2021 7:15 PM		Load data
d----	11/2/2021 11:32 PM		Plotting

\Code\Functions\Analysis

Mode	LastWriteTime	Length	Name
-a----	10/27/2021 5:53 PM	416	animate_order.m
-a----	11/3/2021 7:10 PM	2346	animate_series.m
-a----	11/4/2021 2:10 PM	3070	cellmasks.m
-a----	11/3/2021 6:49 PM	4180	contact_area.m
-a----	11/4/2021 2:11 PM	4461	extract_greys.m
-a----	11/4/2021 1:33 PM	1064	IDtoXY.m
-a----	10/23/2021 5:29 PM	972	XYtoID.m

\Code\Functions\Driver and Settings

Mode	LastWriteTime	Length	Name
-a----	7/6/2021 6:47 PM	19	classifierweights.m
-a----	11/4/2021 10:17 PM	7586	Driver.m
-a----	11/2/2021 2:48 PM	1354	Initialize.m
-a----	10/23/2021 4:28 PM	1999	overwrite_default_settings.m
-a----	10/23/2021 9:08 PM	1470	runtype.m

\Code\Functions\Image processing

Mode	LastWriteTime	Length	Name
d----	11/3/2021 11:30 PM		Fitting
d----	11/3/2021 1:16 PM		Preprocessing
d----	10/22/2021 7:31 PM		Processing
d----	10/23/2021 9:24 PM		Sampling
d----	10/22/2021 7:36 PM		Segmentation

\Code\Functions\Image processing\Fitting

Mode	LastWriteTime	Length	Name
-a----	10/31/2021 6:05 PM	246	approxSplineLength.m
-a----	11/3/2021 10:06 PM	9125	spline_fit.m

\Code\Functions\Image processing\Preprocessing

Mode	LastWriteTime	Length	Name
-a----	10/27/2021 6:21 PM	2907	applythreshold.m
-a----	11/3/2021 11:11 AM	9508	backgroundsubtractv3.m
-a----	10/20/2021 2:55 PM	494	downsample16to8b.m

\Code\Functions\Image processing\Processing

Mode	LastWriteTime	Length	Name
d----	11/3/2021 9:47 PM		Classification
d----	10/23/2021 7:46 PM		Grouping
d----	11/3/2021 11:30 PM		Labeling
d----	10/26/2021 2:39 PM		Tracking

\Code\Functions\Image processing\Processing\Classification

Mode	LastWriteTime	Length	Name
-a----	11/3/2021 11:35 PM	25326	classification.m
-a----	11/3/2021 5:51 PM	8634	objectgrouper.m

\Code\Functions\Image processing\Processing\Grouping

Mode	LastWriteTime	Length	Name
-a----	11/3/2021 11:13 PM	654	datareorganise.m
-a----	11/3/2021 11:09 PM	1858	supergrouper.m

\Code\Functions\Image processing\Processing\Labeling

Mode	LastWriteTime	Length	Name
-a----	11/3/2021 11:30 PM	1582	correctlabels.m
-a----	10/23/2021 2:48 PM	2230	removedoubles.m

\Code\Functions\Image processing\Processing\Tracking

Mode	LastWriteTime	Length	Name
-a----	10/23/2021 2:43 PM	1501	boxtrack.m
-a----	10/26/2021 7:11 PM	3270	pixeltrackerv2.m
-a----	10/23/2021 2:46 PM	580	scancenters.m
-a----	10/31/2021 1:39 PM	1439	unfoldtrackdat.m

\Code\Functions\Image processing\Sampling

Mode	LastWriteTime	Length	Name
-a----	10/31/2021 6:56 PM	4380	bresenhamv2.m
-a----	10/23/2021 9:48 PM	8262	Get_Bounds.m
-a----	11/3/2021 4:06 PM	3760	grouppixels.m

\Code\Functions\Image processing\Segmentation

Mode	LastWriteTime	Length	Name
-a----	10/22/2021 7:36 PM	456	imagelabel.m
-a----	10/22/2021 7:36 PM	4776	imagesegmentation_v2.m

\Code\Functions\Load data

Mode	LastWriteTime	Length	Name
-a----	10/20/2021 5:22 PM	1494	auto_selector_string.m
-a----	10/12/2021 11:37 AM	2119	getdrives.m
-a----	10/20/2021 2:14 PM	4342	read_data_v06.m

\Code\Functions\Plotting

Mode	LastWriteTime	Length	Name
-a----	10/25/2021 7:35 PM	11440	figureplotter_v3.m
-a----	10/31/2021 6:31 PM	3229	imageGrid.m
-a----	11/2/2021 7:40 PM	1133	plotprofiles.m
-a----	10/31/2021 6:37 PM	340	plot_bounds.m
-a----	9/22/2021 5:39 PM	283	quickplotter.m
-a----	10/31/2021 4:03 PM	1013	showframe.m

S4: Online: code availability

<https://github.com/LvdBoogaart/Mosquito-FTIR-thesis>

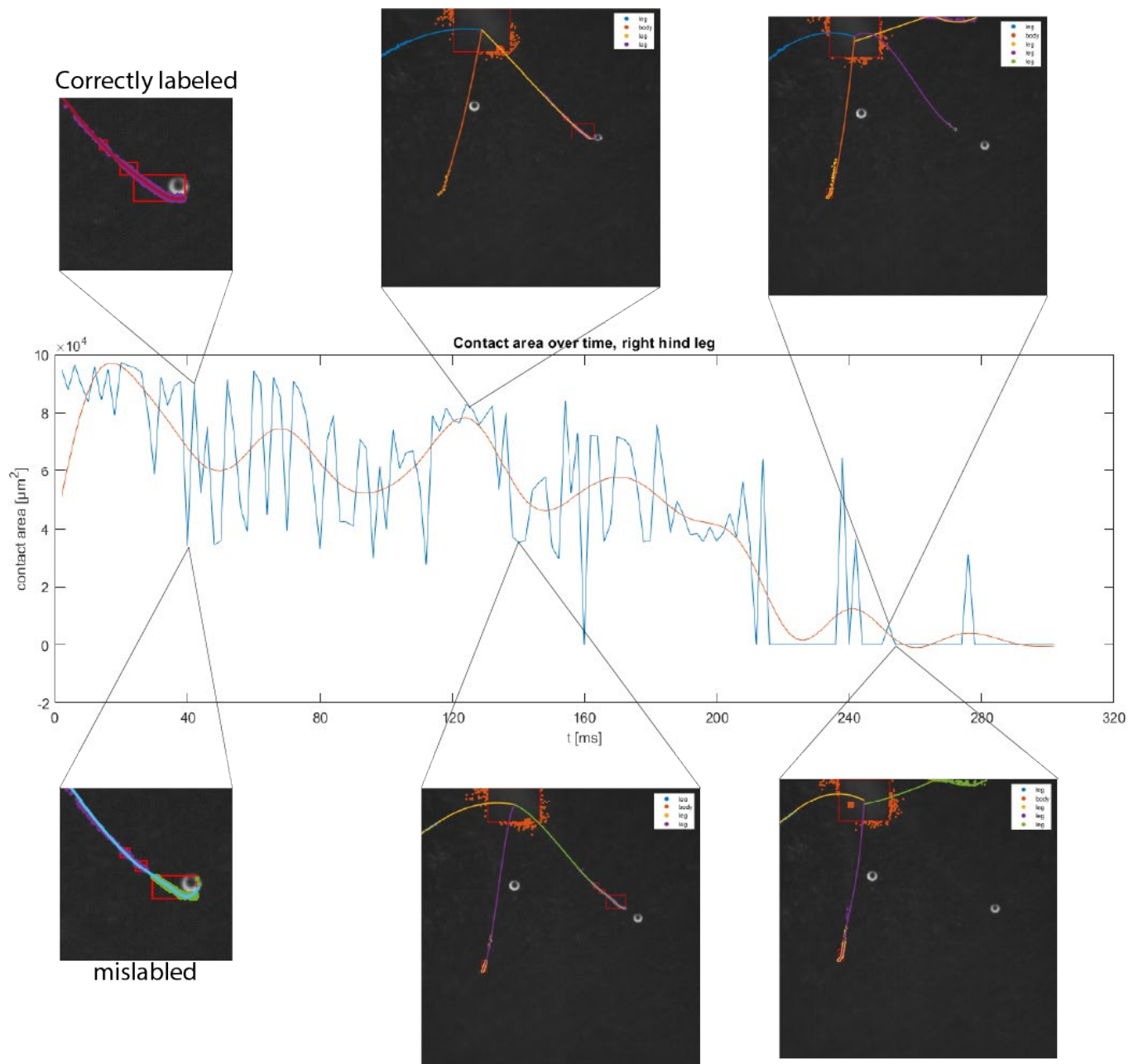
S5: Online: Video of processed PCO signal

<https://youtu.be/hqdaryr2leg>

S6: Table of recordings

Run	Day	local runno	Framerate	Landing	Succesful?	Note
1	03_25	1	2000	Yes	No	Software crash: no Photron signal
2	03_25	2	2000	Yes	No	Software crash: no PCO signal
3	03_26	1	2000	Yes	No	Software crash during save: no Photron signal
4	03_26	2	2000	Yes	Yes	PCO signal SNR is too low
5	03_31	1	500	Yes	Yes	Software issue: Photron 1 run 5 + Photron 2 & PCO run 6 are the same run
6	03_31	2	500	-	-	Software issue: Photron 1 run 5 + Photron 2 & PCO run 6 are the same run
7	03_31	3	500	Yes	Yes	
8	03_31	4	500	Yes	no	
9	03_31	5	500	Yes	yes	Sitting on sensor
10	03_31	6	500	Yes	Yes	Walking over sensor
11	03_31	7	500	Yes	Yes	
12	04_01	1	1000	yes	no	3 mosquitoes, none in center, succesfull landings at outside of target area
13	04_01	2	1000	Yes	yes	Perfect approach
14	04_01	3	1000	Yes	no	Mosquito flying across sensor
15	04_01	4	1000	Yes	no	Mosquito at side of sensor
16	04_01	5	1000	Yes	yes	Mosquito landing top sensor
17	04_01	6	1000	Yes	no	Touchdown center sensor
18	04_02	1	500	Yes	no	Attempted landing center sensor
19	04_02	2	500	no	no	Take-off from side of sensor
20	04_02	3	500	no	no	Leg tapping, Only Photron 1 data (mosquito outside of view of photron 2)
21	04_02	4	500	no	no	Leg tapping

S7: Figure 7 extended



S8. Online video: 2021-03-31 Run6

<https://youtu.be/1qqDew6qGak>

S9. Parafilm puncture



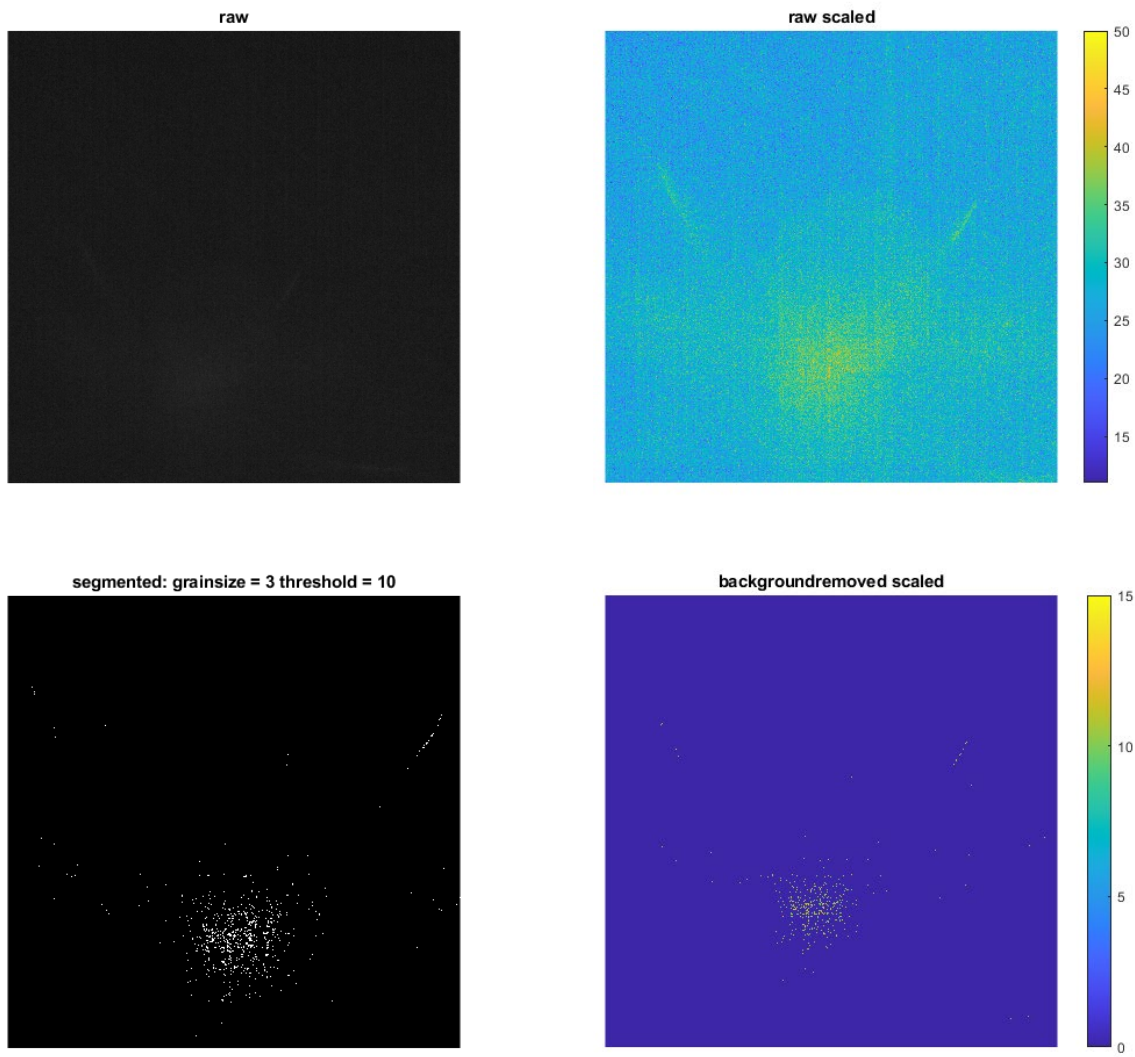
S10. Online video: 2021-04-01 Run2

<https://youtu.be/9v1U7K9ISVs>

S11. Online video: 2021-04-02 Run1

<https://youtu.be/gJTXdxEDWIA>

S12. 1000 FPS PCO data



S13: Digitized lab journal

25/03/2021

1st measurements

goal: successfully collect first batch of data

outline: 3 batches of mosquitoes

B1: 10 mosquitoes on fresh sensor

B2: 10 mosquitoes on same sensor, including CO2 supply

B3: 10 mosquitoes on fresh sensor, including CO2 supply

Experiment:

Start: 9:40, End: 11:30

Temp start: 26.2C Temp end: 27.1C

RH start: 72% RH end: 70%

Batch 1: 9:40 - 10:24 --> Sensor overheated

--> New outline: 2 batches, 2nd part with double mosquitoes and CO2

10:24 - 11:04

- Prepare new sensor

- Remove mosquitoes from arena

- clean arena

Batch 2: 11:04 - 11:30 --> Sensor overheated

Observations:

-After CO2 input (blowing with mouth for ~3 seconds into the arena) mosquito activity increased for about 10 min.

-1 recording of activity made: run folder 2021_03_25_Run1

-More recordings impossible: PCO software crashed during save, sensor overheated before reboot complete.

Future Experiments:

- Find optimal power setting for LED strip

- Standardize CO2 input into system

--> 100% CO2 using flow meter

--> 5% CO2 from tanks

26/03/2021

2nd Measurements + Power setting optimization (for LED strip).

goal: Tune settings, find correct power setting, identify further bottlenecks

Outline: 3 batches, normal experiment

Experiment:

Start: 11:00 End: 12:30

Temp start: 26.9C Temp end: 27.9C

RH start: 69% RH end: 67%

Batch1 11:00 - 11:41

Batch2 11:41 - 11:50

Batch3 11:50 - 12:30

Powersetting: 9V --> T substrate 31C

--> Follow up experiment --> different voltage

Observations:

At least 1 good landing recorded.
dir: 2021_03_26_RUN2...

Steep drop in activity after 11:30
--> try to start earlier.

Follow up experiments:

Power setting of LED's

- Tested 10V for 4 hours: no sensor burst & substrate temperature 34.5C
--> New setting 10V, removed heat pad from setup.

Setup development:

-CO2 supply using flow meter available, next experiments will have more consistent CO2 supply.

31/03/2021

4th measurements @500 FPS

-Checked mosquito age with previous results (30/03/2021) --> Should be well within range.
-Used tap water in stead of sugar water --> significant increase in activity.

Outline: 4 batches of mosquitoes, 8 days old

B1: 16f, 2m

B2: 14f, 3m

B3: 15f, 5m

B4: 11f, 1m

Experiment:

ts = 9:30 te = 12:40
Ts = 26.9C Te = 28.4C
RHs = 71% RHe = 68%

1st Batch, no landings (9:30-10:00)

--> Removed CO2 pump and returned to applying CO2 through blowing

2nd Batch, no landings (10:05-10:07)

--> sensor failure: parafilm tore.

- Aborted experiment, removed mosquitoes from arena, cleaned arena, prepared new sensor.

3rd Bath (11:00-11:40)

- Multiple landings, identified new software problem, camera stopping the recording half way through measurement.

!! Double check all day's data !!

--> Revised camera protocol to continuously monitor recording state

4th Batch (11:45-12:40)

- Multiple landings.

Future experiments:

Decide for one more day of horizontal measurements, because now unsure how much data is collected with software issue.

01/04/2021

5th measurements @1000 FPS

- Changed framerate to 1000 FPS to increase temporal resolution compared to 500 FPS, at higher exposure time compared to 2000 FPS

- Added extra host cue (nylon sock strip -worn for 8 hours) to see if activity increases compared to 31-03-2021

- Used large batches (more mosquitoes were available)

Outline: 4 batches of mosquitoes, 8 days old

B1: 28f, 1m

B2: 26f, 4m

B3: 30f

B4: 30f, 1m

Experiment:

ts = 10:00 te = 12:30

Ts = 26,6C Te = 28,1C

RHs = 68% RHe = 67%

Batch 1 10:00 - 10:40

--> No captures, but good activity

Batch 2 10:40 - 11:15

--> 1 capture

Batch 3 11:15 - 11:45

--> 3 captures

Batch 4 11:45 - 12:30

--> 2 captures

Observations:

- No significant increase of activity visible on substrate that can be attributed to extra host cue (socks was placed around the tunnel, 1

cm wide strip nylon sock ~3 cm from substrate) --> discontinued

- Increased FPS but reduced exposure reduced image quality of PCO significantly on first glance, for sake of redundancy on the image quality,

decided to do final experiments at 500 FPS

- Afternoon used to change the setup from vertical landings to inverse horizontal landings.

(LABJOURNAL has a sketch of the change. See setup folder for setups)

02/04/2021

Inverse Horizontal Landings @500 FPS

- No changes to host cues compared to 01-04-2021

Outline: 4 Batches of Mosquitoes, 8 days old

B1: 18f, 1m

B2: 20f

B3: 17f, 2m

B4: 18f, 2m

Experiment

ts = 10:00 te = 12:30

Ts = 27.0C Te = 28.1C

RHs = 68% RHe = 67%

B1 10:00 - 10:30

--> No landings

B2 10:30 - 11:00

--> No landings

- No landings, cleaning the setup to increase motivation to land

B3&B4 11:10 - 12:30

- No actual landings recorded, only videos of approach and host seeking behaviour
- Mosquitoes would land on the holder, not the parafilm.

Measurements aborted at 12:30 to start setup clean-up and data backup procedure.

Cleaning protocol

Release cages:

- 1) scrub using cold water to remove dirt and particles
- 2) scrub with cotton swab drenched in 30% ethanol to remove odour.
- 3) Rinse with cold tap water
- 4) Dry using paper towels

Release cage grates:

Same procedure, using 70% ethanol instead of 30% ethanol.

Fligh arena:

- 1) Remove mosquitoes using vacuum cleaner
- 2) Dry the arena using paper towels (in case of sensor rupture)
- 3) Clean all inner surfaces using a cotton swab with 15% ethanol
- 4) Dry using paper towels

S14: other videos

<https://www.youtube.com/playlist?list=PLafxcjdFSFi9tyGLTxBSdPdaMy0ruDIOD>

<https://youtu.be/Eo9H2vzAZ4>

<https://youtu.be/CgKcnKJuGGo>

<https://youtu.be/TnH3ICZsW E>

<https://youtu.be/W1e4gLUbeNc>

<https://youtu.be/vG1Z4Qc-rjE>

<https://youtu.be/bR8y8fgV3lw>

<https://youtu.be/1qqDew6qGak>

<https://youtu.be/Jly55u6u8ls>

<https://youtu.be/2wVm9EnEXg4>

https://youtu.be/Ko_1ytmqBis

